PB81-122319

REPORT NO.
UCB/EERC-80/09
MAY 1980

EARTHQUAKE ENGINEERING RESEARCH CENTER

HYBRID MODELLING OF SOIL-STRUCTURE INTERACTION

by

SUNIL GUPTA
TSUNG-WU LIN
JOSEPH PENZIEN
CHAN-SHIOUNG YEH

Report to the National Science Foundation

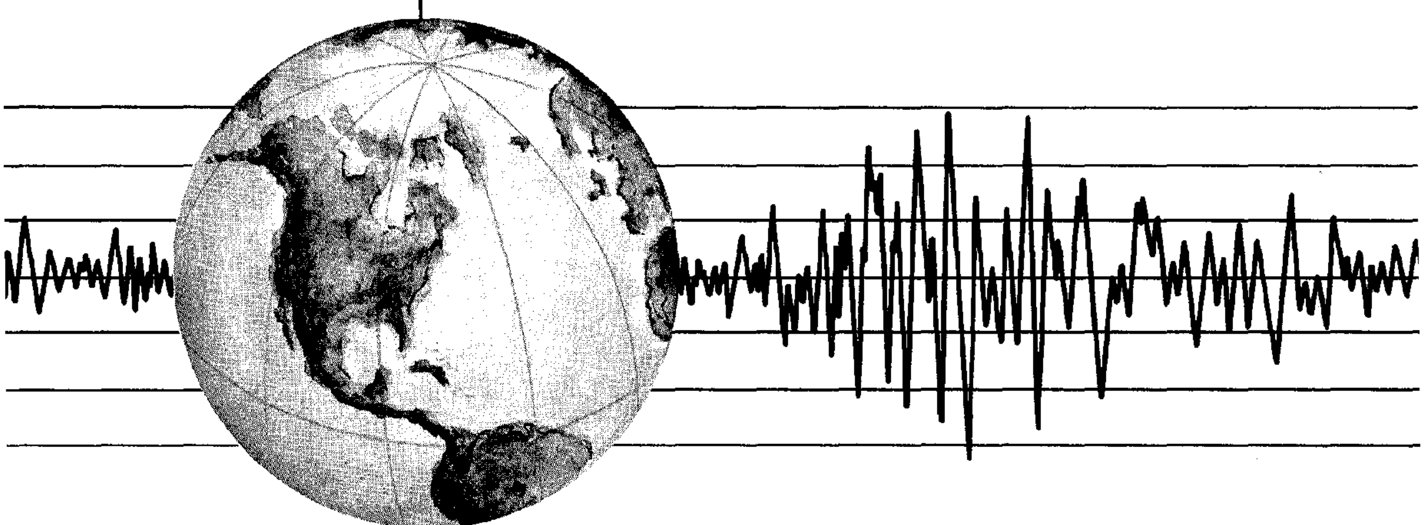

COLLEGE OF ENGINEERING

UNIVERSITY OF CALIFORNIA · Berkeley, California

For sale by the National Technical Information Service, U.S. Department of Commerce, Springfield, Virginia 22161.

See back of report for up to date listing of EERC reports.

50272-101

REPORT DOCUMENTATION PAGE	1. REPORT NO. NSF/RA-800195	2.	3. Recipient's Accession No. PB81 122319
4. Title and Subtitle: Hybrid Modelling of Soil-Structure Interaction			5. Report Date: May 1980
			6.
7. Author(s): S. Gupta, T-W Lin, J. Penzien, C-S Yeh			8. Performing Organization Rept. No.: UCB/EERC-80/09
9. Performing Organization Name and Address: Earthquake Engineering Research Center, University of California, Richmond Field Station, 47th and Hoffman Blvd., Richmond, California 94804			10. Project/Task/Work Unit No.
			11. Contract(C) or Grant(G) No. (C) (G) ENV77-06006
12. Sponsoring Organization Name and Address: National Science Foundation, 1800 G Street, N.W., Washington, D. C. 20550			13. Type of Report & Period Covered
			14.

15. Supplementary Notes

16. Abstract (Limit: 200 words)

A hybrid model for the analysis of soil-structure interaction is proposed which promises to be superior to the currently available methods of analysis. The modelling is achieved by partitioning the total soil-structure system into a near-field and a far-field with hemispherical interface. The near-field, which consists of the structure to be analyzed and a finite region of soil around it, is modelled by the finite element method. For the semi-infinite far-field, impedance matrix corresponding to the interface degrees of freedom is developed which accounts for the loss of energy due to waves travelling away from the foundation.

For torsional vibrations, the far-field impedance matrix can be determined analytically. For general loading conditions a semi-analytical approach is adopted in which the far-field is modelled through continuous impedance functions placed in the three coordinate directions at the interface. These frequency dependent impedance functions are determined by using system identification methods such that the resulting hybrid model reproduces the known compliances of a rigid circular plate on an elastic halfspace. Numerical results obtained using these far-field impedances indicate that the proposed model presents a realistic and economic method for the analysis of three-dimensional soil-structure interaction in surface or embedded structures.

17. Document Analysis a. Descriptors

b. Identifiers/Open-Ended Terms

c. COSATI Field/Group

18. Availability Statement: Release Unlimited	19. Security Class (This Report)	21. No. of Pages
	20. Security Class (This Page)	22. Price

(See ANSI–Z39.18) See Instructions on Reverse OPTIONAL FORM 272 (4–77) (Formerly NTIS–35) Department of Commerce

HYBRID MODELLING OF SOIL-STRUCTURE INTERACTION

by

Sunil Gupta

T. W. Lin

J. Penzien

and

C. S. Yeh

Report to the National Science Foundation

Report No. UCB/EERC-80/09
Earthquake Engineering Research Center
University of California
Berkeley, California

May, 1980

ABSTRACT

A hybrid model for the analysis of soil-structure interaction is proposed which promises to be superior to the currently available methods of analysis. The modelling is achieved by partitioning the total soil-structure system into a near-field and a far-field with hemispherical interface. The near-field, which consists of the structure to be analyzed and a finite region of soil around it,is modelled by the finite element method. For the semi-infinite far-field, impedance matrix corresponding to the interface degrees of freedom is developed which accounts for the loss of energy due to waves travelling away from the foundation.

For torsional vibrations, the far-field impedance matrix can be determined analytically. For general loading conditions a semi-analytical approach is adopted in which the far-field is modelled through continuous impedance functions placed in the three coordinate directions at the interface. These frequency dependent impedance functions are determined by using system identification methods such that the resulting hybrid model reproduces the known compliances of a rigid circular plate on an elastic halfspace. Numerical results obtained using these far-field impedances indicate that the proposed model presents a realistic and economic method for the analysis of three-dimensional soil-structure interaction in surface or embedded structures.

ACKNOWLEDGEMENTS

This investigation was carried out as part of an ongoing U.S.-Taiwan Cooperative Research Program in Earthquake Engineering. The report is based on a Ph.D. dissertation submitted by the first author to the University of California, Berkeley. Financial support, provided by the National Science Foundation under Grant No. ENV-77-06006, is gratefully acknowledged. Computing facilities were provided by the Computer Centers at the University of California, Berkeley, and the Lawrence Berkeley Laboratory.

The authors wish to thank Professors B. A. Bolt and A.K. Chopra for their critical review of the manuscript and Ms. Toni Avery for careful typing.

TABLE OF CONTENTS

	Page
ABSTRACT	i
ACKNOWLEDGEMENTS	ii
TABLE OF CONTENTS	iii
1. INTRODUCTION	1
2. HYBRID MODEL	9
2.1 Near-Field	9
2.2 Far-Field	11
2.3 Hybrid System	12
2.4 Earthquake Input Motion	15
2.5 Dynamic Response of the Hybrid System	16
3. ANALYTICAL SOLUTIONS FOR FAR-FIELD IMPEDANCES	17
3.1 General Equations	17
3.2 Torsional Impedances	21
4. SEMI-ANALYTICAL SOLUTIONS FOR FAR-FIELD IMPEDANCES	31
4.1 Mathematical Modelling	31
4.2 Error Function	38
4.3 Parameter Evaluation	40
5. FINITE ELEMENT MODEL OF NEAR-FIELD USED TO GENERATE FAR-FIELD IMPEDANCES	47
5.1 Variable 4 to 9 Node Isoparametric Element	49
5.2 Element Accuracy for Wave Propagation	57
5.3 Near-Field Finite Element Mesh	59
6. NUMERICAL RESULTS: FAR-FIELD IMPEDANCES AND COMPARISON OF SOLUTIONS	63
6.1 Torsional Loading	63
6.2 General Loadings	64

TABLE OF CONTENTS (CONT'D) Page

7. GENERAL CONCLUSIONS 69

REFERENCES. 71

FIGURES 79

1. INTRODUCTION

Soil-structure interaction has significant influence on the dynamic response of massive embedded structures such as nuclear power plant buildings and offshore gravity towers. Although considerable effort has been made in the past to develop an understanding of this phenomenon, conceptual and computational difficulties still remain primarily due to the three-dimensional, semi-infinite nature of the soil medium. Complex geometries associated with real structures, non-homogeneity and strain dependency of soil properties, scattering of seismic waves from the embedded foundation, and uncertainties associated with input motions are factors which complicate the mathematical modelling process. Rigorous mathematical treatment of these factors is impossible at the present time.

Currently, two basic methods are available for the analysis of soil-structure systems: the continuum method and the finite element method. Both methods involve certain simplifying assumptions regarding the nature of the problem and both have certain advantages and disadvantages over the other [1,2,3].

In the continuum approach (sometimes referred to as the impedance approach or the substructure approach), the foundation is idealized as a rigid massless plate bonded to a semi-infinite halfspace to which the structure is directly coupled as shown in Fig. 1.1(a). Frequency dependent impedance functions for the plate are developed and incorporated into the Fourier transformed equations of motion for the structure by imposing the conditions of compatibility and equilibrium between the structure and the plate. The continuum approach provides a simple and economical three-dimensional model for a large class of practical soil-structure interaction problems. Its obvious disadvantage is the simplistic modelling of the structural foundation as a rigid plate with simple geometries.

Evaluation of the dynamic impedances for the plate requires the solution of a mixed boundary value problem in elastodynamics. This problem is simplified by assuming a stress distribution or a relaxed contact between the plate and the soil. Analytical solutions for the impedance (or compliance) functions for the rigid body modes of a massless circular plate on a homogeneous, isotropic, elastic halfspace have been presented, among others, by Lysmer and Richart [4], Veletsos and Wei [5] and Luco and Westemann [6]. Solutions for layered elastic halfspaces [7-12], viscoelastic halfspaces [13,14] and layered viscoelastic halfspaces [15] are also available. The corresponding solutions for rigid rectangular plates have been presented in Refs. 16-22. The two-dimensional problem of a rigid strip footing on an elastic halfspace has been studied by Oien [23] and Luco and Westemann [24]. Wong and Luco [25] in 1976 developed a method to analyze arbitrary shaped rigid foundations on the surface of viscoelastic halfspaces by expressing the displacements in terms of an integral of Green's function.

Studies of the effect of foundation embedment on response have been rather limited. Continuum solutions are available for dynamic impedances of rigid embedded foundations for antiplane [26-29] and plane strain [30,31] conditions. Luco [32] obtained impedance functions for the torsional vibrations of a rigid hemisphere embedded in a homogeneous elastic halfspace. Apsel and Luco [33] later generalized the above approach for semi-elliptic foundations. Approximate solutions for the dynamic impedances of a vertical rigid circular cylinder have also been obtained by assuming that the pressure distribution under the footing is the same as that for a circular surface footing [34,35,36]. Recently, Apsel [37] presented a method to analyze rigid embedded foundations of arbitrary shapes. This method represents a significant advancement in the state-of-the-art in soil-structure interaction.

The input motion to the foundation in the continuum approach is usually taken as the free-surface ground motion. It may, however, be different from the free-surface motion if the seismic waves are not vertically incident or if the structure is deeply embedded in the soil. The response of a foundation to incoming seismic waves constitutes what is called a scattering problem which has been studied by several authors [27,31,38-40]. Most of these studies are limited to the case of plane SH waves. The interaction of Rayleigh surface waves with footings has been investigated by Iguchi [41] for rectangular foundations and by Simpson [42] for strip footings. These studies indicate that the scattering effects may significantly reduce the free-field motion and induce torsional and rocking motions in addition to translation. Rigid foundations also have a filtering effect on the high frequency content of the incoming seismic waves, filtering out those with wave lengths smaller than the width of the foundation [43-46]. Although such an approach to soil-structure interaction analysis deserves attention, one is limited by lack of knowledge about the wave content of a typical strong motion accelerogram and the angle of incidence of the incoming seismic waves. Recent studies [47,48] have shown that a major constituent of a typical strong motion earthquake are the surface waves; however, their exact proportion and the presence of other types of waves may vary from earthquake to earthquake. In the light of such limitations, it appears reasonable and prudent at present to use the more reliably recorded free-field motions as input to soil-structure systems.

The other approach to the analysis of soil-structure interaction is the application of the finite element method [49,50,51]. In this approach both the structure and the soil are modelled through an assemblage of finite elements, Fig. 1.1(b). An obvious disadvantage of such an approach is that the soil which is essentially semi-infinite in nature has to be modelled by a finite sized model with a rigid lower boundary. This rigid boundary has the effect of trapping energy radiating away from the foundation; thus, introducing artificial resonance conditions in the response. The discretization also causes a filtering effect on the waves in the higher frequency range. These problems may somewhat be mitigated by placing the boundaries far from the structure and by keeping the size of the finite elements sufficiently small. This however leads to a system with a relatively large number of degrees of freedom causing severe penalty on computer time and storage. The analysis is therefore usually restricted to two-dimensions. This inability of the finite element method to properly model the soil as a three-dimensional semi-infinite medium is a major disadvantage. It has been shown [52] that an arbitrary reduction of a three-dimensional problem to two-dimensions not only underestimates the peak amplitude of response but also affects the frequency where it occurs. The overwhelming advantage of the finite element method is that structures with flexible foundations embedded in the soil and having complex geometries can be analyzed without major difficulty. The strain dependency of the soil properties and their spatial variation can also be considered by assigning appropriate material properties to each element.

In an effort to minimize errors associated with a finite size model, special non-reflecting boundaries have been developed. Lysmer and Kuhlemeyer [53] developed an approximate energy absorbing boundary in the form of discrete viscous dampers placed around the boundary of the finite element grid. Other boundaries of similar nature have been proposed by White et al. [54] and Smith [55]. A transmitting boundary for plane and axisymmetric problems was proposed by Waas [56] that was an accurate representation of the radiation boundary conditions. This approach was later extended to axisymmetric problems with arbitrary loading conditions [57]. These analyses are however limited to half-spaces underlain by rigid bed rock. No satisfactory solutions are as yet available for three-dimensional situations where bed rock does not exist at reasonable depths. These viscous and transmitting boundaries, in conjunction with the finite element method, have been used to determine the impedance functions for rigid embedded foundations [58,59]. The viscous boundaries have also been used to simulate the third dimension, in an otherwise two-dimensional analysis of soil-structure interaction, without much physical justification [60,61].

Another variation of the finite element method is the so-called general substructure method [62,63]. In this method, a finite element analysis of the soil region without the structure is first carried out to determine the dynamic stiffness matrix corresponding to the interface degrees of freedom which is later used in soil-structure analysis of the structure. The method has computational advantages over the direct application of the finite element method. However, in the analysis of the soil region, the various limitations pertinent to the finite element method apply. For the simple case of a homogeneous viscoelastic halfspace in plane strain, the dynamic stiffness matrix for the surface degrees of freedom has been developed analytically [64].

Recently, Day [65] used the finite element method in a time-domain analysis to obtain steady state response of a rigid hemispherical foundation. A large finite element mesh is used so that the waves reflected from the rigid boundaries would arrive after the transient solution has been completed; thus, eliminating the influence of the rigid boundaries on response. Close agreement with the closed-form solutions obtained by Luco [32] was observed. This type of analysis is very expensive due to the large number of degrees of freedom involved and its application to three-dimensional cases remains impractical.

It is apparent from the previous discussion that it is difficult to properly model three-dimensional embedded structures with flexible foundations using the existing methods of analysis. The continuum approach which can easily treat the three-dimensional semi-infinite nature of the soil is limited to the analysis of rigid foundations with simple geometries. The finite element method on the other hand has the advantage that it can easily accommodate complex geometries such as those produced by structural embedment and variable soil properties can also be considered. However, it can not properly model the three-dimensional semi-infinite soil medium which accounts for radiation damping in the system. It is the objective of this investigation to develop a simple, rational, and economical hybrid model for the analysis of soil-structure interaction which takes advantage of the good features of the currently available methods and which minimizes their bad features. This model is obtained by partitioning the entire soil-structure system into a near-field and a far-field. The near-field is modelled by the finite element method whereas the far-field is modelled in the form of an impedance matrix. As will be shown in Chapter 2, the equations of motion for the hybrid model are obtained by combining the near- and far-field equations in the frequency domain using the concepts of substructuring. Since modelling of the near-field through the finite element method is a standard structural analysis procedure, the main thrust of this investigation is in the determination of the far-field impedances which account for the semi-infinite soil medium. In Chapter 3, the far-field impedance matrix for the case of torsional vibrations is developed by solving the actual radiation boundary value problem. However, it is pointed out that to solve such a boundary value problem for general loading conditions is mathematically intractable at present. Therefore, for general three-dimensional loadings, a semi-analytical approach is presented in Chapter 4 which makes use of system identification procedures to determine the far-field impedance functions. The type of finite element used in modelling the near-field is presented in Chapter 5. Numerical results for the far-field impedances are presented in Chapter 6 along with solutions obtained from the resulting hybrid model which are compared with closed form solutions for the rigid plate on an elastic halfspace. Significant conclusions of the research are presented in Chapter 7.

2. HYBRID MODEL

For hybrid modelling, the soil-structure system is partitioned into a near-field and a far-field. The near-field is modelled through standard structural analysis techniques, such as the finite element method, whereas the far-field is modelled through an impedance matrix which accounts for the semi-infinite nature of the foundation medium. The combined model provides a simple but powerful and economical method of treating soil-structure interaction in three-dimensional form.

2.1 Near-Field

The near-field as shown in Fig. 2.1(b) consists of the structure to be analysed under the prescribed loading conditions and a finite portion of the soil medium encompassing irregular base geometries such as those produced by embedment.

The entire near-field is modelled in three-dimensional form using the finite element method which makes it possible to realistically model the complex geometrical shapes associated with real structures. Spatial variations of soil properties within the near-field can also be effectively taken into account by assigning appropriate material properties to each soil finite element. Several types of finite elements are available to suit particular situations: beam elements, two-dimensional triangular and rectangular elements, shell elements, and three-dimensional solid elements. For example, if the structure is the containment shell of a nuclear power plant it may be modelled by shell elements. The soil in the near-field should be modelled by three-dimensional solid elements unless the nature of the problem is such that two-dimensional behavior is justified.

Conceptually, the finite element method can be applied to two- and three-dimensional problems with equal ease. However, the analyst is often limited by the amount of computer storage available. In the direct application of the finite element method, a three-dimensional analysis of the soil-structure system is usually not feasible because of the large system required to minimize the spurious reflections of waves from the artificial boundaries. In the hybrid model, the semi-infinite foundation medium is effectively modelled through a far-field impedance matrix; thus, the size of the near-field and consequently the number of degrees of freedom in the system can be kept relatively small. If the near-field possesses geometric and material axisymmetry, a reduction in the number of degrees of freedom can also be achieved by using axisymmetric finite elements [66,67].

The ability of the finite element near-field to transmit waves depends upon the assumed displacement field within and the size of each element. Higher order elements which have quadratic displacement fields transmit waves more accurately than do elements having linear displacement fields. Having selected the type of finite element to be used, care should be taken to make sure that the finite element mesh is fine enough to be able to transmit waves having frequencies over the entire range of interest. A variable 3 to 9 node isoparametric finite element is used in this study for the modelling of the near-field. It is very effective in reproducing curved boundaries and for the same number of nodes provides a higher degree of accuracy. The formulation of this element and its effectiveness in wave propagation problems are discussed in detail in Chapter 5.

2.2 Far-Field

The far-field is treated herein as a homogeneous halfspace of linearly elastic isotropic solid representing the semi-infinite foundation soil. It shares a common interface with the near-field along which the nodal points are common to both. In the present investigation, the interface between the near- and far-fields is chosen to be hemispherical. The far-field is therefore a halfspace with a hemispherical surface cavity as shown in Fig. 2.1(c). The choice of hemispherical boundary is judicious because any singularities in the form of sharp corners are avoided and the mathematical boundary conditions are easy to satisfy.

The far-field accounts for loss of energy in the form of waves travelling away from the foundation. An accurate model of the far-field which properly accounts for this radiation damping has so far been difficult to accomplish. In this report, a far-field impedance matrix which relates the far-field forces to the far-field displacements at the interface degrees of freedom is developed. This impedance matrix when combined with near-field equations of motion very effectively and efficiently simulates the total soil-structure system. The development of the far-field impedance matrix requires the solution of a set of partial differential equations with prescribed boundary conditions on the interface. For the case of torsional loading, it is possible to carry out this rigorous analysis and develop the corresponding far-field impedance matrix. However, for general loading conditions, it does not appear feasible to solve such a boundary value problem. For the general case, therefore, a semi-analytical approach is adopted in which the far-field is modelled through continuous three-component impedance functions placed at the interface. These frequency dependent impedance functions are obtained through methods of system identification.

2.3 Hybrid System

The equations of motion for the isolated near-field finite element idealization can be written as

$$\underline{M}\ddot{\underline{u}} + \underline{C}\dot{\underline{u}} + \underline{K}\underline{u} = \underline{p}(t) + \underline{f}(t) \tag{2.1}$$

in which $\underline{u}$ is the nodal point displacement vector (including interface nodal displacements) relative to the free-field motion and $\dot{\underline{u}}$ and $\ddot{\underline{u}}$ are the corresponding velocity and acceleration vectors, respectively. The load vector $\underline{p}(t)$ may be due to earthquake ground motion, wind or any other arbitrary external forces. $\underline{f}(t)$ is the vector of interaction forces which has non-zero components corresponding to the interface degrees of freedom only. $\underline{M}$ and $\underline{K}$ are mass and stiffness matrices, respectively, and $\underline{C}$ is the viscous damping matrix which accounts for energy loss in the near-field due to material damping.

In the consistant mass formulation, $\underline{M}$ is a full matrix whose off-diagonal terms are not zero implying a coupling between the inertia forces. However, it has been observed [68,69] that a lumped mass approximation which ignores such coupling is sufficient and provides results that are comparable in accuracy to those obtained using consistant mass matrix. Also, since the lumped mass matrix is diagonal, a substantial saving in computer storage is achieved.

Damping matrix $\underline{C}$ is also a full matrix in general. However, its individual elements are difficult to determine. In conventional dynamic analysis, this difficulty is often overcome by performing a modal decomposition of the undamped equations of motion and assigning modal damping ratios to the lower significant modes of vibration. Such an approach to soil-structure systems is not valid because in general the structure and the soil posses different damping characteristics leading to coupling between different modes. It is, therefore, necessary to define the complete damping matrix. In most cases this can be achieved by specifying modal damping ratios separately for the structure and for the soil region and then developing mass and stiffness proportional Rayleigh damping matrix [69]. An alternative, and sometimes more convenient, way of defining damping in soil-structure systems is to assume constant hysteretic damping in both the structure and the soil [63].

The equations of motion for the near-field can be transformed into frequency domain giving

$$(-\omega^2\underline{M} + i\omega\underline{C} + \underline{K})\ \underline{U}(\omega) = \underline{P}(\omega) + \underline{F}(\omega) \tag{2.2}$$

or,

$$\underline{S}(\omega)\underline{U}(\omega) = \underline{P}(\omega) + \underline{F}(\omega) \tag{2.3}$$

where,

$$\underline{S}(\omega) = -\omega^2\underline{M} + i\omega\underline{C} + \underline{K} \tag{2.4}$$

is the frequency dependent, complex valued impedance matrix characterizing the mass, damping and stiffness properties of the near-field. $\underline{P}(\omega)$ and $\underline{U}(\omega)$ are the Fourier transforms of the load vector and displacement vector, respectively. $\underline{F}(\omega)$ is the Fourier transform of the interaction vector and ω is the excitation frequency.

If as shown in Fig. 2.1(b), the vector $\underline{u}$ of nodal point displacements is separated into two parts: $\underline{u}_b$ corresponding to the nodal displacements at the boundary common to near-field and far-field, and $\underline{u}_s$ corresponding to the nodal displacements elsewhere in the near-field, Eq. 2.3 can be written as

$$\begin{bmatrix} \underline{S}_{ss} & \underline{S}_{sb} \\ \\ \underline{S}_{bs} & \underline{S}_{bb} \end{bmatrix} \begin{Bmatrix} \underline{U}_s \\ \\ \underline{U}_b \end{Bmatrix} = \begin{Bmatrix} \underline{P}_s \\ \\ \underline{P}_b \end{Bmatrix} + \begin{Bmatrix} \underline{0} \\ \\ \underline{F}_b \end{Bmatrix} \tag{2.5}$$

in which $\underline{F}_b$ represents the interaction forces at the interface between the near-field and the far-field.

For the isolated far-field, the dynamic force-deflection relationship is

$$\underline{S}^f(\omega)\,\underline{U}_f(\omega) = \underline{R}_f(\omega) \tag{2.6}$$

where $\underline{S}^f(\omega)$ is the far-field impedance matrix which has to be determined by a separate analysis. In rigorous form, it is a full matrix the elements of which characterize the mass, damping, and stiffness characteristics of the far-field. It is complex valued and frequency dependent.

The equations of motion for the far-field are incorporated into the frequency domain near-field equations by invoking the conditions of compatibility and equilibrium at the interface; i.e.,

$$\underline{U}_f = \underline{U}_b \tag{2.7}$$

and

$$\underline{F}_f + \underline{F}_b = \underline{0} \tag{2.8}$$

Substitution of Eqs. 2.6, 2.7 and 2.8 into Eq. 2.5, leads to the following equations of motion for the hybrid system in the frequency domain:

$$\begin{bmatrix} \underline{S}_{ss} & \underline{S}_{sb} \\ \\ \underline{S}_{bs} & \underline{S}_{bb}+\underline{S}^f \end{bmatrix} \begin{Bmatrix} \underline{U}_s \\ \\ \underline{U}_b \end{Bmatrix} = \begin{Bmatrix} \underline{P}_s \\ \\ \underline{P}_b \end{Bmatrix} \tag{2.9}$$

or,

$$\hat{\underset{\sim}{S}}(\omega)\underset{\sim}{U}(\omega) = \underset{\sim}{P}(\omega) \tag{2.10}$$

where $\hat{\underset{\sim}{S}}(\omega)$ is the impedance matrix of the hybrid system including the near- and the far-fields.

A reduction in the number of unknowns in Eq. 2.10 can be achieved by expressing the structural displacements in terms of the lower significant normal modes of the fixed-base structure as discussed in Refs. 63 and 70.

2.4 Earthquake Input Motion

Definition of a realistic input motion is important for the earthquake response analysis of soil-structure systems. The seismic energy arriving at a particular site will depend upon several factors such as the fault rupture mechanism, the location and distance of the site relative to the earthquake epicenter, the intervening and local soil conditions, and the presence of topographical features such as mountains and canyons [71]. A complete characterization of an earthquake ground motion unique to a particular site cannot be obtained within the present state of art; therefore, one must rely upon the strong ground motion records obtained during past earthquakes or upon synthetically generated ground motions.

In the hybrid model, the seismic input is applied at the interface between the near-field and the far-field. Since in the hybrid modelling the size of the near-field can be kept small, the same free-field ground motion can often be applied at the entire boundary. Although this neglects the rocking and torsional motions generated by spatial variations of the ground motion, the error introduced will be quite small for structures whose lateral dimensions are small in comparision to the wave lengths of the incoming seismic waves. It must be emphasized, however, that the lack of knowledge of an appropriate input motion is not a limitation of the hybrid model itself. It only reflects the present state of the art and the need for additional research effort in this area. If the spatial variation of the earthquake ground motion is known, it can be applied to the hybrid model without any difficulty.

2.5 Dynamic Response of Hybrid System

Once the input motion has been defined, the Fourier amplitude $\underline{P}(\omega)$ of the resulting load vector $\underline{p}(t)$ can be obtained from

$$\underline{P}(\omega) = \int_0^{T_d} \underline{p}(t) e^{-i\omega t} \, dt \tag{2.11}$$

where T_d is the time duration of excitation. The solution $\underline{U}(\omega)$ of Eq. 2.10 for discrete values of the excitation frequency completely characterizes response in the frequency domain. The time histories of response can then be obtained by the Fourier synthesis of the complex frequency response into time domain using

$$\underline{u}(t) = \frac{1}{2\pi} \int_{-\infty}^{\infty} \underline{U}(\omega) e^{i\omega t} \, d\omega \tag{2.12}$$

The Fourier transforms of Eqs. 2.11 and 2.12 are carried out using Fast Fourier Transform (FFT) techniques which are very efficient and economical on digital computers [72].

3. ANALYTICAL SOLUTIONS FOR FAR-FIELD IMPEDANCES

3.1 General Equations

The far-field which is a semi-infinite halfspace with a surface hemispherical cavity of radius R is shown in Fig. 3.1(a) along with the chosen spherical frame of reference. For a linearly elastic isotropic continuum the small-displacement equations of motions in spherical coordinates are [73]

$$\left.\begin{aligned}
\rho \frac{\partial^2 u_r}{\partial t^2} &= (\lambda+2\mu) \frac{\partial \Delta}{\partial r} - \frac{2\mu}{r\text{Sin}\phi} \frac{\partial (\omega_\theta \text{Sin}\phi)}{\partial \phi} + \frac{2\mu}{r\text{Sin}\phi} \frac{\partial \omega_\phi}{\partial \theta} \\
\rho \frac{\partial^2 u_\phi}{\partial t^2} &= (\lambda+2\mu) \frac{1}{r} \frac{\partial \Delta}{\partial \phi} - \frac{2\mu}{r\text{Sin}\phi} \frac{\partial \omega_r}{\partial \theta} + \frac{2\mu}{r} \frac{\partial (r\omega_\theta)}{\partial r} \\
\rho \frac{\partial^2 u_\theta}{\partial t^2} &= (\lambda+2\mu) \frac{1}{r\text{Sin}\phi} \frac{\partial \Delta}{\partial \theta} - \frac{2\mu}{r} \frac{\partial (r\omega_\phi)}{\partial r} + \frac{2\mu}{r} \frac{\partial \omega_r}{\partial \phi}
\end{aligned}\right\} \tag{3.1}$$

where u_r, u_ϕ, u_θ are the radial, tangential and, circumferential components of the displacement, respectively, and

$$\Delta = \frac{1}{r^2 \text{Sin}\phi} \left[\frac{\partial (u_r r^2 \text{Sin}\phi)}{\partial r} + \frac{\partial (u_\phi r \text{Sin}\phi)}{\partial \phi} + \frac{\partial (u_\theta r)}{\partial \theta} \right] \tag{3.2a}$$

is the dilatation and,

$$\begin{aligned}
2\omega_r &= \frac{1}{r^2 \text{Sin}\phi} \left[\frac{\partial}{\partial \phi} (u_\theta r \text{Sin}\phi) - \frac{\partial}{\partial \theta} (u_\phi r) \right] \\
2\omega_\phi &= \frac{1}{r\text{Sin}\phi} \left[\frac{\partial u_r}{\partial \theta} - \frac{\partial (u_\theta r \text{Sin}\phi)}{\partial r} \right] \\
2\omega_\theta &= \frac{1}{r} \left[\frac{\partial (u_\phi r)}{\partial r} - \frac{\partial u_r}{\partial \phi} \right]
\end{aligned} \tag{3.2b}$$

are the rotations. ρ is the mass density and λ and μ are Lame's constants.

It is difficult to solve Eqs. 3.1 in their original form. However, if u_r, u_ϕ and u_θ are eliminated by using Eq. 3.2, one gets

$$\rho \frac{\partial^2 \Delta}{\partial t^2} = (\lambda+2\mu)\left[\frac{1}{r^2}\frac{\partial}{\partial r}(r^2\frac{\partial \Delta}{\partial r}) + \frac{1}{r^2 \mathrm{Sin}\phi}\frac{\partial}{\partial \phi}(\mathrm{Sin}\phi\frac{\partial \Delta}{\partial \phi}) + \frac{1}{r^2\mathrm{Sin}^2\phi}\frac{\partial^2 \Delta}{\partial \theta^2}\right]$$

$$\rho \frac{\partial^2 \omega_r}{\partial t^2} = \mu\left[\frac{\partial^2 \omega_r}{\partial r^2} + \frac{4}{r}\frac{\partial \omega_r}{\partial r} + \frac{2}{r^2}\omega_r + \frac{1}{r^2\mathrm{Sin}\phi}\frac{\partial}{\partial \phi}(\mathrm{Sin}\phi\frac{\partial \omega_r}{\partial \phi}) + \frac{1}{r^2\mathrm{Sin}^2\phi}\frac{\partial^2 \omega_r}{\partial \theta^2}\right] \tag{3.3}$$

$$\rho \frac{\partial^2 \omega_\phi}{\partial t^2} = \mu\left[\frac{1}{r}\frac{\partial^2(\omega_\phi r)}{\partial r^2} + \frac{1}{r^2\mathrm{Sin}^2\phi}\frac{\partial^2 \omega_\phi}{\partial \theta^2} - \frac{1}{r^2\mathrm{Sin}^2\phi}\frac{\partial^2(\omega_\theta \mathrm{Sin}\phi)}{\partial\phi\partial\theta} + \frac{1}{r}\frac{\partial^2 \omega_r}{\partial r\partial\phi}\right]$$

$$\rho \frac{\partial^2 \omega_\theta}{\partial t^2} = \mu\left[\frac{1}{r}\frac{\partial^2(\omega_\theta r)}{\partial r^2} + \frac{1}{r^2}\frac{\partial}{\partial\phi}\frac{1}{\mathrm{Sin}\phi}\frac{\partial(\omega_\theta\mathrm{Sin}\phi)}{\partial\phi} - \frac{1}{r^2}\frac{\partial}{\partial\phi}(\frac{1}{\mathrm{Sin}\phi}\frac{\partial\omega_\phi}{\partial\theta}) - \frac{1}{r\mathrm{Sin}\phi}\frac{\partial^2\omega_r}{\partial r\partial\theta}\right]$$

These uncoupled P- and S-wave equations are easy to solve for the dilatation Δ, and rotations ω_r, ω_ϕ, ω_θ. The displacements u_r, u_ϕ and u_θ can then be obtained by substituting the expressions for Δ, ω_r, ω_ϕ and ω_θ into Eqs. 3.1. Proceeding in this fashion, general solutions of Eqs. 3.1 are [74],

$$
\left.\begin{aligned}
u_r(r,\phi,\theta,t) &= \sum_{m=o}^{\infty} \sum_{n=o}^{\infty} u_r^{mn}(r,\phi) \left.\begin{matrix}\text{Cos}\\ \text{Sin}\end{matrix}\right\} m\theta \cdot e^{i\omega t} \\
u_\phi(r,\phi,\theta,t) &= \sum_{m=o}^{\infty} \sum_{n=o}^{\infty} u_\phi^{mn}(r,\phi) \left.\begin{matrix}\text{Cos}\\ \text{Sin}\end{matrix}\right\} m\theta \cdot e^{i\omega t} \\
u_\theta(r,\phi,\theta,t) &= \sum_{m=o}^{\infty} \sum_{n=o}^{\infty} u_\theta^{mn}(r,\phi) \left.\begin{matrix}\text{Sin}\\ -\text{Cos}\end{matrix}\right\} m\theta \cdot e^{i\omega t}
\end{aligned}\right\} \tag{3.4}
$$

where,

$$
\begin{aligned}
u_r^{mn} &= \left[-\frac{1}{p^2} \frac{d}{dr} h_n(pr) A_{mn} - \frac{n(n+1)}{mk^2} \frac{h_n(kr)}{r} C_{mn} \right] P_n^m(\text{Cos}\phi) \\
u_\phi^{mn} &= \left[-\frac{1}{p^2} \frac{h_n(pr)}{r} A_{mn} - \frac{1}{mk^2} \frac{1}{r} \frac{d}{dr} (r h_n(kr)) C_{mn} \right] \frac{dP_n^m(\cos\phi)}{d\phi} \\
&\quad + \frac{m}{n(n+1)} h_n(kr) B_{mn} \frac{P_n^m(\text{Cos}\phi)}{\text{Sin}\phi} \qquad (3.5) \\
u_\theta^{mn} &= \left[\frac{m}{p^2} \frac{h_n(pr)}{r} A_{mn} + \frac{1}{k^2} \frac{1}{r} \frac{d}{dr} (r h_n(kr)) C_{mn} \right] \frac{P_n^m(\text{Cos}\phi)}{\text{Sin}\phi} - \\
&\quad \frac{1}{n(n+1)} h_n(kr) B_{mn} \frac{dP_n^m(\text{Cos}\phi)}{d\phi}
\end{aligned}
$$

in which $h_n(\cdot)$ are the spherical Hankel functions of the first kind, $P_m^n(\cdot)$ are the associated Legendre polymonials of the first kind, and

$$p^2 = \frac{\rho\omega^2}{(\lambda+2\mu)}$$

$$k^2 = \frac{\rho\omega^2}{\mu}$$

where ω is the excitation frequency and A_{mn}, B_{mn} and, C_{mn} are the, as yet, unknown constants of integration which have to be determined from the boundary conditions.

To determine the dynamic force-deflection relationship for the far-field, unit tractions are imposed at node i on the interface in each coordinate direction. The resulting displacement field on the interface then provides the influence coefficients of the dynamic flexibility matrix for the far-field which can be inverted to give the general three-dimensional far-field impedance matrix.

The pertinent boundary conditions that must be satisfied are the following:

a. On the hemispherical interface $r = R$, $-\pi/2 \leq \phi \leq \pi/2$, for a unit traction in the r-direction,

$$\left.\begin{aligned} \sigma_{rr} &= \delta(\phi-\phi_i)\ \delta(\theta-\theta_i)e^{i\omega t} \\ \sigma_{r\phi} &= 0 \\ \sigma_{r\theta} &= 0 \end{aligned}\right\} \tag{3.6a}$$

with similar conditions in ϕ- and θ-directions.

b. On the free-surface $r \geq R$, $\phi = \pm\ \pi/2$,

$$\sigma_{\phi r} = \sigma_{\phi\phi} = \sigma_{\phi\theta} = 0 \tag{3.6b}$$

where δ is the Dirac's delta function.

Unfortunately, at present it does not seem possible to satisfy the boundary conditions given above and to determine the far-field impedance matrix for general three-dimensional problems. However, a solution to this formulation can be obtained for the case of torsional vibration.

3.2 Torsional Impedances

If advantage is taken of the natural axisymmetry of the far-field then for the case of torsional vibration, it is possible to solve the radiation boundary value problem as discussed in Sec. 3.1 and to obtain a torsional impedance matrix for the far-field. Under torsional excitations with respect to the z-axis (ϕ=0), the only non-vanishing displacement is the circumferential component u_θ. Because of axisymmetry the displacements are independent of the angle θ and only one quadrant in the $\theta = 0$ plane has to be considered, Fig. 3.1(b). For steady state vibrations, we can write

$$u_\theta(r,\phi,t) = U_\theta(r,\phi,\omega)e^{i\omega t} \tag{3.7}$$

where the amplitude function u_θ must staisfy the equation of motion

$$\frac{1}{r^2}\frac{\partial}{\partial r}\left(r^2\frac{\partial U_\theta}{\partial r}\right) + \frac{1}{r^2 \mathrm{Sin}\phi}\frac{\partial}{\partial \phi}\left(\mathrm{Sin}\phi\,\frac{\partial U_\theta}{\partial \phi}\right) - \frac{U_\theta}{r^2 \mathrm{Sin}^2\phi} + k^2 U_\theta = 0 \tag{3.8}$$

where,

$k = \omega/C_s$

ω = excitation frequency

$C_s = \sqrt{G/\rho}$, the shear wave velocity

G = shear modulus, and

ρ = mass density.

On the surface of the hemispherical cavity, a shear force $1 \cdot e^{i\omega t}$ is applied at the nodal circle $\phi = \phi_i$ in the circumferential direction. The boundary conditions are then described by

$$\sigma_{r\theta} = G\left(\frac{\partial U_\theta}{\partial r} - \frac{U_\theta}{r}\right)e^{i\omega t} = -\frac{1}{2\pi R\ \mathrm{Sin}\phi}\ \delta(\phi-\phi_i)e^{i\omega t} \tag{3.9}$$

at $r=R$, $0\leq\phi\leq\pi/2$, and

$$\sigma_{\phi\theta} = \frac{G}{r}\left(\frac{\partial U_\theta}{\partial \phi} - U_\theta \mathrm{Cot}\phi\right)e^{i\omega t} = 0 \tag{3.10}$$

at $r\geq R$, $\phi = \pi/2$.

3.2.1 Continuous Approach [75]

Equation 3.8 can be solved by the method of separation of variables. Let,

$$U_\theta(r,\phi,\omega) = f(r)\cdot g(\phi) \tag{3.11}$$

Substitution of Eq. 3.11 into Eq. 3.8 leads to two uncoupled equations; one in r-direction and the other in ϕ-direction, i.e.,

$$\frac{d}{dr}\left(r^2\frac{df}{dr}\right) + (k^2r^2-\lambda^2)f = 0 \tag{3.12}$$

$$\frac{d}{d\phi}\left(\mathrm{Sin}\phi\frac{dg}{d\phi}\right) + \left(\lambda^2\mathrm{Sin}\phi - \frac{1}{\mathrm{Sin}\phi}\right)g = 0 \tag{3.13}$$

The solution of Eq. 3.12 is

$$f(r) = A_n H_{\nu_n}(kr) \tag{3.14}$$

where,

$$\nu_n = \sqrt{\lambda_n^2 + \frac{1}{4}} \tag{3.15}$$

and $H_{\nu_n}(\cdot)$ is the Hankel function of the first kind representing a wave travelling away from the origin (r=0) into the halfspace ($r \to \infty$).

The solution of Eq. 3.13 gives the eigen vectors

$$g(\phi) = P_n^1(\text{Cos}\phi) \tag{3.16}$$

and the eigen values

$$\lambda_n^2 = n(n+1), \; n = 1,3,5,---\infty \tag{3.17}$$

where $P_n^1(\cdot)$ are the associated Legendre polynomials of first kind with rank one. The boundary condition given by Eq. 3.10 restricts the order of Legendre polynomials to odd numbers in the above solution

$$U_\theta(r,\phi,\omega) = \sum_{n=1,3,..}^{\infty} A_n \, h_n(kr) P_n^1(\text{Cos}\phi) \tag{3.18}$$

where $h_n(\cdot)$ are now the spherical Hankel functions and A_n is an arbitrary constant which will be determined from the boundary condition given by Eq. 3.9. Substitution of Eq. 3.18 into Eq. 3.9 gives

$$\sum_{n=1,3..}^{\infty} A_n \left\{ nb_o h_{n-1}(b_o) - (n+1)b_o h_{n+1}(b_o) - h_n(b_o) \right\} P_n^1(\text{Cos}\phi) = - \frac{1}{2\pi RG} \frac{\delta(\phi-\phi_i)}{\text{Sin}\phi} \tag{3.19}$$

where b_o is a non-dimensional frequency defined by $b_o = \frac{\omega R}{C_s}$.

With the aid of the orthogonality condition for $P_n^1(\alpha)$, namely

$$\int_{-1}^{+1} P_n^1(\alpha) \; P_m^1(\alpha) \; d\alpha = \begin{cases} 0 & m \neq n \\ \dfrac{2}{(2n+1)} \dfrac{(n+1)!}{(n-1)!} & m = n \end{cases} \tag{3.20}$$

and the recursion formula of $h_n(\alpha)$

$$\alpha h_{n-1}(\alpha) = (2n+1)h_n(\alpha) - \alpha h_{n+1}(\alpha) \tag{3.21}$$

A_n can be evaluated giving

$$A_n = \frac{1}{2\pi RG} \frac{(2n+1)}{n(n+1)} \frac{P_n^1(\cos\phi_i)}{D_n(b_o)} \tag{3.22}$$

where

$$D_n(b_o) = b_o h_{n+1}(b_o) - (n-1)h_n(b_o) \tag{3.23}$$

Substitution of Eq. 3.22 into 3.18 gives at r=R

$$U_\theta(R,\phi,b_o;\phi_i) = \frac{1}{2\pi RG} \sum_{n=1,3,}^{\infty} \frac{(2n+1)}{n(n+1)} \frac{P_n^1(\cos\phi_i)P_n^1(\cos\phi)h_n(b_o)}{D_n(b_o)} \tag{3.24}$$

which is the displacement field on the interface due to a unit force distributed uniformly along the nodal circle $\phi=\phi_i$.

Elements C_{ji}^f of the flexibility matrix(or compliance matrix) are defined as the displacement at node j due to a unit force at node i. Therefore,

$$C_{ji}^f = U_\theta(R,\phi_j,b_o;\phi_i) \tag{3.25}$$

A far-field compliance matrix $\underline{C}^f$ can therefore be assembled which upon inversion gives the far-field impedance matrix $\underline{S}^f$,

$$\underline{S}^f = \underline{C}^{f^{-1}} \tag{3.26}$$

The far-field impedance matrix so developed relates the far-field forces to the far-field displacements as indicated by Eq. 2.6. It is complex valued and depends upon the non-dimensional frequency b_o, shear modulus G, and the far-field radius R.

Although the solutions developed in this section are theoretically "exact", it must be recognized that they are not consistent with the near-field finite element idealization in which the displacements are usually assumed to have a linear or quadratic variation over an element. The displacement field given by Eq. 3.18 (or 3.24) however is a function of the Legendre polynomials. The imposition of the conditions given by Eq. 2.7 therefore guarantees the compatibility of displacements only at the nodes, but not along the entire interface. This is illustrated in Fig. 3.2(a). To get meaningful results, it is therefore necessary to have a large number of closely spaced nodes on the boundary so that compatibility violations are minimized. This is apparent from the large errors observed in the numerical solutions presented in Chapter 6. The following consistent approach is therefore developed which results in a significant improvement in the modelling of the far-field.

3.2.2 Consistent Approach

In this section, the far-field impedance matrix for the case of torsional vibrations is developed using an approach that is consistent with the finite element idealization of the near-field; thus, avoiding the noncompatibility of displacements associated with the far-field impedance matrix developed in the previous section.

As before separation of variables is used to find the solution of Eq. 3.7 leading to the uncoupled Eqs. 3.12 and 3.13. Since in the r-direction no discretization of the far-field is involved, the continuum solutions obtained earlier (Eqs. 3.14 and 3.15) are used. This ensures proper modelling of the semi-infinite soil medium.

In the ϕ-direction, however, an equivalent discrete eigen value problem is solved instead of using the closed-form solutions given by Eqs. 3.16 and 3.17. This is done by discretizing the domain $\phi=0$ to $\phi=\pi/2$ into line elements and using the same interpolation functions as used in the near-field finite elements. Therefore for element p, one can write

$$g^p(\phi) = \underline{N}_p \underline{v}^p \qquad (3.27)$$

where $\underline{N}_p$ is the row vector of interpolation functions and $\underline{v}^p$ is a vector containing the nodal values of the function $g(\phi)$. For quadratic elements, the interpolation functions as shown in Fig. 3.2 are,

$$N_1 = \frac{1}{2}(1-t) - \frac{1}{2}(1-t^2)$$

$$N_2 = 1-t^2$$

$$N_3 = \frac{1}{2}(1+t) - \frac{1}{2}(1-t^2)$$

where, for equally spaced nodes

$$t = \frac{\phi-\phi_2}{\phi_o}$$

Substituting Eq. 3.27 into Eq. 3.13 and using standard finite element techniques [76], one obtains the following eigen value problem

$$(\underline{K} - \lambda^2 \underline{M})\ \underline{v} = \underline{0} \qquad (3.28)$$

where

$$\underline{K} = \sum_p \underline{K}^p; \quad \underline{M} = \sum_p \underline{M}^p$$

with element matrices given by

$$\underline{K}^p = \int_p \underline{N}'^T_p \underline{N}'_p \, \text{Sin}\phi d\phi + \int_p \underline{N}^T_p \underline{N}_p \frac{1}{\text{Sin}\phi} d\phi \tag{3.29}$$

$$\underline{M}^p = \int_p \underline{N}^T_p \underline{N}_p \, \text{Sin}\phi d\phi \tag{3.30}$$

where $\underline{N}'_p$ is the derivative of the interpolation functions with respect to ϕ.

Eigen value problem 3.28 can be solved by standard methods giving eigen vectors $\underline{v}_n$ and eigen values λ_n^2 for $n = 1,2,....N_b$ where N_b is the total number of nodes on the interface. These eigen values and eigen vectors are analogous to those given by Eqs. 3.16 and 3.17.

Substituting Eqs. 3.14 and 3.27 into 3.11, the displacement field within an element can be expressed as

$$U^p_\theta(r,\phi,\omega) = \sum_{n=1,2,}^{N_b} A_n \underline{N}_p \underline{v}^p_n \frac{H_{\nu_n}(kr)}{H_{\nu_n}(kR)} \tag{3.31}$$

where $H_{\nu_n}(kR)$ has been introduced as a normalizing factor to simplify equations developed subsequently.

For $r = R$, Eq. 3.3 gives the displacement field at the interface in the form

$$U^p_\theta(R,\phi,\omega) = \sum_{n=1,2,}^{N_b} A_n \underline{N}_p \underline{v}^p_n = \underline{N}_p \underline{U}^p_f \tag{3.32}$$

where in an element

$$\underline{U}_f{}^p = \sum_{n=1,2}^{N_b} A_n \underline{v}^p_n$$

The corresponding vector for interface nodal displacements in the circumferential direction is

$$\underline{U}_f = \sum_{n=1,2}^{N_b} A_n \underline{v}_n = \underline{V}\,\underline{A} \tag{3.33}$$

In the above equation, $\underline{V}$ is the matrix of eigen vectors and $\underline{A}$ is the vector of unknown constants A_n which can be obtained from the relation

$$\underline{A} = \underline{V}^{-1}\ \underline{U}_f \tag{3.34}$$

The shear stress as given by Eq. 3.9 is

$$\sigma_{r\theta} = G\left[\frac{\partial U_\theta}{\partial r} - \frac{U_\theta}{r}\right]$$

Making use of Eq. 3.31, the shear stress at the interface r = R becomes

$$\sigma_{r\theta}^{\ p} = \frac{G}{R}\sum_{n=1,2}^{N_b} \underline{N}_p\ \underline{v}_n^p \left[b_o \frac{H_{\nu_{n-1}}(b_o)}{H_{\nu_n}(b_o)} - (\nu_n + 3/2)\right] A_n \tag{3.35}$$

where b_o is the non-dimensional frequency defined earlier. The equivalent nodal forces on the boundary can now be obtained as

$$\underline{R}_f^{\ p} = 2\pi R^2 \int_p \underline{N}_p^T\ \sigma_{r\theta}^{\ p}\ \mathrm{Sin}\phi d\phi$$

which become upon substitution of Eq. 3.35.

$$\underline{R}_f^{\ p} = 2\pi RG \sum_{n=1,2}^{N_b} \left(\int_p \underline{N}_p^T\ \underline{N}_p \mathrm{Sin}\phi d\phi\right)\ \underline{v}_n^p \left[b_o \frac{H_{\nu_{n-1}}(b_o)}{H_{\nu_n}(b_o)} - (\nu_n + 3/2)\right] A_n$$

Summing up over all the elements, one obtains

$$\underline{R}_f = 2\pi RG\ \underline{M}\ \underline{V}\ \underline{H}\ \underline{A} \tag{3.36}$$

where $\underline{H}$ is a diagonal matrix whose elements are

$$H_{nn} = b_o \frac{H_{\nu_{n-1}}(b_o)}{H_{\nu_n}(b_o)} - (\nu_n + 3/2) \tag{3.37}$$

Finally, substituting Eq. 3.34 into Eq. 3.36 gives

$$\underline{R}_f = 2\pi RG\ \underline{M}\ \underline{V}\ \underline{H}\ \underline{V}^{-1}\ \underline{U}_f$$

or

$$\underline{R}_f = \underline{S}^f \; \underline{U}_f$$

where the desired far-field impedance matrix

$$\underline{S}^f(b_o) = 2\pi RG \; \underline{M} \; \underline{V} \; \underline{H} \; \underline{V}^{-1} \tag{3.38}$$

is a full matrix containing complex frequency dependent coefficients.

The advantage of using this approach to develop the far-field impedance matrix is that the displacement field given by Eq. 3.32 is consistent with the displacement on the boundary of the near-field as shown in Fig. 3.2(b). Therefore, the compatibility of displacements along the entire interface between the near- and far-fields is satisfied. Also, the displacements are expressed in terms of a finite number of eigen vectors as opposed to an infinite sum required for the continuous approach.

Numerical solutions using the far-field impedance matrices developed by continuous and consistent approach are presented in Chapter 6.

4. SEMI-ANALYTICAL SOLUTIONS FOR FAR-FIELD IMPEDANCES

Analytical solutions as described in Chapter 3 are limited to torsional vibrations. As previously mentioned, solutions for non-axisymmetric cases appear to be mathematically intractable at present. The following semi-analytical approach is therefore developed using concepts of system identification to determine the far-field impedances for general three-dimensional loadings.

4.1 Mathematical Modelling

The far-field, which is a semi-infinite halfspace with hemispherical cavity, is modelled by continuously distributed impedance functions placed in three coordinate directions on the interface between the near- and far-fields. Conceptually the far-field may, therefore, be thought of as a Winkler type foundation (uncoupled over the interface) characterized by complex impedance functions: the real part representing stiffness and the imaginary part representing radiation damping. This is a realistic assumption if the displacements are smooth and slowly varying functions over the interface, which can be assured by placing the interface at a reasonable distance from the structure. These continuous impedance functions are then discretized at the boundary nodal points to obtain a far-field impedance matrix.

In general, for horizontally layered halfspaces, the impedance functions can be expressed in terms of a Fourier series retaining only the symmetric terms in ϕ due to axisymmetry of the far-field; thus giving

$$\left.\begin{aligned} S_R(R,\phi,\omega) &= \sum_{n=o}^{\infty} S_{Rn}(R,\omega)\ \mathrm{Cos}\,n\phi \\ S_\phi(R,\phi,\omega) &= \sum_{n=o}^{\infty} S_{\phi n}(R,\omega)\ \mathrm{Cos}\,n\phi \\ S_\theta(R,\phi,\omega) &= \sum_{n=o}^{\infty} S_{\theta n}(R,\omega)\ \mathrm{Cos}\,n\phi \end{aligned}\right\} \qquad (4.1)$$

Preceding page blank

where S_R, S_ϕ, and S_θ are the far-field impedance functions per unit area in the directions normal, tangential and circumferntial to the hemispherical interface as shown in Fig. 4.1(a). Coefficients S_{Rn}, $S_{\phi n}$, and $S_{\theta n}$ are complex valued functions of the interface radius R and the excitation frequency ω. The number of terms required in Eqs. 4.1 to properly represent the far-field will depend upon the complexity of layering. However, due to the Winkler assumption, only the first term in each coordinate direction is needed for homogeneous, isotropic halfspaces.

The discrete far-field impedances for node i on the interface are obtained by integrating the continuous boundary impedances over the tributary area A_i which extends halfway to the nodes adjacent to node i as shown in Fig. 4.1(a). Therefore, in the normal direction, the discrete impedance at node i is

$$S_R^i = \iint_{A_i} S_R(R,\phi,\omega)\,dA \tag{4.2}$$

Since, in spherical coordinates

$$dA = (Rd\phi)\ (R\sin\phi d\theta)$$

Eq. 4.2 becomes

$$S_R^i = R^2 \int_{\phi_1^i}^{\phi_2^i} \int_{\theta_1^i}^{\theta_2^i} S_R(R,\phi,\omega)\sin\phi d\phi\ d\theta \tag{4.3a}$$

Similarily in the tangential and circumferential directions,

$$S_\phi^i = R^2 \int_{\phi_1^i}^{\phi_2^i} \int_{\theta_1^i}^{\theta_2^i} S_\phi(R,\phi,\omega)\sin\phi d\phi\ d\theta \tag{4.3b}$$

$$S_{\theta}^{i} = R^2 \int_{\phi_1^i}^{\phi_2^i} \int_{\theta_1^i}^{\theta_2^i} S_{\theta}(R,\phi,\omega)\mathrm{Sin}\phi d\phi\ d\theta \tag{4.3c}$$

Thus, for each node on the interface, a 3 x 3 diagonal impedance matrix is obtained leading, in general, to a $3N_b$ x $3N_b$ diagonal far-field impedance matrix, N_b being the number of nodes on the interface.

In the present investigation, the far-field considered is homogeneous and isotropic for which, as mentioned previously, it is sufficient to consider the far-field impedances to be uniformly distributed. Therefore, only the constant terms in Eq. 4.1 are retained, giving

$$\left.\begin{aligned} S_R(R,\phi,\omega) &= S_{R0}(R,\omega) = \eta_R + i\xi_R \\ S_\phi(R,\phi,\omega) &= S_{\phi 0}(R,\omega) = \eta_\phi + i\xi_\phi \\ S_\theta(R,\phi,\omega) &= S_{\theta 0}(R,\omega) = \eta_\theta + i\xi_\theta \end{aligned}\right\} \tag{4.4}$$

where η's and ξ's are the real and imaginary part, respectively, of the unknown far-field impedance functions. These impedance functions are determined by using system identification methods such that the resulting hybrid model reproduces the known response functions of a rigid massless circular plate on a uniform elastic halfspace. Because of axi-symmetry of the system under consideration, it is necessary to consider only one quadrant in the θ=0 plane as shown in Fig. 4.1(b) where the nodal points actually describe nodal circles.

For torsional and vertical vibrations of the rigid plate, the displacements in the far-field will be constant around the nodal circles. The discretized far-field nodal impedances in an axisymmetric formulation can therefore be obtained from Eqs. 4.3 by simply extending the limits of integration in the θ-direction from 0 to 2π instead of from θ_1^i to θ_2^i. Thus, for torsional vibrations, the nodal impedances are

$$\left.\begin{aligned} S_R^i &= S_\phi^i = 0 \\ S_\theta^i &= R^2 \int_{\phi_1^i}^{\phi_2^i} \int_0^{2\pi} S_\theta(R,\phi,\omega)\,\mathrm{Sin}\phi\,d\phi\,d\theta \end{aligned}\right\} \tag{4.5}$$

Substituting Eq. 4.4 into Eq. 4.5 gives

$$S_\theta^i = (\eta_\theta + i\xi_\theta).2\pi R^2 \int_{\phi_1^i}^{\phi_2^i} \mathrm{Sin}\phi\,d\phi = (\eta_\theta + i\xi_\theta).A_i \tag{4.6}$$

where

$$A_i = 2\pi R^2 \int_{\phi_1^i}^{\phi_2^i} \mathrm{Sin}\phi\,d\phi \tag{4.7}$$

is the area of the tributary strip shown in Fig. 4.1(b).

Similarily for vertical vibrations, since the circumferential displacements are zero, the discrete impedances at node i can be obtained as

$$\left.\begin{aligned} S_R^i &= R^2 \int_{\phi_1^i}^{\phi_2^i} \int_0^{2\pi} S_R(R,\phi,\omega)\,\mathrm{Sin}\phi\,d\phi\,d\theta \\ S_\phi^i &= R^2 \int_{\phi_1^i}^{\phi_2^i} \int_0^{2\pi} S_\phi(R,\phi,\omega)\,\mathrm{Sin}\phi\,d\phi\,d\theta \\ S_\theta^i &= 0 \end{aligned}\right\} \tag{4.8}$$

Again making use of Eqs. 4.4, one gets

$$\left.\begin{aligned} S_R^i &= (\eta_R + i\xi_R)\ A_i \\ S_\phi^i &= (\eta_\phi + i\xi_\phi)\ A_i \end{aligned}\right\} \tag{4.9}$$

For the coupled translational and rocking mode of vibration, the displacements around a nodal circle are not uniform but instead are given by

$$u_r = u_r^i \operatorname{Cos}\theta$$

$$u_\phi = u_\phi^i \operatorname{Cos}\theta$$

$$u_\theta = -\ u_\theta^i \operatorname{Sin}\theta \ .$$

This non-uniform condition introduces $\operatorname{Cos}^2\theta$ and $\operatorname{Sin}^2\theta$ terms in Eqs. 4.5 and 4.8 which can be explained in terms of the principle of virtual work: If a real displacement u_r^i is applied at node i, then the resulting force around the nodal circle is

$$f_r = S_R .\ u_r^i \operatorname{Cos}\theta \tag{4.10}$$

Therefore, the work done by the virtual displacement δu_r is

$$\delta w = \iint \delta u_r f_r dA = R^2 \int_{\phi_1^i}^{\phi_2^i} \int_0^{2\pi} \delta u_r f_r \operatorname{Sin}\phi d\phi\ d\theta \tag{4.11}$$

Choosing the virtual displacement distribution to be of the same form as the actual displacement field, substitution of Eq. 4.10 into Eq. 4.11 gives

$$\begin{aligned} \delta w &= R^2 \iint \delta u_r^i \operatorname{Cos}\theta .\ S_R\ u_r^i \operatorname{Cos}\theta .\ \operatorname{Sin}\phi d\phi\ d\theta \\ &= \delta u_r^i \left(R^2 \int_{\phi_1^i}^{\phi_2^i} \int_0^{2\pi} S_R(R,\phi,\omega) \operatorname{Sin}\phi .\ \operatorname{Cos}^2\theta d\phi\ d\theta \right) u_r^i \end{aligned}$$

; thus,

$$S_R^i = R^2 \int_{\phi_1^i}^{\phi_2^i} \int_0^{2\pi} S_R(R,\phi,\omega)\,\mathrm{Sin}\phi d\phi\ \mathrm{Cos}^2\theta d\theta$$

Similarily, in the ϕ- and θ-directions

$$\left.\begin{aligned} S_\phi^i &= R^2 \int_{\phi_1^i}^{\phi_2^i} \int_0^{2\pi} S_\phi(R,\phi,\omega)\,\mathrm{Sin}\phi\ d\phi\ \mathrm{Cos}^2\theta\ d\theta \\ S_\theta^i &= R^2 \int_{\phi_1^i}^{\phi_2^i} \int_0^{2\pi} S_\theta(R,\phi,\omega)\,\mathrm{Sin}\phi d\phi\ \mathrm{Sin}^2\theta\ d\theta \end{aligned}\right\} \quad (4.12)$$

Since

$$\int_0^{2\pi} \mathrm{Cos}^2\theta\ d\theta = \int_0^{2\pi} \mathrm{Sin}^2\theta d\theta = \pi$$

Eqs. 4.12 reduce to

$$\left.\begin{aligned} S_R^i &= (\eta_R + i\xi_R)\pi R^2 \int_{\phi_1^i}^{\phi_2^i} \mathrm{Sin}\phi d\phi = (\eta_R + i\xi_R).A_i/2 \\ S_\phi^i &= (\eta_\phi + i\xi_\phi)\pi R^2 \int_{\phi_1^i}^{\phi_2^i} \mathrm{Sin}\phi d\phi = (\eta_\phi + i\xi_\phi).A_i/2 \\ S_\theta^i &= (\eta_\theta + i\xi_\theta)\pi R^2 \int_{\phi_1^i}^{\phi_2^i} \mathrm{Sin}\phi d\phi = (\eta_\theta + i\xi_\theta).A_i/2 \end{aligned}\right\} \quad (4.13)$$

which are the work equivalent discrete impedances at node i in the normal, tangential, and circumferential directions, respectively. The factor of 1/2 in the above equations reflects the fact that due to the Cosθ and Sinθ variation of displacements around nodal circles,the total work done is half of that done when the displacements are uniform.

Equations 4.6, 4.9 and 4.13 give rise to the following impedance matrices in spherical coordinates for node i:

$$\underset{1x1}{\tilde{\underline{S}}^{i}} = A_i \; (\eta_\theta + i\xi_\theta) \tag{4.14a}$$

for torsional vibrations,

$$\underset{2x2}{\tilde{\underline{S}}^{i}} = A_i \begin{bmatrix} (\eta_R + i\xi_R) & 0 \\ 0 & (\eta_\phi + i\xi_\phi) \end{bmatrix} \tag{4.14b}$$

for vertical vibrations, and

$$\underset{3x3}{\tilde{\underline{S}}^{i}} = \frac{A_i}{2} \begin{bmatrix} (\eta_R + i\xi_R) & 0 & 0 \\ 0 & (\eta_\phi + i\xi_\phi) & 0 \\ 0 & 0 & (\eta_\theta + i\xi_\theta) \end{bmatrix} \tag{4.14c}$$

for coupled translation and rocking.

These impedance matrices must be transformed into cylindrical coordinates to be compatible with the corresponding nodal point displacements used for the axisymmetric finite elements in the near-field. As shown in Fig. 4.2, the displacements in these two coordinate systems are related by

$$\begin{Bmatrix} u_{\tilde{r}} \\ u_\phi \\ u_\theta \end{Bmatrix} = \begin{bmatrix} \text{Sin}\phi & \text{Cos}\phi & 0 \\ \text{Cos}\phi & -\text{Sin}\phi & 0 \\ 0 & 0 & 1 \end{bmatrix} \begin{Bmatrix} u_r \\ u_z \\ u_\theta \end{Bmatrix} = \underline{\Phi} \begin{Bmatrix} u_r \\ u_z \\ u_\theta \end{Bmatrix} \tag{4.15}$$

where $\underline{\Phi}$ is the displacement transformation matrix. The nodal impedances in cylindrical coordinates can therefore be obtained as

$$\underline{S}^i = \underline{\Phi}_i^T \, \underline{\tilde{S}}^i \, \underline{\Phi}_i \tag{4.16}$$

The far-field impedance for the entire interface can then be assembled as

$$\underline{S}^f = \begin{bmatrix} \underline{S}^1 & & & \\ & \underline{S}^2 & & \\ & & \ddots & \\ & & & \underline{S}^{N_b} \end{bmatrix} \tag{4.17}$$

which is an $N_b \times N_b$ diagonal matrix for torsional vibrations, a $2N_b \times 2N_b$ tridiagonal matrix for vertical vibrations, and a $3N_b \times 3N_b$ tridiagonal matrix for coupled translation and rocking vibrations.

The far-field impedance matrices so obtained can be employed in the hybrid modelling of the rigid massless circular plate on an elastic half-space as discussed in Chapter 2, yielding equations of motion

$$\underline{S}(\omega) \; \underline{u}(\omega) = p(\omega) \tag{4.18}$$

for the three modes of vibration of the plate.

4.2 Error Function

For a prescribed value of excitation frequency ω and for assumed values of the far-field impedances, matrix Eq. 4.18 can be solved to yield the complex harmonic displacement vector $\underline{u}(\omega)$ which includes the displacement amplitudes (compliances) of the rigid massless circular plate. The resulting compliances are a function of the assumed far-field impedances and will be in error with the analytical solutions. To minimize the errors involved, an error function containing the sum of the squared errors of all the plate compliances is formed giving,

$$
\begin{aligned}
J(\underline{\beta},\omega) &= \sum_{i=1}^{NC} \left| U_i(\underline{\beta},\omega) - C_i(\omega) \right|^2 \\
&= \sum_{i=1}^{NC} \left[\mathrm{Re}(U_i) - \mathrm{Re}(C_i) \right]^2 + \sum_{i=1}^{NC} \left[\mathrm{Im}(U_i) - \mathrm{Im}(C_i) \right]^2
\end{aligned}
\tag{4.19}
$$

where, $\underline{\beta}$ is an n-dimensional vector containing all of the far-field impedance coefficients, $U_i = U_i(\underline{\beta},\omega)$ are the compliances of the plate as generated from Eq. 4.18 for the hybrid model, $C_i = C_i(\omega)$ are the known plate compliances generated from analytical elasticity solutions, and NC is the number of plate compliances considered in the solution.

The analytical solutions for the rigid massless circular plate in the torsional, vertical and coupled translational and rocking modes of vibration are presented in Refs. 4, 5, and 6. These dynamic compliances are defined by the matrix equation

$$
\begin{Bmatrix} \Delta_T \\ \Delta_V \\ \Delta_H \\ \Delta_M \end{Bmatrix} = \begin{bmatrix} C_{TT} & 0 & 0 & 0 \\ 0 & C_{VV} & 0 & 0 \\ 0 & 0 & C_{HH} & C_{HM} \\ 0 & 0 & C_{MH} & C_{MM} \end{bmatrix} \begin{Bmatrix} T \\ V \\ H \\ M \end{Bmatrix}
$$

Therefore, five independent compliance functions are available, namely, C_{TT}, C_{VV}, C_{HH}, C_{HM} ($C_{MH} = C_{HM}$) and C_{MM} , which are plotted in Fig. 4.3.

In the present investigation, since the far-field is uniform, the vector of far-field impedances from Eq. 4.4 is

$$
\underline{\beta} = \langle \eta_R, \xi_R, \eta_\phi, \xi_\phi, \eta_\theta, \xi_\theta \rangle \tag{4.20}
$$

Thus, there are six parameters that must be determined.

4.3 Parameter Evaluation

Methods of system identification are used to systematically adjust the originally assumed values of the far-field impedance coefficients so that the error function $J(\underline{\beta},\omega)$ is minimized for discrete values of ω, thus giving the far-field impedance vector $\underline{\beta}$ over the frequency range of interest.

There are several iterative methods reported in literature [77] which could be used for this purpose. Most of these methods use the so-called gradient techniques in which new values for the components in vector $\underline{\beta}$ are obtained by following in the direction of the negative gradient of the error function in the n-dimensional parameter space. The method selected for the present study is the modified Gauss-Newton method which makes use of information on second derivatives, thus, resulting in an improved convergence rate. The Gauss-Newton method is obtained by expanding the error function $J(\underline{\beta},\omega)$ into a Taylor's series and equating the gradient to 0, resulting in the equation

$$\underline{\beta}_i = \underline{\beta}_{i-1} - \lambda\, \underline{h}^{-1}(\underline{\beta}_{i-1},\omega)\ \underline{g}\ (\underline{\beta}_{i-1},\omega) \tag{4.21}$$

where $\underline{\beta}_{i-1}$ and $\underline{\beta}_i$ are the parameter vectors at iterative steps i-1 and i, respectively,

$$\underline{g}(\underline{\beta}_{i-1},\omega) = < \frac{\partial J}{\partial \beta_1}, \frac{\partial J}{\partial \beta_2}, \ldots, \frac{\partial J}{\partial \beta_n} > \tag{4.22}$$

is the gradient vector and,

$$\underline{h}(\underline{\beta}_{i-1},\omega) = \begin{bmatrix} \dfrac{\partial^2 J}{\partial \beta_1{}^2} & \cdot\ \cdot & \dfrac{\partial^2 J}{\partial \beta_1 \partial \beta_n} \\ \vdots & & \\ \dfrac{\partial^2 J}{\partial \beta_n \partial \beta_1} & \cdot\ \cdot & \dfrac{\partial^2 J}{\partial \beta_n{}^2} \end{bmatrix} \tag{4.23}$$

is the nxn Hessian matrix the inverse of which modifies both the magnitude and the direction of the steepest descent given by the negative gradient. Scalar λ is a positive step-size parameter selected to ensure a decrease in error within each iteration cycle. Equation 4.21 may also be written as

$$\underline{\beta}_i = \underline{\beta}_{i-1} - \lambda\, \underline{d}_{i-1} \tag{4.24}$$

where

$$\underline{d}_{i-1} = \underline{h}^{-1}(\underline{\beta}_{i-1},\omega)\ \underline{g}\ (\underline{\beta}_{i-1},\omega) \tag{4.25}$$

is the search direction given by the modified Gauss-Newton method.

The components of the gradient vector in Eq. 4. 22 are obtained by taking the derivative of the error function at $\underline{\beta}_{i-1}$, i.e.,

$$\begin{aligned} \frac{\partial J}{\partial \beta_j} = {} & 2 \sum_{i=1}^{NC} \Big[\mathrm{Re}(U_i) - \mathrm{Re}(C_i) \Big] \frac{\partial \mathrm{Re}(U_i)}{\partial \beta_j} \; + \\ & 2 \sum_{i=1}^{NC} \Big[\mathrm{Im}(U_i) - \mathrm{Im}(C_i) \Big] \frac{\partial \mathrm{Im}(U_i)}{\partial \beta_j} \end{aligned} \tag{4.26}$$

Similarily, the coefficients of the Hessian matrix are

$$\frac{\partial^2 J}{\partial\beta_j \partial\beta_k} = 2 \sum_{i=1}^{NC} \left\{ \left[Re(U_i) - Re(C_i) \right] \frac{\partial^2 Re(U_i)}{\partial\beta_j \partial\beta_k} + \frac{\partial Re(U_i)}{\partial\beta_j} \frac{\partial Re(U_i)}{\partial\beta_k} \right\} +$$

$$2 \sum_{i=1}^{NC} \left\{ \left[Im(U_i) - Im(C_i) \right] \frac{\partial^2 Im(U_i)}{\partial\beta_j \partial\beta_k} + \frac{\partial Im(U_i)}{\partial\beta_j} \frac{\partial Im(U_i)}{\partial\beta_k} \right\} \tag{4.27}$$

Since the effort required to calculate the second derivatives in Eq. 4.27 is prohibitive, the modified Gauss-Newton method approximates the coefficients of the Hessian matrix by

$$\frac{\partial^2 J}{\partial\beta_j \partial\beta_k} \doteq 2 \sum_{i=1}^{NC} \left[\frac{\partial Re(U_i)}{\partial\beta_j} \frac{\partial Re(U_i)}{\partial\beta_k} + \frac{\partial Im(U_i)}{\partial\beta_j} \frac{\partial Im(U_i)}{\partial\beta_k} \right] \tag{4.28}$$

Such an approximation is justifiable in the near vicinity of the minimum where $U_i \doteq C_i$; however, it can be considerably in error away from the minimum. Therefore, if the initial estimates of the vector $\underline{\beta}$ are considerably in error, convergence may be slow initially.

The above approximation given by Eq. 4.28, makes the Hessian matrix positive semi-definite, a property that the original matrix based on Eq. 4.27 does not posses. To ensure that the inverse of the Hessian matrix in Eq. 4.21 does exist, it is necessary only to add a small positive constant to the diagonal elements, which has the effect of altering the direction of search.

It must also be recognized that the response quantity $U_i(R,\omega)$ is not an explicit function of $\underline{\beta}$ but obtained through a numerical process involving the solution of Eq. 4.18. The partial derivatives $\frac{\partial U_i}{\partial\beta_j}$ in Eqs. 4.26 and 4.28, therefore, have to be replaced by the finite differences $\dfrac{\Delta U_i}{\Delta \beta_j}$.

The error function $J(\underline{\beta},\omega)$ defines an n-dimensional surface which in two dimensions is easy to visualize as shown in Fig. 4.4. The modified Gauss-Newton method is an iterative process in which the error is minimized by obtaining successively better estimates of the far-field impedance vector $\underline{\beta}$ until a point $\underline{\beta}^*$ is located where slope of the error surface approaches zero. The slope of the error profile at a point $\underline{\beta}_i$ along the search direction $\underline{d}_{i-1}$ is obtained by differentiating the error function with respect to the step size λ, giving

$$\alpha_{i-1}(\underline{\beta}_i) = - \underline{g}^T(\underline{\beta}_i,\omega)\ \underline{d}_{i-1} \tag{4.29}$$

At any step i-1, a typical iteration cycle proceeds as follows -- The far-field impedance matrices corresponding to the parameter vector $\underline{\beta}_{i-1}$ are formed as explained in Sec. 4.1 which are then combined with the near-field finite element equations to give the equations of motion Eq. 4.18 for the hybrid model. These equations are solved to obtain the responses U_i of the rigid plate and the error is evaluated according to Eq. 4.19. The slope of the error surface, $\alpha_{i-1}(\underline{\beta}_{i-1})$, at that point is then obtained by substituting $\underline{\beta}_{i-1}$ for $\underline{\beta}_i$ in Eq. 4.29 and compared against a specified tolerance on slope sufficiently close to zero. If the slope is less than the specified tolerance then it means that the error surface is flat (or nearly flat) at that point and the error J is minimized. The parameter vector $\underline{\beta}_{i-1}$ in that case is the desired far-field impedance vector $\underline{\beta}^*$. If not, then a line search along the search direction $\underline{d}_{i-1}$ is made as shown in Fig. 4.4. According to Eq.4.24, each value of the step size parameter λ defines a different point $\underline{\beta}_i$ along this direction. Within a line search the step size λ is systematically adjusted in such a way that a point $\underline{\beta}_i$ is obtained where the slope of the error profile is sufficiently small and the error is minimized in that direction. For a detailed discussion on how a line search is conducted for the step size determination, see the report by Matzen and McNiven [78]. The parameter vector $\underline{\beta}_i$ so obtained is then used as the next point in the iteration process. The tolerance on slope within a line search affects the number of steps required to determine the step size for which the error profile reaches a minimum in the search direction. If a crude line stopping tolerance is specified the process may take fewer steps within each line search but may require a large number of iterations to reach the true minima as indicated by dashed lines in Fig. 4.4. It has therefore been recommended that a moderate amount of effort be spent in the step length determination. How accurately the true minimum is determined depends upon the specified criteria for overall convergence. If a strict tolerance on slope is specified, the process may take longer to converge, but the minimum will be determined more accurately.

To start the iterative process one must have an initial estimate $\underline{\beta}_o$ of the far-field impedance functions. The success of the method depends upon the accuracy of this estimate. If the starting vector $\underline{\beta}_o$ is far from the true minimum, the convergence may be very slow. It is possible that, although the iterative process converges to a minimum, the error at that point is still large. This implies one of two things -- either it is a local minimum, or it is a global minimum but the model chosen for the far-field impedances is not adequate. In the first eventuality, one may start from a different set of starting values $\underline{\beta}_o$ until the true minimum is achieved. In the second case, one may try including higher terms in the Fourier expansion of Eqs. 4.1. If that does not work either, then it implies that the chosen model is not realistic. If, however, at the minimum the error approaches zero, it signifies that the chosen mathematical model for the far-field impedances is adequate and that the iterative process has converged to the true minimum.

5. FINITE ELEMENT MODEL OF NEAR-FIELD USED TO GENERATE FAR-FIELD IMPEDANCES

The vibrations of a rigid massless circular plate on a uniform elastic halfspace constitutes an axisymmetric problem. The near-field can therefore be modelled by axisymmetric finite elements. In the analysis of axisymmetric bodies subjected to arbitrary non-axisymmetric loadings, both the loads and the displacements are expanded in terms of a Fourier series [66]. Therefore, if a cylindrical frame of reference as shown in Fig. 5.1 is used, the displacements u_r, u_z and u_θ in the radial, vertical and circumferential directions, respectively, can be written as

$$\left.\begin{aligned}
u_r(r,z,\theta) &= \sum_{n=0}^{\infty} u_{rn}(r,z)\ \mathrm{Cos}n\theta + \sum_{n=0}^{\infty} \hat{u}_{rn}(r,z)\mathrm{Sin}n\theta \\
u_z(r,z,\theta) &= \sum_{n=0}^{\infty} u_{zn}(r,z)\ \mathrm{Cos}n\theta + \sum_{n=0}^{\infty} \hat{u}_{zr}(r,z)\ \mathrm{Sin}n\theta \\
u_\theta(r,z,\theta) &= \sum_{n=0}^{\infty} -u_{\theta n}(r,z)\ \mathrm{Sin}n\theta + \sum_{n=0}^{\infty} \hat{u}_{\theta n}(r,z)\ \mathrm{Cos}n\theta
\end{aligned}\right\} \qquad (5.1)$$

which contain symmetric and anti-symmetric components about the $\theta=0$ axis. These generalized displacements are functions of r and z only and do not depend upon θ. Thus, what was originally a three-dimensional problem is reduced to a two-dimensional problem with substantial reduction in total number of degrees of freedom. The introduction of the negative sign in the sine term for the circumferential displacement has the effect of yielding the same stiffness matrix for both symmetric and antisymmetric components. Similarly, the applied forces can be expressed in the form,

Preceding page blank

$$\left.\begin{aligned}
f_r(r,z,\theta) &= \sum_{n=0}^{\infty} f_{rn}(r,z)\ \mathrm{Cos}n\theta + \sum_{n=0}^{\infty} \hat{f}_{rn}(r,z)\ \mathrm{Sin}n\theta \\
f_z(r,z,\theta) &= \sum_{n=0}^{\infty} f_{zn}(r,z)\ \mathrm{Cos}n\theta + \sum_{n=0}^{\infty} \hat{f}_{zn}(r,z)\ \mathrm{Sin}n\theta \\
f_\theta(r,z,\theta) &= \sum_{n=0}^{\infty} - f_{\theta n}(r,z)\ \mathrm{Sin}n\theta + \sum_{n=0}^{\infty} \hat{f}_{\theta n}(r,z)\ \mathrm{Cos}n\theta
\end{aligned}\right\} \tag{5.2}$$

Due to the orthogonality conditions of the trigonometric functions in the above expressions, a set of uncoupled equations of motion of the form

$$\underline{M}_n \ddot{\underline{u}}_n + \underline{K}_n \underline{u}_n = \underline{p}_n \tag{5.3}$$

can be obtained for each Fourier term, as shown later in this chapter. The solution procedure consists of solving Eq. 5.3 for each Fourier amplitude and then combining them according to Eq. 5.1 to obtain the total displacement field. This leads to a very economical method of analysis for axisymmetric bodies subject to arbitrary loads if the number of terms required in the Fourier representation of the applied loads and the resulting displacements is small. In particular, the torsional, vertical and coupled translation and rocking vibrations of a rigid circular plate can be represented by only a single term each as shown in Fig. 5.2. For torsion, only the first (n=0) antisymmetric term is required; thus

$$\begin{aligned}
u_r(r,z,\theta) &= 0 \\
u_z(r,z,\theta) &= 0 \\
u_\theta(r,z,\theta) &= \hat{u}_{\theta 0}(r,z)
\end{aligned}$$

Vertical vibrations can be represented by the first symmetric term in Eq. 5.1 giving

$$u_r(r,z,\theta) = u_{r0}(r,z)$$

$$u_z(r,z,\theta) = u_{z0}(r,z)$$

$$u_\theta(r,z,\theta) = 0$$

Coupled translation and rocking vibrations are represented by the second (n=1) symmetric term giving

$$u_r(r,z,\theta) = u_{r1}(r,z)\ \mathrm{Cos}\theta$$

$$u_z(r,z,\theta) = u_{z1}(r,z)\ \mathrm{Cos}\theta$$

$$u_\theta(r,z,\theta) = -\ u_{\theta 1}(r,z)\ \mathrm{Sin}\theta$$

5.1 Variable 4 to 9 Node Isoparametric Element

The element used in this study is a gradrilateral element described by 4 to 9 nodes as shown in Fig. 5.3. A triangular element is treated as a degenerate gradrilateral by specifying two of the corner nodes to be the same. Because of the axisymmetric nature of the problem, the element actually describes a toroidal volume and nodal points are nodal circles in r-θ plane. The element which was originally presented for plane and axisymmetric problems [79] has been extended here to axisymmetric problems with non-axisymmetric loadings.

Interpolation Functions:

In an isoparametric formulation of the finite element method the coordinates of any point within an element are interpolated as

$$\left.\begin{aligned} r &= \sum_{i=1}^{q} N_i(s,t)\,r_i \\ z &= \sum_{i=1}^{q} N_i(s,t)\,z_i \end{aligned}\right\} \qquad (5.4)$$

where q is the number of nodes used to define the element which may be anywhere from 4 to 9; r_i and z_i are the coordinates of the nodes i=1,..., q and where N_i, the interpolation functions in the natural coordinates system (s,t) are defined in Table 1.

The displacement field within an element is also approximated by the same interpolation functions. Therefore, from Eqs. 5.1

$$\left.\begin{aligned} u_r &= \sum_{n=0}^{\infty} \sum_{i=1}^{q} N_i u^i_{rn} \operatorname{Cos} n\theta + \sum_{n=0}^{\infty} \sum_{i=1}^{q} N_i \hat{u}^i_{nr} \operatorname{Sin} n\theta \\ u_z &= \sum_{n=0}^{\infty} \sum_{i=1}^{q} N_i u^i_{zn} \operatorname{Cos} n\theta + \sum_{n=0}^{\infty} \sum_{i=1}^{q} N_i \hat{u}^i_{zn} \operatorname{Sin} n\theta \\ u_\theta &= \sum_{n=0}^{\infty} \sum_{i=1}^{q} -N_i u^i_{\theta n} \operatorname{Sin} n\theta + \sum_{n=0}^{\infty} \sum_{i=1}^{q} N_i \hat{u}^i_{\theta n} \operatorname{Cos} n\theta \end{aligned}\right\} \qquad (5.5a)$$

where u^i_{rn}, u^i_{zn}, and $u^i_{\theta r}$ are the symmetric components and $\hat{u}^i_{rn}$, $\hat{u}^i_{zn}$, and $\hat{u}^i_{\theta n}$, the antisymmetric components of the nodal point displacements. In the expressions to follow, however, the antisymmetric components have not been shown for the sake of simplicity in presentation. Eqs. 5.5a in matrix form can be written as,

$$\begin{Bmatrix} u_r \\ u_z \\ u_\theta \end{Bmatrix} = \sum_{n=0}^{\infty} \begin{bmatrix} \underline{N} \operatorname{Cos} n\theta & 0 & 0 \\ 0 & \underline{N} \operatorname{Cos} n\theta & 0 \\ 0 & 0 & -\underline{N} \operatorname{Sin} n\theta \end{bmatrix} \begin{Bmatrix} \underline{u}_{rn} \\ \underline{u}_{zn} \\ \underline{u}_{\theta n} \end{Bmatrix} \qquad (5.5b)$$

or

$$\underline{u} = \sum_{n=0}^{\infty} \underline{N}_n \underline{u}_n \qquad (5.5c)$$

where

$$\underline{N} = < N_1, N_2, \ldots, N_q >$$

and

$$\underline{u}_{rn} = \begin{Bmatrix} u_{rn}^1 \\ u_{rn}^2 \\ \cdot \\ \cdot \\ \cdot \\ u_{rn}^q \end{Bmatrix} ; \quad \underline{u}_{zn} = \begin{Bmatrix} u_{zn}^1 \\ u_{zn}^2 \\ \cdot \\ \cdot \\ \cdot \\ u_{zn}^q \end{Bmatrix} ; \quad \underline{u}_{\theta n} = \begin{Bmatrix} u_{\theta n}^1 \\ u_{\theta n}^2 \\ \cdot \\ \cdot \\ \cdot \\ u_{\theta n}^q \end{Bmatrix}$$

Stress-Strain Relationship:

For three-dimensional isotropic elasticity, the stresses are related to the strains by

$$\begin{Bmatrix} \sigma_{rr} \\ \sigma_{zz} \\ \sigma_{\theta\theta} \\ \sigma_{rz} \\ \sigma_{r\theta} \\ \sigma_{z\theta} \end{Bmatrix} = \begin{bmatrix} C_{11} & C_{12} & C_{13} & & & \\ C_{21} & C_{22} & C_{23} & & & \\ C_{31} & C_{32} & C_{33} & & & \\ & & & C_{44} & & \\ & & & & C_{55} & \\ & & & & & C_{66} \end{bmatrix} \begin{Bmatrix} \varepsilon_{rr} \\ \varepsilon_{zz} \\ \varepsilon_{\theta\theta} \\ 2\varepsilon_{rz} \\ 2\varepsilon_{r\theta} \\ 2\varepsilon_{z\theta} \end{Bmatrix} \tag{5.6a}$$

or,

$$\underline{\sigma} = \underline{C}\ \underline{\varepsilon} \tag{5.6b}$$

where,

$$C_{11},\ C_{22},\ C_{33} = \frac{2G(1-\nu)}{(1-2\nu)}$$

$$C_{12},\ C_{21},\ C_{13},\ C_{31},\ C_{23},\ C_{32} = \frac{2G}{(1-2\nu)}$$

$$C_{44},\ C_{55},\ C_{66} = G$$

in which G is the shear modulus and ν is Poisson's ratio.

Strain-Displacement Relationship:

The three-dimensional strain-displacement relationship in cylindrical coordinates is

$$\underline{\varepsilon} = \begin{Bmatrix} \varepsilon_{rr} \\ \varepsilon_{zz} \\ \varepsilon_{\theta\theta} \\ 2\varepsilon_{rz} \\ 2\varepsilon_{r\theta} \\ 2\varepsilon_{z\theta} \end{Bmatrix} = \begin{bmatrix} \frac{\partial}{\partial r} & 0 & 0 \\ 0 & \frac{\partial}{\partial z} & 0 \\ \frac{1}{r} & 0 & \frac{1}{r}\frac{\partial}{\partial \theta} \\ \frac{\partial}{\partial z} & \frac{\partial}{\partial r} & 0 \\ \frac{1}{r}\frac{\partial}{\partial \theta} & 0 & -\frac{1}{r} + \frac{\partial}{\partial r} \\ 0 & \frac{1}{r}\frac{\partial}{\partial \theta} & \frac{\partial}{\partial z} \end{bmatrix} \begin{Bmatrix} u_r \\ u_z \\ u_\theta \end{Bmatrix} \tag{5.7}$$

Making use of Eqs. 5.5b, one obtains

$$\underline{\varepsilon} = \sum_{n=0}^{\infty} \begin{bmatrix} \underline{N},r \text{ Cos}n\theta & 0 & 0 \\ 0 & \underline{N},z \text{ Cos}n\theta & 0 \\ \frac{1}{r}\underline{N} \text{ Cos}n\theta & 0 & -\frac{1}{r}\underline{N}n \text{ Cos}n\theta \\ \underline{N},z \text{ Cos}n\theta & \underline{N},r \text{ Cos}n\theta & 0 \\ -\frac{1}{r}\underline{N}n \text{ Sin}n\theta & 0 & (\frac{1}{r}\underline{N}-\underline{N},r) \text{ Sin}n\theta \\ 0 & -\frac{1}{r}\underline{N}n \text{ Sin}n\theta & -\underline{N},z \text{ Sin}n\theta \end{bmatrix} \begin{Bmatrix} \underline{u}_{rn} \\ \underline{u}_{zn} \\ \underline{u}_{\theta n} \end{Bmatrix} \tag{5.8a}$$

or,

$$\underline{\varepsilon} = \sum_{n=0}^{\infty} \underline{B}_n \; \underline{u}_n \tag{5.8b}$$

Since the interpolation functions N_i are given in terms of the natural coordinates (s,t), the partial derivatives $\underline{N}_{,r}$ and $\underline{N}_{,z}$ in Eq. 5.8a are obtained by inverting the chain rule.

$$\begin{Bmatrix} \frac{\partial}{\partial s} \\ \\ \frac{\partial}{\partial t} \end{Bmatrix} = \begin{bmatrix} \frac{\partial r}{\partial s} & \frac{\partial z}{\partial s} \\ \\ \frac{\partial r}{\partial t} & \frac{\partial z}{\partial t} \end{bmatrix} \begin{Bmatrix} \frac{\partial}{\partial r} \\ \\ \frac{\partial}{\partial z} \end{Bmatrix} = \underline{J} \begin{Bmatrix} \frac{\partial}{\partial r} \\ \\ \frac{\partial}{\partial z} \end{Bmatrix} \tag{5.9}$$

where $\underline{J}$ is the Jacobian matrix, the elements of which can be obtained by differentiating Eq. 5.4, e.g.,

$$\frac{\partial r}{\partial s} = \sum_{i=1}^{q} \frac{\partial N_i}{\partial s} r_i \tag{5.10}$$

Upon inversion of Eq. 5.9, one gets

$$\begin{Bmatrix} \frac{\partial}{\partial r} \\ \\ \frac{\partial}{\partial z} \end{Bmatrix} = \frac{1}{|\underline{J}|} \begin{bmatrix} \frac{\partial z}{\partial t} & -\frac{\partial z}{\partial s} \\ \\ -\frac{\partial r}{\partial t} & \frac{\partial r}{\partial s} \end{bmatrix} \begin{Bmatrix} \frac{\partial}{\partial s} \\ \\ \frac{\partial}{\partial t} \end{Bmatrix} \tag{5.11}$$

where

$$|\underline{J}| = \frac{\partial r}{\partial s}\frac{\partial z}{\partial t} - \frac{\partial r}{\partial t}\frac{\partial z}{\partial s} \tag{5.12}$$

is the determinant of the Jacobian matrix which must always be positive to satisfy Eq. 5.11. A non-positive Jacobian $|\underline{J}|$ implies that the transformation from global to natural coordinates is not unique. This may be caused by the angle between adjacent sides of the element being greater than 180° or by node sequencing errors during input. The Jacobian also represents the conversion of the volume differential dV from global to natural coordinates:

$$dV = (rd\theta)\ drdz = (rd\theta)\left|\underline{J}\right|\ dsdt \tag{5.13}$$

Element Matrices:

The element stiffness and mass matrices can be obtained by using the principle of virtual displacements which can be stated as

$$\int_V \delta\underline{u}^T\underline{\ddot{u}}\rho dV + \int_V \delta\underline{\varepsilon}^T\underline{\sigma}dV - \int_V \delta\underline{u}^T\underline{f}dV = 0 \tag{5.14}$$

Upon substituting Eqs. 5.5c, 5.6b and 5.8b into Eq. 5.14, one gets for element e

$$\sum_{m=0}^{\infty} \delta\underline{u}_m^{eT} \left\{ \sum_{n=0}^{\infty} \left(\int_{V^e} \rho \underline{N}_m^T \underline{N}_n\ dV\ \underline{\ddot{u}}_n^e + \int_{V^e} \underline{B}_m^T \underline{C}\ \underline{B}_n\ dV\ \underline{u}_n^e - \int_{V^e} \underline{N}_m^T \underline{f}\ dV \right) \right\} = 0 \tag{5.15a}$$

or,

$$\sum_{m=0}^{\infty} \delta\underline{u}_m^{eT} \left\{ \sum_{n=0}^{\infty} \left(\underline{M}_{mn}^e\ \underline{\ddot{u}}_n^e + \underline{K}_{mn}^e\ \underline{u}_n^e - \underline{p}_{mn}^e \right) \right\} = 0 \tag{5.15b}$$

which leads to the coupled equations of motion

$$\underline{M}_{mn}^e\ \underline{\ddot{u}}_n^e + \underline{K}_{mn}^e\ \underline{u}_n^e - \underline{p}_{mn}^e = 0 \tag{5.16a}$$

where,

$$\left.\begin{aligned} \underline{M}_{mn}^e &= \iiint_{V^e} \rho N_m^T N_n\ rdrdz\ d\theta \\ \underline{K}_{mn}^e &= \iiint_{V^e} \underline{B}_m^T\ \underline{C}\ \underline{B}_n\ rdrdz\ d\theta \\ \underline{p}_{mn}^e &= \iiint_{V^e} \underline{N}_m^T\ \underline{f}\ rdrdz\ d\theta \end{aligned}\right\} \tag{5.17a}$$

are the consistent mass matrix, stiffness matrix and load vector, respectively, for element e. The above integrals can be transformed to the natural coordinate system of the element using Eq. 5.13; thus, one obtains

$$\left.\begin{aligned}
\underline{M}^e_{mn} &= |\underline{J}| \int_{-1}^{+1}\int_{-1}^{+1}\int_{0}^{2\pi} \rho \underline{N}_m^T \underline{N}_n \, r \, ds dt \, d\theta \\
\underline{K}^e_{mn} &= |\underline{J}| \int_{-1}^{+1}\int_{-1}^{+1}\int_{0}^{2\pi} \underline{B}_m^T \underline{C} \, \underline{B}_n \, r \, ds dt \, d\theta \\
\underline{p}^e_{mn} &= |\underline{J}| \int_{-1}^{+1}\int_{-1}^{+1}\int_{0}^{2\pi} \underline{N}_m^T \underline{f} \, r \, ds dt \, d\theta
\end{aligned}\right\} \tag{5.17b}$$

in which r can be expressed in terms of interpolation functions as given by Eq. 5.4.

In the above equations, integration in the θ-direction can be carried out explicitly, giving rise to the following integrals:

$$\left.\begin{aligned}
I_1 &= \int_0^{2\pi} \text{Cos}m\theta \, \text{Cos}n\theta \, d\theta = \begin{cases} 0 & m \neq n \\ 2\pi & m = n = 0 \\ \pi & m = n \geq 1 \end{cases} \\
I_2 &= \int_0^{2\pi} \text{Sin}m\theta \, \text{Sin}n\theta \, d\theta = \begin{cases} 0 & m \neq n \\ 0 & m = n = 0 \\ \pi & m = n \geq 1 \end{cases} \\
I_3 &= \int_0^{2\pi} \text{Sin}m\theta \, \text{Cos}n\theta \, d\theta = 0 \text{ for all m and n}
\end{aligned}\right\} \tag{5.18}$$

Since these integrals equal zero for $m \neq n$, it follows that

$$\left.\begin{matrix} \underline{M}^e_{mn} \\ \underline{K}^e_{mn} \\ \underline{p}^e_{mn} \end{matrix}\right\} = 0 \quad \text{for } m \neq n$$

and Eqs. 5.16a reduce to the uncoupled form

$$\underline{M}^e_n \, \ddot{\underline{u}}^e_n + \underline{K}^e_n \, \underline{u}^e_n = \underline{p}^e_n \tag{5.16b}$$

for each Fourier amplitude. Equations 5.3, presented in the beginning of this Chapter for the finite element idealization of the near-field can now be obtained from Eq. 5.16b by standard assembly procedures.

In the s and t-directions, the integrals of Eq. 5.17b are evaluated numerically using the Gaussian quadrature. Both 2 x 2 and 3 x 3 integration points are possible as shown in Fig. 5.4. However, for a 9-node element, only 3 x 3 integration is recommended to ensure stability.

The consistent mass matrix obtained in the above formulation has non-zero off-diagonal elements. However, as mentioned in Chapter 2, for most practical problems a lumped mass representation is sufficient. Therefore, in the present investigation a lumped mass matrix is formed by scaling the diagonal terms of the consistent mass matrix so that their sum is equal to the total mass of the element.

The element presented herein offers a flexible, efficient, and reliable means of analyzing plane and axisymmetric problems. Since the isoparametric formulation allows accurate modelling of curved boundaries, this element is especially suited for the present investigation where the interface between the near- and far-fields is hemispherical. The accuracy and stability characteristics of the element have been studied previously [79] where it was noted that the addition of the ninth node to the center of the more conventional 8-node isoparametric element increases its reliability under geometric distortion. In the following, the accuracy of the element in wave propagation problems is examined and recommendations are made about the largest size of the elements to be used.

5.2 Element Accuracy for Wave Propagation

The effectiveness of the finite element to transmit waves is studied by analyzing the problem of one-dimensional wave propagation through a semi-infinite rod constrained to undergo motion only in the longitudinal direction which has been the subject of a similar investigation in the past [68]. The displacement field within the homogeneous rod, when subject to a unit harmonic displacement as shown in Fig. 5.5(a) can be obtained by solving the corresponding wave equation giving

$$u_z(z,\omega) = \text{Cos}\,\frac{\omega}{C_p}\,z - i\,\text{Sin}\,\frac{\omega}{C_p}\,z \tag{5.19}$$

where

$$C_p = \sqrt{\frac{M}{\rho}}$$

is the compressional wave velocity, and

$$M = \frac{2G(1-\nu)}{1-2\nu}$$

is the constrained modulus for the rod.

Since the only stress component at a horizontal section through the rod is the normal stress $\sigma = \rho C_p \dot{u}_z$, a valid finite model can be obtained by applying this stress to a finite portion of the rod through uniform dampers with constant $C_D = \rho C_p$ as shown in Fig. 5.5(b). The resulting finite system maintains dynamic equilibrium and behaves like the semi-infinite rod.

A plane-strain finite element analysis of the rod was performed using the isoparametric element presented in the previous section. The length of the finite model was conveniently chosen to be equal to one wave length. Three different finite element meshes were considered as shown in Fig. 5.6. The first two meshes were modelled by 9-node elements, whereas 8-node elements (without the center node) were used in the third mesh. The size of the finite elements in the direction of wave propagation was 1/3-rd of the wave length, λ, in the first mesh and 1/4-th in the second and third mesh. Only the vertical degree of freedom was allowed at each node. The stiffness and mass matrices for the finite element models described above were obtained by a computer program that was developed for this purpose. The distributed damping stresses at the boundary of the finite element model can be replaced by the work equivalent nodal damping values. These are equal to $bC_D/6$ at the side nodes, and $2bC_D/3$ at the center node of each element where b is the width of the element. Since there is no material damping in the rod, this dashpot representation leads to a diagonal damping matrix for the system having non-zero components corresponding only the the boundary nodal points.

The resulting equations of motion were solved for the steady state displacements in the rod due to the applied unit harmonic displacement boundary condition. The numerical solutions so obtained are compared with the true solutions (Eq. 5.19) in Fig. 5.7. Although both consistent and lumped mass formulations were considered, the results presented in Fig. 5.7 are for the lumped mass formulation only. It is observed from this figiure that when the size of the 9-node finite elements is 1/4-th of the wave length, the numerical results are in excellent agreement with the true solutions. The maximum error is about 3% for the real part and less than 2% for the imaginary part. The use of consistent mass matrix instead of lumped mass matrix resulted in only a slight improvement in the real part. For the first mesh, where the size of the finite elements used is 1/3-rd of the wave length, the maximum errors are about 17% and 8% for the real and imaginary parts, respectively. The importance of including the center node is apparent from the results for the third mesh which are in significant error with the true solutions even though the size of the elements used is 1/4-th of the wave length.

Since the above error analysis pertains to one-dimensional wave propagation, the errors may be higher for more complex two- or three-dimensional wave propagation. However, it serves as a useful guideline in selecting the size of the elements in the finite element mesh. It is recommended that 9-node elements be used as much as possible and that the size of these elements be no greater than 1/4-th of the wave length corresponding to the highest frequency of interest.

5.3 Near-Field Finite Element Mesh

The near-field in the hybrid modelling of the rigid circular plate on a uniform elastic halfspace is idealized by the axisymmetric finite element presented in the previous section. The finite element mesh used is as shown in Fig. 5.8. There are 73 quadrilateral elements in the mesh. The total number of nodes is 317 out of which 17 are on the interface. These boundary nodes are numbered last so that the near-field impedance matrix can be partitioned as discussed in Chapter 2. To keep the errors associated with the finite element mesh small, 9-node elements, which were shown to be so effective for wave propagation, are used as much as possible. These elements on the boundary also reproduce the hemispherical interface correctly. The largest dimension of elements anywhere in the mesh is approximately 1/4th of the wave length corresponding to a non-dimensional frequency ($\omega R/C_s$) of 9.0. It is, therefore, anticipated that errors in the displacement field, for frequencies below this value will not be greater than 5%. Such a refined mesh was deemed necessary in this investigation to ensure that the far-field impedances, identified using this mesh, are not unduely influenced by the near-field discretization.

The stiffness and lumped mass matrices for the near-field are obtained using a computer program specifically developed for this purpose. For those elements with nodes in contact with the rigid plate the stiffness and mass matrices are transformed so as to be consistent with the rigid body motions of the plate. The stiffness matrix is stored using an active column scheme to minimize computer storage. Since material damping is not being considered in this investigation, the near-field damping matrix is identically equal to zero.

TABLE 1

INTERPOLATION FUNCTIONS

$N_1 = \frac{1}{4}(1+s)(1+t)$	$-\frac{1}{2}N_5$			$-\frac{1}{2}N_8$	$-\frac{1}{4}N_9$
$N_2 = \frac{1}{4}(1-s)(1+t)$	$-\frac{1}{2}N_5$	$-\frac{1}{2}N_6$			$-\frac{1}{4}N_9$
$N_3 = \frac{1}{4}(1-s)(1-t)$		$-\frac{1}{2}N_6$	$-\frac{1}{2}N_7$		$-\frac{1}{4}N_9$
$N_4 = \frac{1}{4}(1+s)(1-t)$			$-\frac{1}{2}N_7$	$-\frac{1}{2}N_8$	$-\frac{1}{4}N_9$
$N_5 = \frac{1}{2}(1-s^2)(1+t)$					$-\frac{1}{4}N_9$
$N_6 = \frac{1}{2}(1-s)(1-t^2)$					$-\frac{1}{4}N_9$
$N_7 = \frac{1}{2}(1-s^2)(1-t)$					$-\frac{1}{4}N_9$
$N_8 = \frac{1}{2}(1+s)(1-t^2)$					$-\frac{1}{4}N_9$
$N_9 = \frac{1}{2}(1-s^2)(1-t^2)$					$-\frac{1}{4}N_9$

Note: Include N_5 to N_9 only if nodes 5 to 9 are defined for the element.

6. NUMERICAL RESULTS: FAR-FIELD IMPEDANCES AND COMPARISON OF SOLUTIONS

6.1 Torsional Loading

Computer programs were developed to evaluate the torsional far-field impedance matrices using the continuous [75] and consistent approach presented in Chapter 3. In the continuous approach, far-field impedance matrices are not related to the order of finite elements on the boundary of the near-field. In the consistent formulation, quadratic interpolation functions consistent with the near-field are used to generate the far-field impedances. The far-field impedance matrices so obtained are combined with the near-field finite element equations and the resulting hybrid model solved for response of the plate under a unit harmonic torque.

The plate compliances obtained from the hybrid model are compared with the closed-form solutions in Figure 6.1. In this figure, the non-dimensional frequency a_o is defined to be equal to $\omega a/C_s$, "a" being the radius of the rigid circular plate. It is observed that for the consistent approach both the real and imaginary parts of response are in close agreement with the known compliances. The error in the real part varies from about 4% at a_o = .2 to about 6% at a_o = 3.0. The corresponding errors in the imaginary part are about 1% to 4%. Since these errors are a combination of the modelling errors in the near- and far-fields, they reflect the effectiveness of the consistent approach in modelling the far-field, and the accuracy of the chosen finite element mesh for the near-field. Solutions obtained using the continuous approach are, however, in considerable error, especially after a_o = 1.8. An oscillatory behaviour in response, absent in the consistent approach, is also observed. The displacement at the interface, using the two approaches, are plotted in Figs. 6.2(a) and (b) for $a_o = 1$ and 3, respectively. At both frequencies, the consistent approach gives smoothly varying displacements over the entire interface which, in the absence of theoretical solutions, may be expected to be a good approximation of the true far-field displacements. The solutions obtained using the continuous approach are again found to be in significant error. These discrepancies in solutions using the continuous approach may be attributed in part to the non-compatibility and displacements at the interface, and in part to the fact that the infinite series of Eq. 3.24 has been truncated to a finite member of terms.

6.2 General Loadings

For general loading conditions, the far-field impedances are generated using the system identification approach outlined in Chapter 4. Since the modified Gauss-Newton algorithm for parameter adjustment is an iterative process requiring repeated solution of the equations,

$$\begin{array}{cc} \begin{array}{c} 3N_s \\ 3N_b \end{array} & \left[\begin{array}{c|c} \underline{S}_{ss} & \underline{S}_{sb} \\ \hline \underline{S}_{bs} & \underline{S}_{bb}+\underline{S}^{f}(\beta) \end{array}\right] \left\{\begin{array}{c} \underline{u}_s \\ \hline \underline{u}_b \end{array}\right\} = \left\{\begin{array}{c} \underline{p}_s \\ \hline \underline{p}_b \end{array}\right\} \\ & \begin{array}{cc} 3N_s & \quad 3N_b \end{array} \end{array}$$

advantage must be taken of the fact that at a particular frequency, only the elements of the far-field impedance matrix are modified. Therefore, in the computer program developed, the forward reduction of the above equations is stopped after the first $3N_s$ equations at which stage the coefficient matrix appears as shown below,

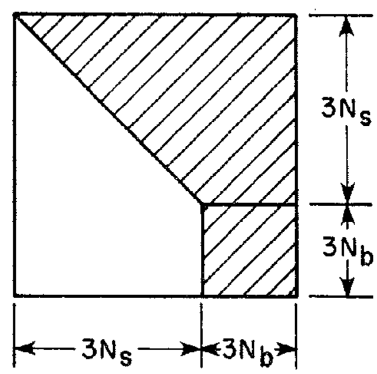

Within any iteration, then, the solution procedure requires the repeated reduction of $3N_b$ x $3N_b$ submatrix and back substitution to obtain the plate response. Since the number of nodes on the interface (N_b) is significantly smaller than the nodes elsewhere in the near-field (N_s), a great saving in computer time is achieved. Also, since the material damping is not considered, only the far-field impedance matrix has complex valued coefficients. Therefore, in the computer program, complex storage is assigned only to the submatrix $\underset{=}{S}_{bb} + \underset{=}{S}^f$ resulting in substantial reduction in storage requirements.

The far-field impedance functions, $\eta_R + i\xi_R$ in the normal direction, $\eta_\phi + i\xi_\phi$ in the tangential direction, and $\eta_\theta + i\xi_\theta$ in the circumferential direction are determined by minimizing the error function (Eq. 4.19) which is formed by considering the response of the plate in all the three modes of vibrations, namely - torsional, vertical, and coupled translation and rocking. Far-field impedances so obtained are presented in Figs. 6.3 - 6.5 as a function of the non-dimensional frequency, b_o. For any particular frequency, these uniformly distributed far-field impedances are directly proportional to the shear modulus G, and inversly proportional to the interface radius R. The discretized far-field impedances at any node, which are obtained by multiplying the continuous impedances by the appropriate tributary area A_i (Eq. 4.7), are therefore directly proportional to both G and R, an observation consistent with the theoretical solutions of Eq. 3.38. The far-field impedance functions presented are for a Poisson's ratio of 1/3, a value which is fairly representative for soils. Since the impedance functions for surface footings are known to be fairly insensitive to variations in Poisson's ratio [5], the far-field impedance functions developed may be used for other values of Poisson's ratio without much loss in accuracy.

The dynamic response of the rigid circular plate, using these far-field impedances are compared with the available solutions in Fig. 6.6 for Poisson's ratio of 1/3. It is apparent from this figure that the proposed hybrid model is very effective in reproducing the theoretical solutions. The discrepancies observed in the coupling compliances, C_{MH}, which are plotted in Fig. 6.11, may be due to the assumption of relaxed boundary conditions in the theoretical solutions. For torsional vibrations, the displacement field at the interface is also compared with that obtained by consistent approach in Fig. 6.7 which is analogous to Fig. 6.2. From these figures it is apparent that the system identification approach, although approximate, predicts the displacements much more accurately than the continuous approach.

Far-field impedances must, in principle, be related only to the interface radius, R. However, due to the approximate and numerical nature of the modelling, these impedances may be expected to be influenced by the near-field model used in the system identification process. The far-field impedances were generated for an R/a ratio of 3.0 which was initially selected to ensure smoothly varying displacements at the interface. To investigate their range of applicability, these impedances were employed to calculate the compliances of the rigid plate for three other R/a ratios of 4.0, 2.4 and 1.935 by changing the radius of the plate. These compliances are compared with their values obtained from the closed form solutions in Figs. 6.8 to 6.10 for a Poisson's ratio of 1/3. The agreement in solutions for R/a ratios of 4.0 and 2.4 is still very good, the errors being of the order of 5 to 10%. Solutions for R/a = 1.935, which represents an extreme case of the far-field being placed at a distance less than two times the radius of plate, are also in reasonable agreement except for the real part of rocking compliance, C_{MM}, which has errors of the order of 20%. For all the results presented, the errors in imaginary parts are generally much smaller than in the real parts. Finally, the identified impedances are used in the hybrid modelling of a rigid embedded hemispherical foundation whose response to torsional excitations has been evaluated analytically[32]. The finite element mesh used is shown in Fig.6.12 which was obtained by modifying the mesh of Fig. 5.8. The results are presented in Fig. 6.13 which indicates that the numerical solutions are within about 10% of the analytical solutions.

The results presented above demonstrate the validity of modelling the far-field through continuously distributed impedance functions for general loading conditions. The impedance functions developed are applicable to a wide range of practical situations and can be successfully employed in the hybrid modelling of soil-structure interaction.

7. GENERAL CONCLUSIONS

The hybrid model presented herein for treating three-dimensional soil-structure interaction of surface supported or embedded structures shows great promise of being superior to the two basic methods now being used, namely, the substructure (or impedance) method and the finite element method.

The far-field impedances required by this method can be generated for cases involving layered foundations and for cases involving visco-elastic foundation materials. The basic method can even be used for cases involving nonlinear hysteretic soil behavior in the near-field by using equivalent linearization techniques allowing a frequency domain solution or by using frequency independent (averaged values over predominant frequency band) far-field impedances allowing a solution of the nonlinear problem in the time domain.

REFERENCES

1. Hadjian, A. H., Luco, J.E. and Tsai, N.C., "Soil-Structure Interaction: Continuum or Finite Element?", Nuclear Engineering and Design, Vol. 31, 151-167, 1974.

2. Lysmer, J., "Analytical Procedures in Soil Dynamics", Report No. EERC-78/29, Earthquake Engineering Research Center, University of California, Berkeley, California, December 1978.

3. Chen, W.W.H., Chatterjee, M. and Day, S.M., "Seismic Response Analysis for a Deeply Embedded Nuclear Power Plant", 5th International Conference on Structural Mechanics in Reactor Technology, Berlin, West Germany, August 1979.

4. Lysmer, J. and Richart, F.E., Jr., "Dynamic Response of Footings to Vertical Loadings", Journal of the Soil Mechanics and Foundations Division, ASCE, Vol. 92, No. SM1, 65-91, January 1966.

5. Veletsos, A. S. and Wei, Y.T., "Lateral and Rocking Vibrations of Footings", Journal of the Soil Mechanics and Foundations Division, ASCE, Vol. 97, No. SM9, 1227-1248, September 1971.

6. Luco, J.E. and Westmann, R.A., "Dynamic Response of Circular Footings", Journal of the Engineering Mechanics Division, ASCE, Vol. 97, No. EM5, 1381-1395, October 1971.

7. Arnold, R.N., Bycroft, G.N., and Warburton, G.B., "Forced Vibrations of a Body on an Infinite Elastic Solid", Journal of Applied Mechanics, ASME, Vol. 22, No. 3, 391-400, 1955.

8. Bycroft, G.N., "Forced Vibrations of a Rigid Circular Plate on a Semi-Infinite Elastic Space or on an Elastic Stratum", Philosophical Transactions, Royal Society of London, 327-368, 1956.

9. Warburton, G.B., "Forced Vibrations of a Body on an Elastic Stratum", Journal of Applied Mechanics, ASME, Vol. 24, 55-58, 1957.

10. Kashio, J., "Steady State Response of a Circular Disk Resting on a Layered Medium", Ph.D. Thesis, Rice University, Houston, Texas, 1970.

11. Wei, Y., "Steady State Response of Certain Foundation Systems", Ph.D. Thesis, Rice University, Houston, Texas, 1971.

12. Luco, J.E., "Impedance Functions for a Rigid Foundation on a Layered Medium", Nuclear Engineering and Design, Vol. 31, 204-217, 1974.

13. Veletsos, A.S. and Verbic, B., "Vibration of Viscoelastic Foundations", Earthquake Engineering and Structural Dynamics, Vol. 2, 87-102, 1973.

14. Veletsos, A.S. and Nair, V.V.D., "Torsional Vibration of Viscoelastic Foundations", Journal of the Geotechnical Engineering Division, ASCE, Vol. 100, 225-246, 1974.

15. Luco, J.E., "Vibrations of a Rigid Disc on a Layered Viscoelastic Medium", Nuclear Engineering, Vol. 36, No. 3, 325-340, 1976.

16. Kobori, T., Minai, R., Suzuki, T. and Kusakabe, K., "Dynamic Ground Compliance of Rectangular Foundations", Proceedings of the 16th Japan National Conference for Applied Mechanics, 1966.

17. Awojobi, A.O., "Harmonic Rocking of Rigid Rectangular Body on a Semi-Infinite Elastic Medium", Journal of Applied Mechanics, Vol. 33, 547-552, 1966.

18. Kobori, T., Minai, R. and Suzuki, T., "Dynamic Ground Compliance of Rectangular Foundation on an Elastic Stratum", Proceedings, 2nd Japan National Symposium on Earthquake Engineering, Japan, 261-266, 1966.

19. Kobori, T., Minai, R. and Suzuki, T., "Dynamic Ground Compliance of Rectangular Foundation on an Elastic Stratum over a Semi-Infinite Rigid Medium", Annual Report, Disaster Prevention Research Institute of Kyoto University, No. 10A, 315-341, 1967.

20. Kobori, T., Minai, R., Suzuki, T. and Kusakabe, K., "Dynamic Ground Compliance of a Rectangular Foundation on a Semi-Infinite Viscoelastic Medium", Annual Report, Disaster Prevention Research Institute of Kyoto University, No. 11A, 349-367, 1968.

21. Kobori, T., Minai, R. and Suzuki, T., "The Dynamic Ground Compliance of a Rectangular Foundation on a Viscoelastic Stratum", Bulletin, Disaster Prevention Research Institute, Kyoto University, 389-429, March 1971.

22. Kobori, T and Suzuki, T., "Foundation Vibrations on a Viscoelastic Multi-layered medium", Proceedings, Third Japan Earthquake Engineering Symposium, Tokyo, 493-499, 1970.

23. Oien, M.A., "Steady State Motion of a Rigid Strip Bonded to an Elastic Halfspace", Journal of Applied Mechanics, ASME, Vol. 8, No. E2, 328-334, June 1971.

24. Luco, J.E. and Westmann, R.A., "Dynamic Response of a Rigid Footing Bonded to an Elastic Halfspace", Journal of Applied Mechanics, ASME, Vol. 39, No. E2, 527-534, June 1972.

25. Wong, H.L. and Luco, J.E., "Dynamic Response of Rigid Foundations of Arbitrary Shape", Earthquake Engineering and Structural Dynamics, Vol. 4, No. 6, 579-587, 1976.

26. Luco, J.E., "Dynamic Interaction of a Shear Wall with the Soil", Journal of The Engineering Mechanics Division, ASCE, Vol. 95, 333-346, 1969.

27. Thau, S.A. and Umek, A., "A Transient Response of Buried Foundation to Antiplane Shear Waves", Journal of Applied Mechanics, ASME, Vol. 40, 1061-1066, 1973.

28. Wong, H.L. and Trifunac, M.D., "Interaction of a Shear Wall with the Soil for Incident Plane SH Waves: Elliptical Rigid Foundations", Bulletin of the Seismological Society of America, Vol. 64, 1825-1842, 1974.

29. Luco, J.E., Wong, H.L. and Trifunac, M.D., "A Note on The Dynamic Response of Rigid Embedded Foundations", International Journal of Earthquake Engineering and Structural Mechanics, Vol. 4, No. 2, 119-128, 1975.

30. Thau, S.A. and Umek, A., "Coupled Rocking and Translating Vibrations of a Buried Foundation", Journal of Applied Mechanics, ASME, Vol. 41, 697-702, 1974.

31. Dravinski, M. and Thau, S.A., "Multiple Diffractions of Elastic Waves by a Rigid Rectangular Foundation: Plane-Strain Model", Journal of Applied Mechanics, ASME, Vol. 43, 291-294, 1976.

32. Luco, J.E., "Torsional Response of Structures for SH Waves: The Case of Hemispherical Foundations", Bulletin of the Seismological Society of America, Vol. 66, 109-123, 1976.

33. Apsel, R.J. and Luco, J.E., "Torsional Response of Rigid Embedded Foundations", Journal of the Engineering Mechanics Division, ASCE, Vol. 102, 957-970, 1976.

34. Novak, M. and Beredugo, Y.O., "Vertical Vibrations of Embedded Footings", Journal of the Soil Mechanics and Foundations Division, ASCE, Vol. 98, 1291-1310, 1972.

35. Novak, M. and Sachs, K., "Torsional and Coupled Vibration of Embedded Footings", Earthquake Engineering and Structural Dynamics, Vol. 2, 11-33, 1973.

36. Beredugo, Y.O. and Novak, M., "Coupled Horizontal and Rocking Vibration of Embedded Footings", Canadian Geotechnical Journal, Vol. 9, 477-497, 1972.

37. Apsel, R.J., "Dynamic Green's Function for Layered Media and Applications to Boundary Value Problems", Ph.D. Thesis, University of California, San Diego, California, 1979.

38. Flitman, L.M., "On the Motion of a Rigid Strip-Mass on an Elastic Halfspace and Excited by a Seismic Wave", Journal of Applied Math. Mech., Vol. 26, 1583-1604, 1962.

39. Luco, J.E., "Torsional Response of Structures to Obliquely Incident Seismic SH Waves", Earthquake Engineering Structural Dynamics, Vol. 4, 207-219, 1976.

40. Wong, H.L. and Luco, J.E., "Dynamic Response of Rectangular Foundations to Obliquely Incident Seismic Waves", Earthquake Engineering and Structural Dynamics, Vol. 6, 3-16, 1978.

41. Iguchi, M., "Basic Study on the Behaviour of Long Dimensional Size Buildings During Earthquakes", Proceedings, 4th Japan Earthquake Engineering Symposium, Tokyo, 783-790, 1975.

42. Simpson, I.C., "On the Interaction of Rayleigh Surface Waves With Structures", Earthquake Engineering and Structural Dynamics, Vol. 6, 247-263, 1978.

43. Newmark, N.M., "Torsion of Symmetrical Buildings", Proceedings, 4th World Conference on Earthquake Engineering", Santiago, Chile, Vol. 2, 1969.

44. Iguchi, M., "Seismic Response With Consideration of Both Phase Difference of Ground Motion and Soil-Structure Interaction", Proceedings, Japan Earthquake Engineering Symposium, Tokyo, Japan, 211-218, 1973.

45. Crouse, C.B. and Jennings, P.C., "Soil-Structure Interaction During the San Fernando Earthquake", Bulletin of the Seismological Society of America, Vol. 65, 13-36, 1975.

46. Scanlan, R.H., "Seismic Wave Effects on Soil-Structure Interaction", Earthquake Engineering and Structural Dynamics, Vol. 4, 379-388, 1976.

47. Trifunac, M.D., "Response Envelope Spectrum and Interpretation of Strong Earthquake Ground Motion", Bulletin of the Seismological Society of America, Vol. 61, 343-356, 1971.

48. Hanks, T.C., "Strong Ground Motion Following the San Fernando, California, Earthquake: Ground Displacements", Bulletin of the Seismological Society of America, Vol. 65, 193-225, 1975.

49. Seed, H.B. and Lysmer, J., "Soil-Structure Interaction Analysis by Finite Element Methods, State-of-the-Art", Transactions, 4th International Conference on Structural Mechanics in Reactor Technology, SMIRT 4, Vol. K(a), Paper K2/1, 1-11, San Francisco, 1977.

50. Lysmer, J., Seed, H.B., Udaka, T. and Hwang, R.N., "LUSH - A Computer Program for Complex Response Analysis of Soil-Structure Systems", Report No. EERC 74-4, Earthquake Engineering Research Center, University of California, Berkeley, California, 1974.

51. Valera, J.E., Seed, H.B., Tsai, C.F. and Lysmer, J., "Seismic Soil-Structure Interaction Effects at Humbolt Bay Power Plant", Journal of the Geotechnical Engineering Division, ASCE, Vol. 103, No. GT10, 1143-1161, 1977.

52. Luco, J.E. and Hadjian, A.H., "Two-Dimensional Approximations to the Three-Dimensional Soil-Structure Interaction Problem", Nuclear Engineering and Design, Vol. 31, 195-203, 1974.

53. Lysmer, J. and Kuhlemeyer, R.L., "Finite Dynamic Model for Infinite Media", Journal of the Engineering Mechanics Division, ASCE, Vol. 95, No. EM4, 859-877, 1969.

54. White, W., Vallippan, S. and Lee, I.K., "Unified Boundary for Finite Dynamic Models", Journal of the Engineering Mechanics Division, ASCE, Vol. 103, No. EM5, 949-964, 1977.

55. Smith, W.D., "A Nonreflecting Plane Boundary for Wave Propagation Problems", Journal of Computational Physics, Vol. 15, 492-503, 1974.

56. Waas, G., "Linear Two-Dimensional Analysis of Soil Dynamic Problems in Semi-Infinite Layered Media", Ph.D. Thesis, University of California, Berkeley, California, 1972.

57. Kausel, E, "Forced Vibrations of Circular Footings on Layered Media", MIT Research Report R74-11, Massachusetts Institute of Technology, Cambridge, Mass., 1974.

58. Kausel, E. and Roësset, J.E., "Dynamic Stiffness of Circular Foundations", Journal of the Engineering Mechanics Division", Vol. 101, No. EM6, 771-785, 1975.

59. Kawano, K., "Application of the Finite Element Method for Dynamic Analysis of Soil-Structure Interaction", Ph.D. Dissertation, Department of Civil Engineering, Kyoto University, Kyoto, Japan, 1979.

60. Lysmer, J., Udaka, T., Tsai, C.-F. and Seed, H.B., "FLUSH - A Computer Program for Approximate 3-D Analysis of Soil-Structure Interaction Problems", Report No. EERC 75-30, Earthquake Engineering Research Center, University of California, Berkeley, California, 1975.

61. Gomez-Masso, A., Lysmer, J., Chen, J.-C. and Seed, H.B., "Soil Structure Interaction in Different Seismic Environments", Report No. EERC 79-18, Earthquake Engineering Research Center, University of California, Berkeley, California, 1979.

62. Vaish, A.K. and Chopra, A.K., "Earthquake Finite Element Analysis of Structure-Foundation Systems", Journal of Engineering Mechanics Division, ASCE, Vol. 100, 1101-1116, 1974.

63. Gutierrez, J.A., "A Substructure Method for Earthquake Analysis of Structure-Soil Interaction", Report No. EERC 76-9, Earthquake Engineering Research Center, University of California, Berkeley, California, 1976.

64. Dasgupta, G. and Chopra, A.K., "Dynamic Stiffness Matrices for Homogeneous Viscoelastic Halfspaces", Report No. EERC 77-26, Earthquake Engineering Research Center, University of California, Berkeley, California, 1977.

65. Day, S.M. and Frazier, G.A., "Seismic Response of Hemispherical Foundation", Journal of the Engineering Mechanics Division, ASCE, Vol. 105, No. EM1, 29-41, 1979.

66. Wilson, E.L., "Structural Analysis of Axisymmetric Solids", Journal of American Institute of Aeronautics and Astronautics, Vol. 3, No. 12, December 1965.

67. Ghosh, S. and Wilson, E. L., "Dynamic Stress Analysis of Axisymmetric Structures Under Arbitrary Loading", Report No. EERC 69-10, Earthquake Engineering Research Center, University of California, Berkeley, California, 1969.

68. Kuhlemeyer, R.L. and Lysmer, J., "Finite Element Accuracy for Wave Propagation Problems", Journal of the Soil Mechanics and Foundations Division, ASCE, Vol. 99, No. SM5, 421-427, 1973.

69. Clough, R.W. and Penzien, J., Dynamics of Structures, McGraw Hill, 1975.

70. Penzien, J. and Tseng, W.S., "Three-Dimensional Dynamic Analysis of Fixed Offshore Platforms", Symposium on Numerical Methods in Offshore Engineering, Swansea, London, January 1977.

71. "Seismic Input and Soil-Structure Interaction", Report No. NUREG/CR-0693, Report to USNRC, D'Appolonia Consulting Engineers, Pittsburg, Pennsylvania, February 1979.

72. Cooley, J.W. and Tuckey, J.W., "An Algorithm for the Machine Calculation of Complex Fourier Series", Mathematics of Computations, Vol. 19, 297-301, 1965.

73. Love, A.E.H., The Mathematical Theory of Elasticity, 4th ed., Cambridge University Press, 1927.

74. Sezawa, K., "Further Studies on Rayleigh-Waves Having some Azimuthal Distribution", Bulletin of Earthquake Research Institute, Tokyo, Vol. 6, 1-18, 1929.

75. Yeh, C.S., Lin, T.W. and Penzien, J., "Dynamic Response of an Embedded Structure under a Dynamic Torque", Proceedings of 6th Asian Regional Conference on Soil Mechanics and Foundation, Engineering, Singapore, 1979.

76. Zienkiewicz, O.C., The Finite Element Method, 3rd Edition, McGraw Hill, 1977.

77. Bekey, G.A., "System Identification - An Introduction and a Survey", Simulation, Vol. 5, No. 4, 151-166, 1970.

78. Matzen, V.C. and McNiven, H.D., "Investigation of the Inelastic Characteristics of a Single Story Steel Structure Using System Identification and Shaking Table Experiments", Report No. EERC 76-20, Earthquake Engineering Research Center, University of California, Berkeley, California, 1976.

79. Hollings, J.P. and Wilson, E.L., "3-9 Node Isoparametric Planar or Axisymmetric Finite Element", Report No. UC SESM 78-3, Department of Civil Engineering, University of California, Berkeley, California, December 1977.

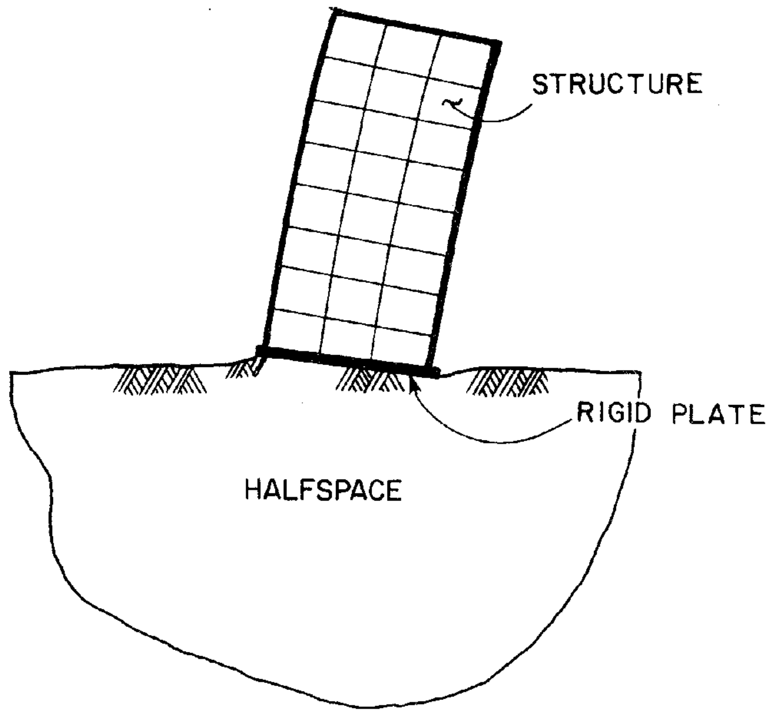

(a) CONTINUUM APPROACH

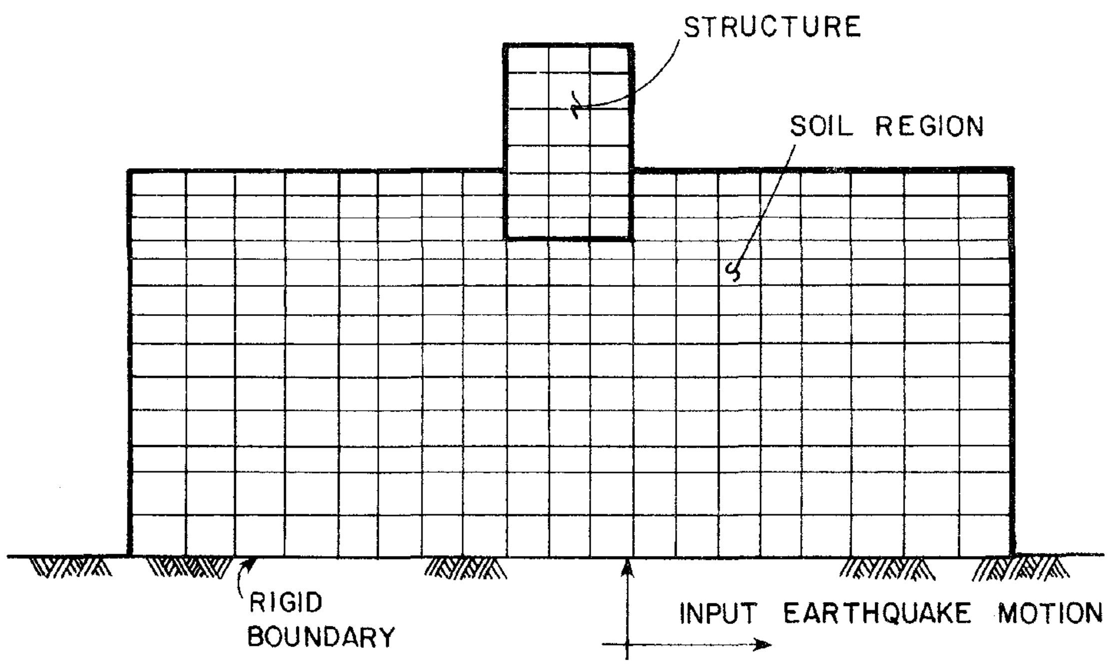

(b) FINITE ELEMENT APPROACH

FIG. 1.1 BASIC METHODS FOR THE ANALYSIS OF SOIL-STRUCTURE INTERACTION

Preceding page blank

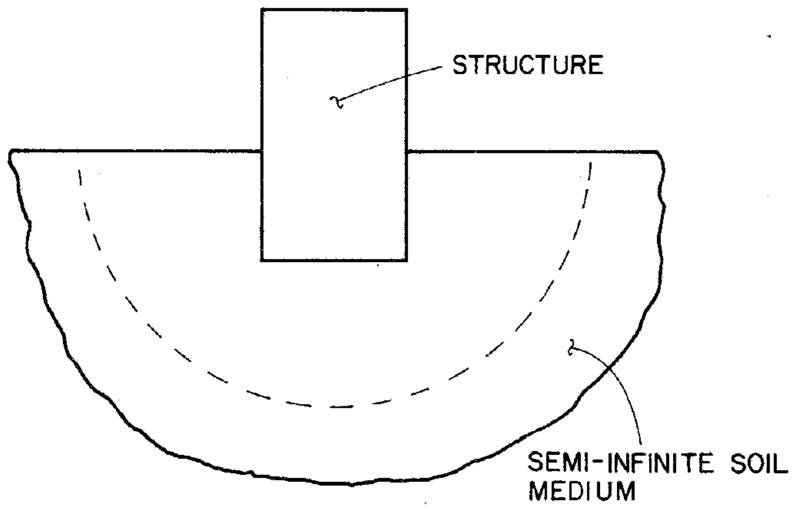

(a) SOIL-STRUCTURE SYSTEM

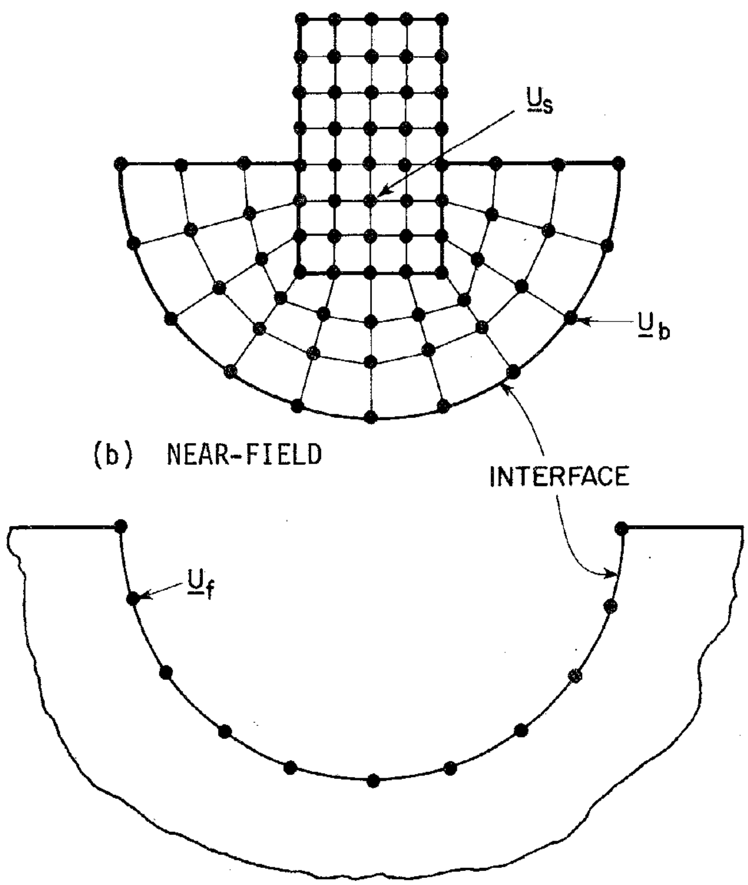

(b) NEAR-FIELD

(c) FAR-FIELD

FIG. 2.1 HYBRID MODELLING OF SOIL-STRUCTURE INTERACTION

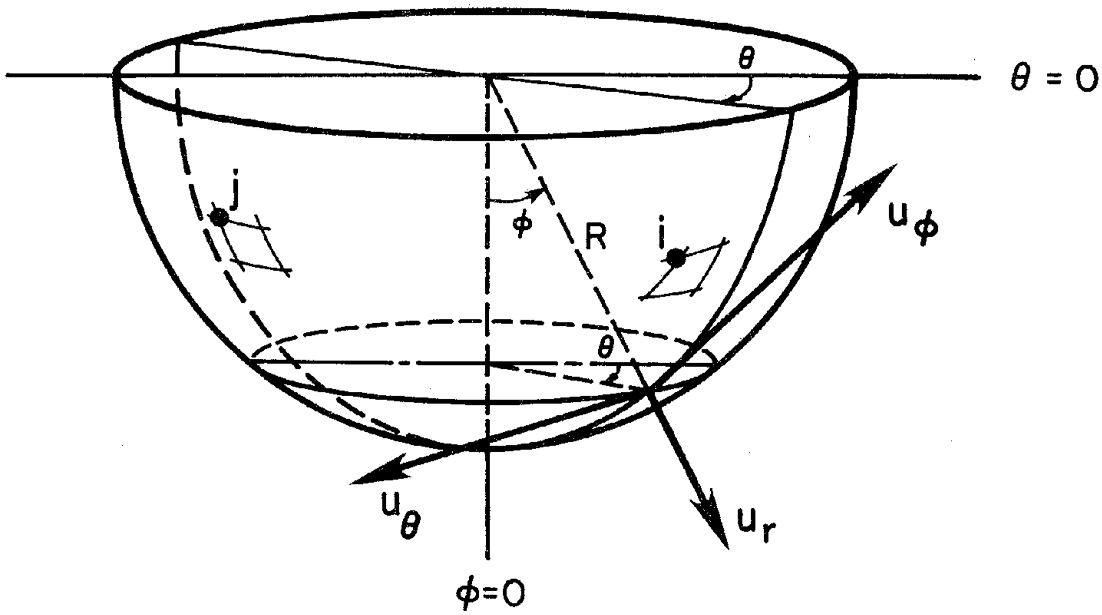

(a) THREE-DIMENSIONAL FORMULATION

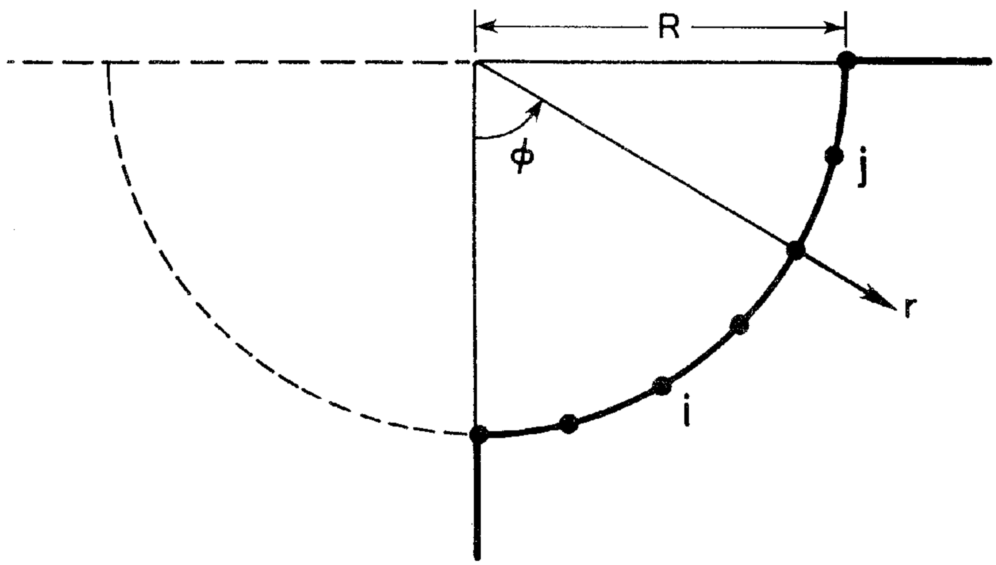

(b) AXISYMMETRIC FORMULATION

FIG. 3.1 FAR-FIELD WITH HEMISPHERICAL SURFACE CAVITY

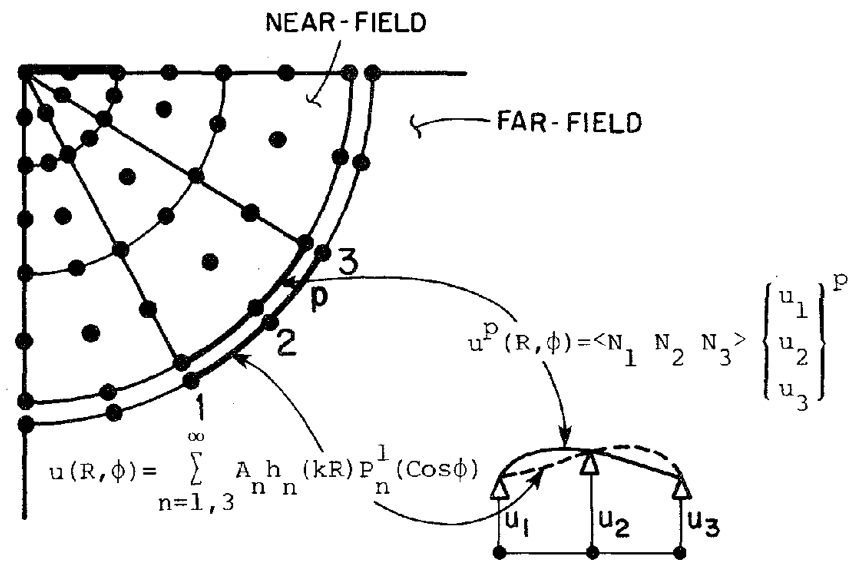

(a) CONTINUOUS APPROACH

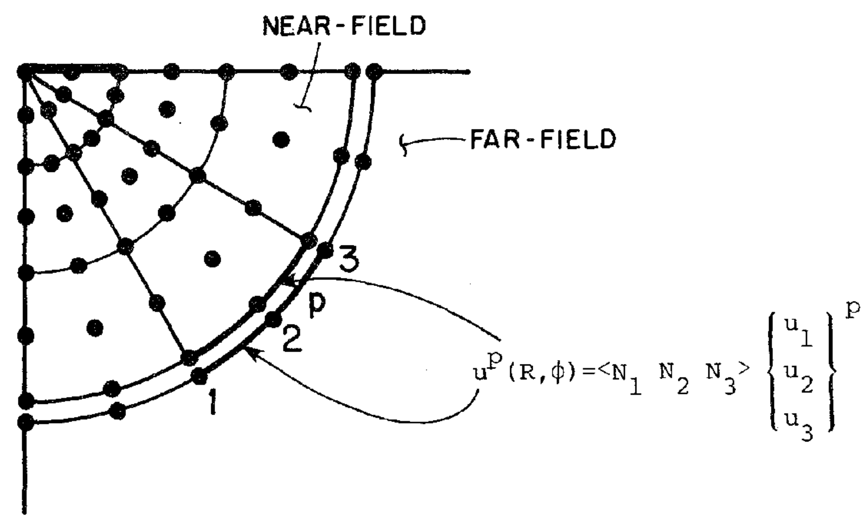

(b) CONSISTENT APPROACH

FIG. 3.2 COMPATIBILITY CONDITIONS AT THE INTERFACE

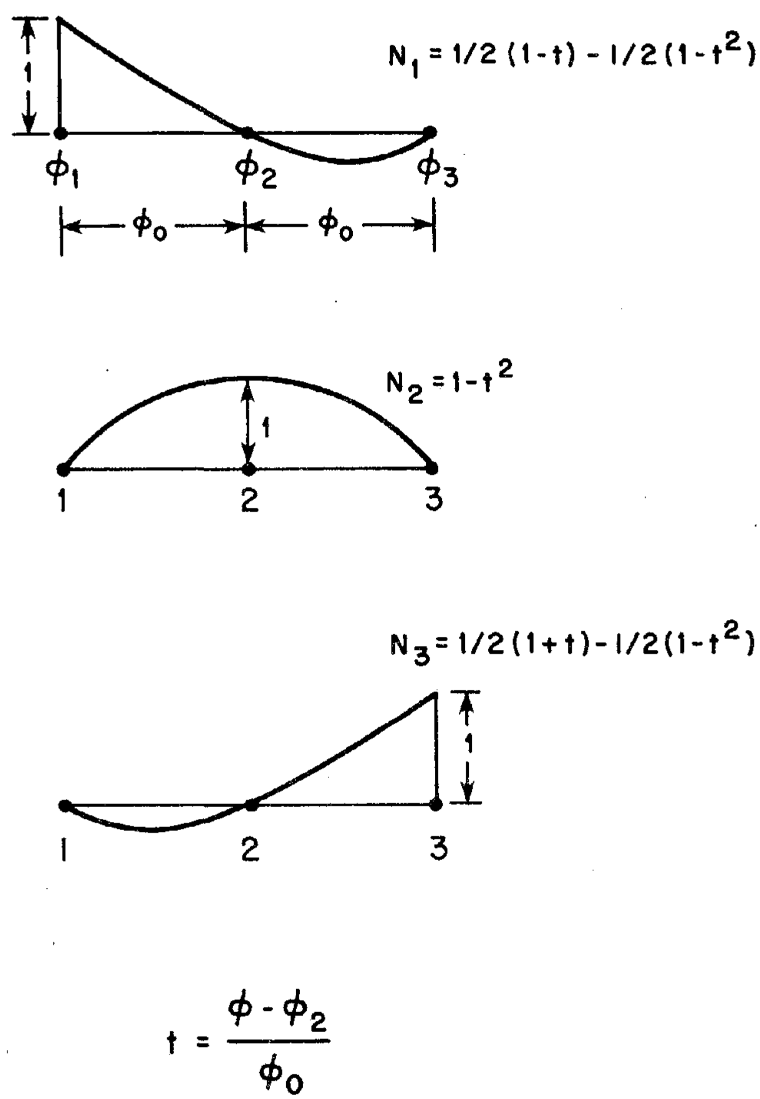

FIG. 3.3 QUADRATIC INTERPOLATION FUNCTIONS

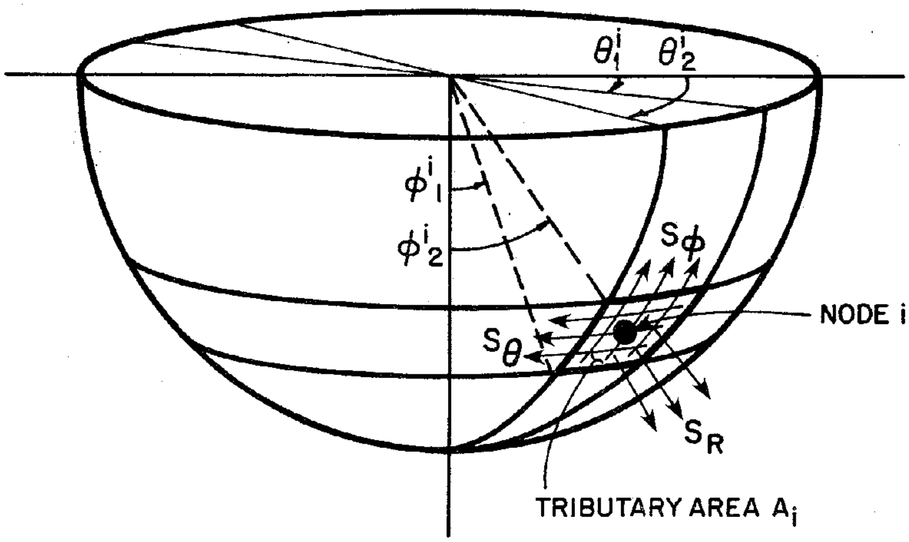

(a) CONTINUOUS FAR-FIELD IMPEDANCES

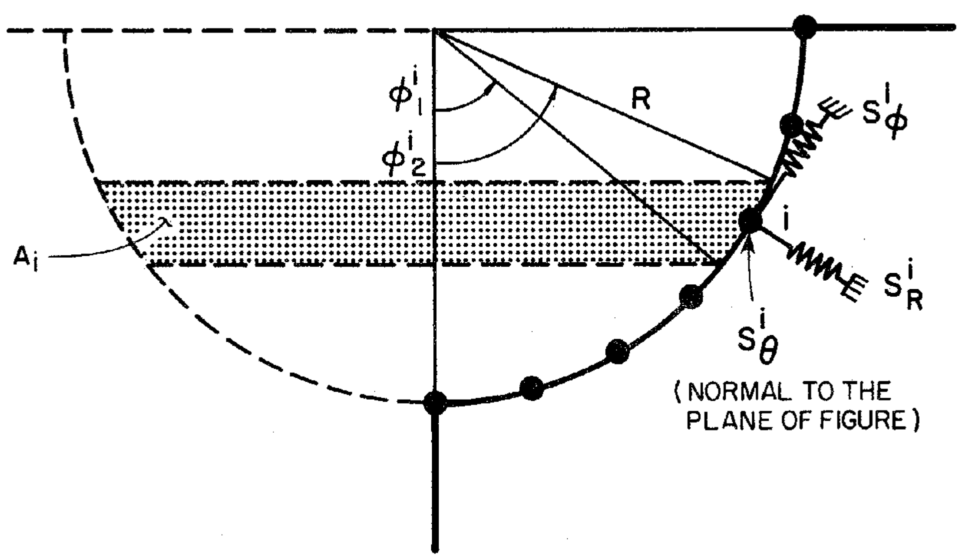

(b) DISCRETIZED IMPEDANCES IN AXISYMMETRIC FORMULATION

FIG. 4.1 FAR-FIELD MODELLING BY IMPEDANCE FUNCTIONS

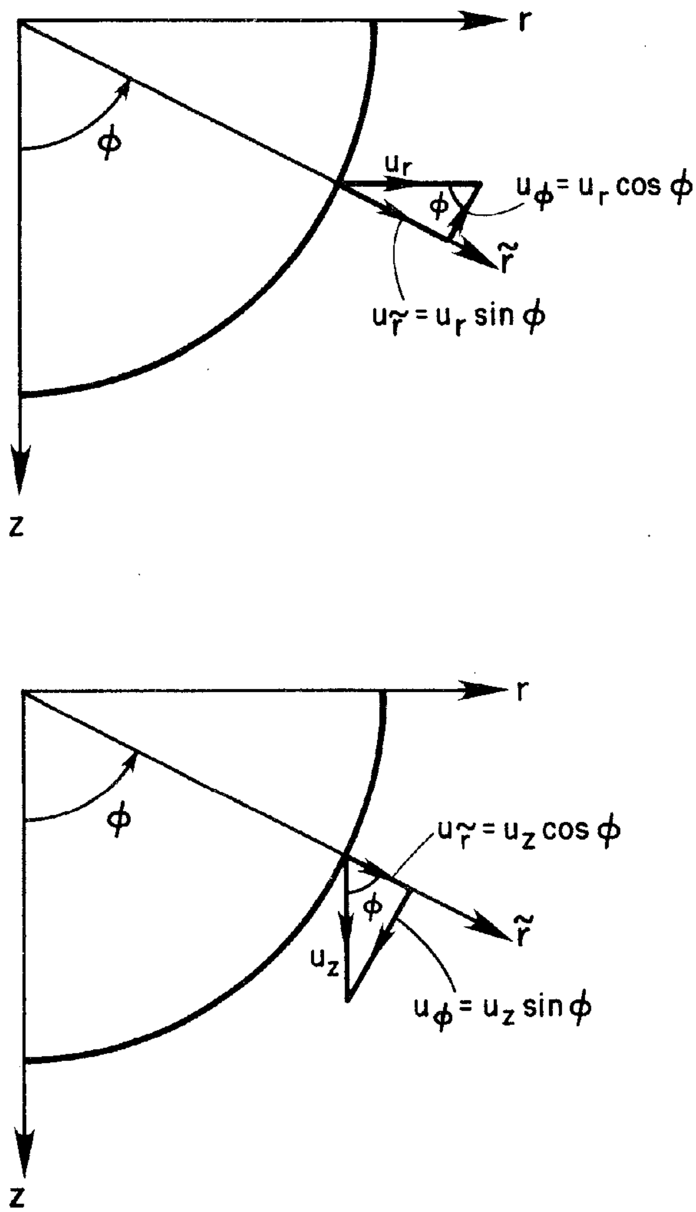

FIG. 4.2 RELATIONSHIP OF DISPLACEMENTS BETWEEN SPHERICAL AND CYLINDRICAL COORDINATES

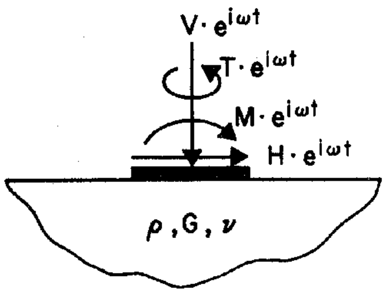

(a) APPLIED LOADING

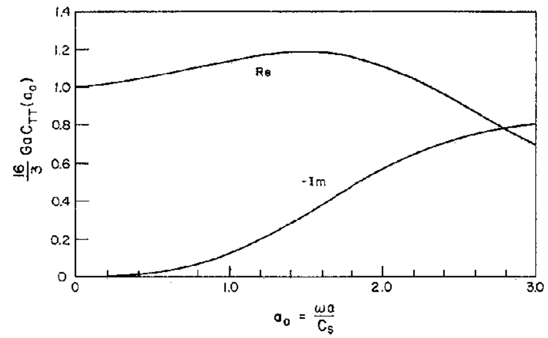

(b) TORSIONAL RESPONSE

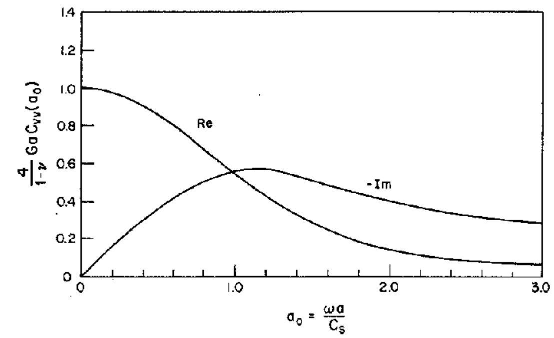

(c) VERTICAL RESPONSE

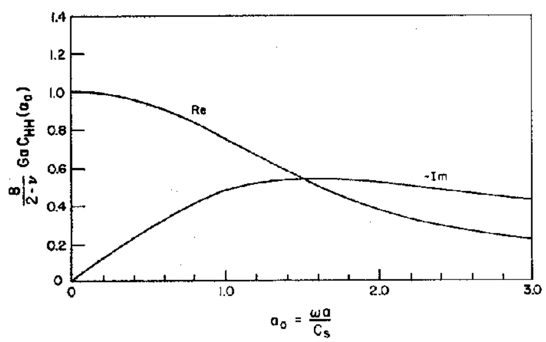

(d) TRANSLATIONAL RESPONSE

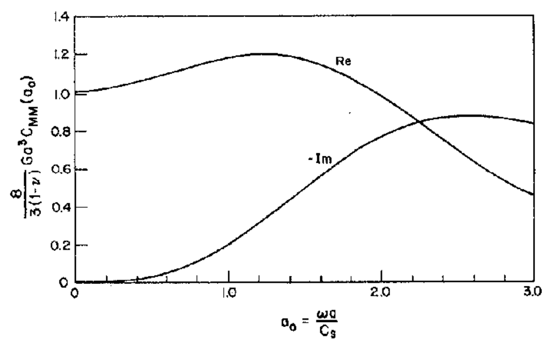

(e) ROCKING RESPONSE

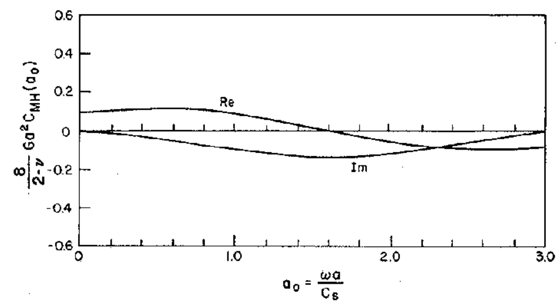

(f) COUPLING TERM

FIG. 4.3 ANALYTICAL SOLUTIONS FOR THE RIGID CIRCULAR PLATE

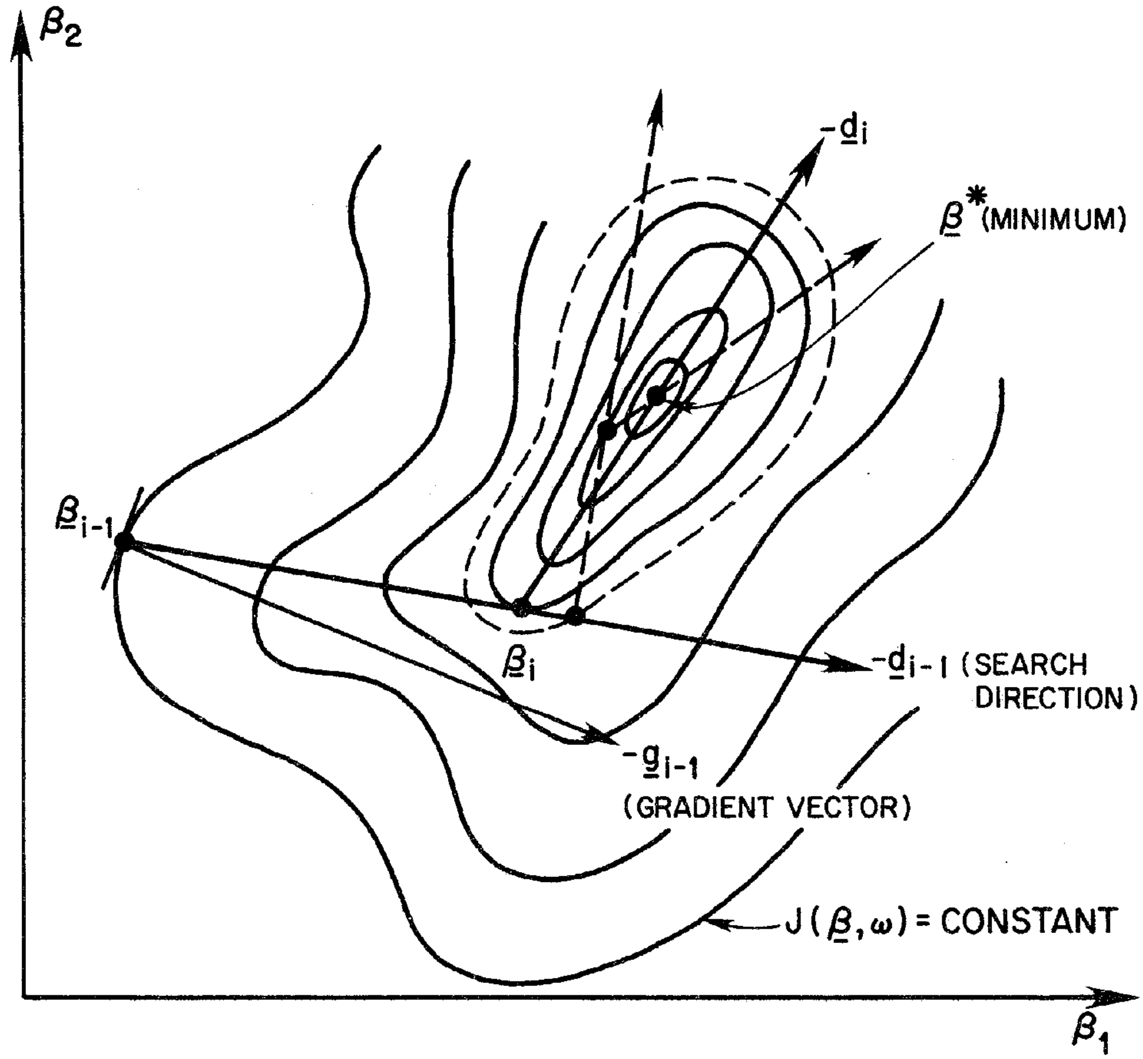

FIG. 4.4 ERROR SURFACE FOR TWO PARAMETERS

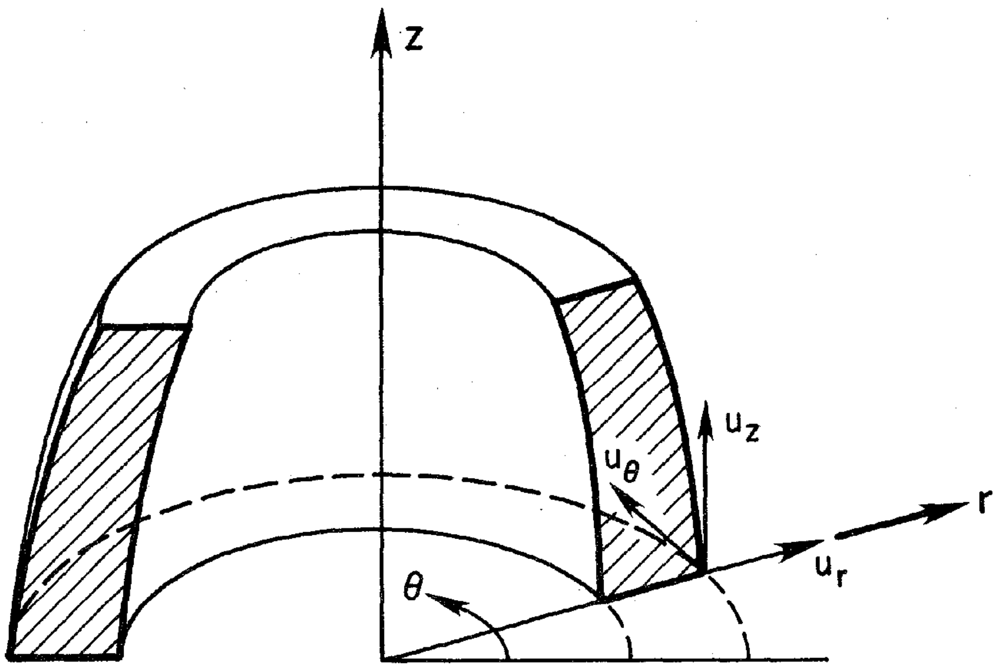

FIG. 5.1 AXISYMMETRIC SOLID IN CYLINDRICAL COORDINATE SYSTEM

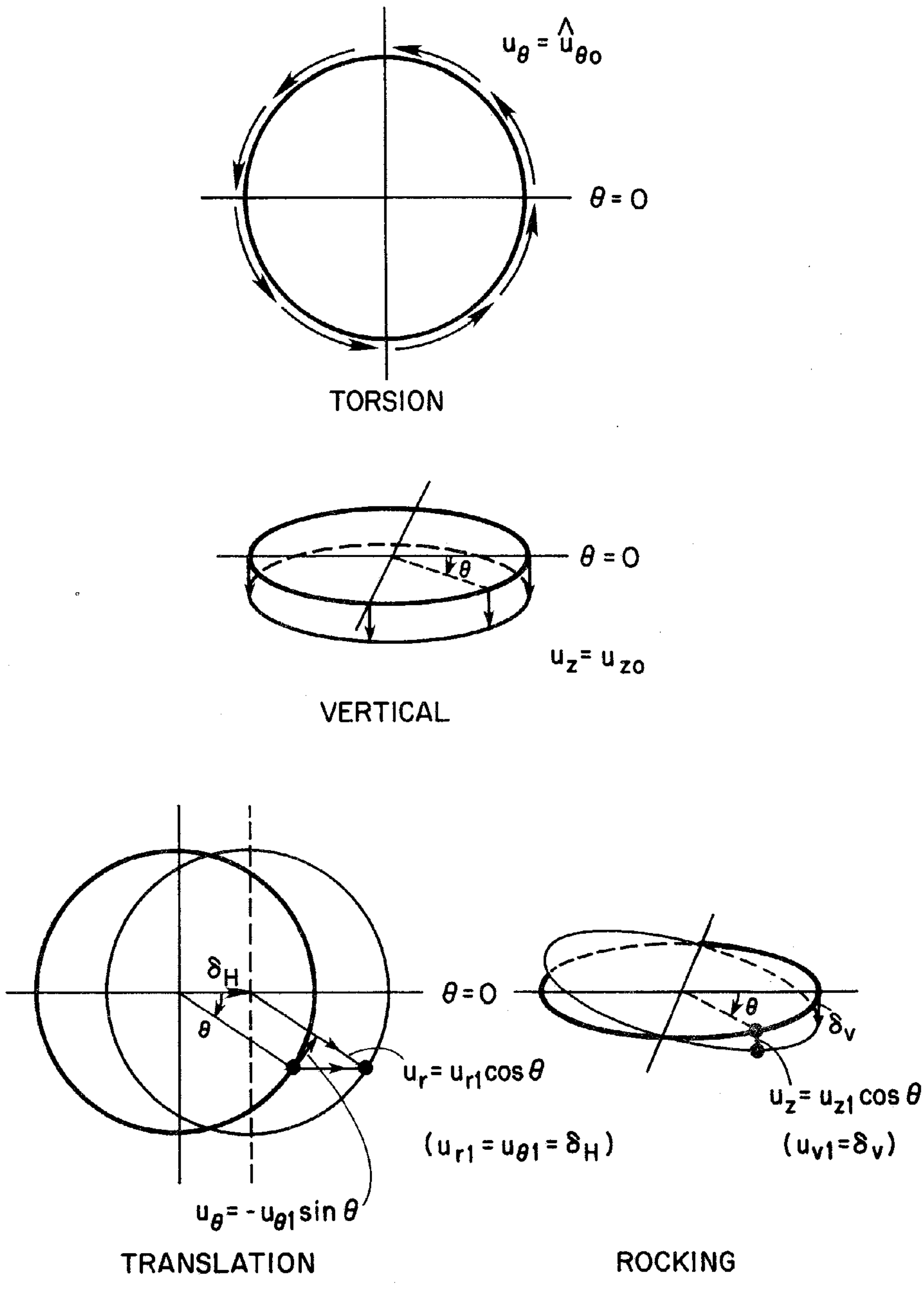

FIG. 5.2 DISPLACEMENT FIELDS DUE TO THE RIGID BODY MOTIONS OF THE CIRCULAR PLATE

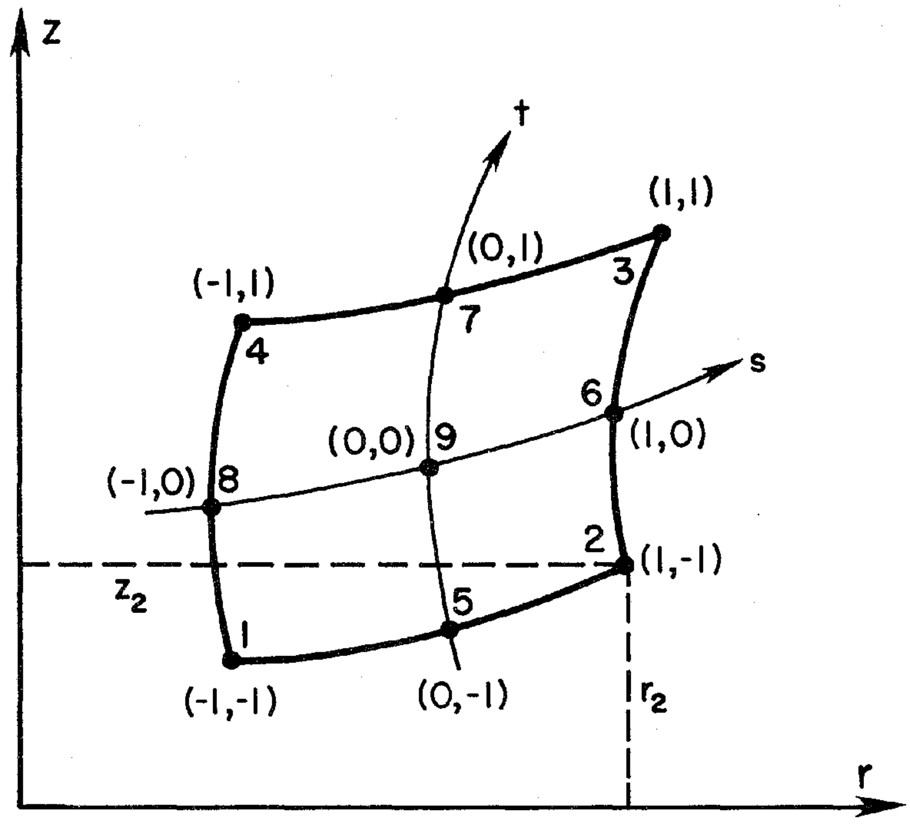

FIG. 5.3 ISOPARAMETRIC ELEMENT IN GLOBAL AND NATURAL COORDINATE SYSTEMS

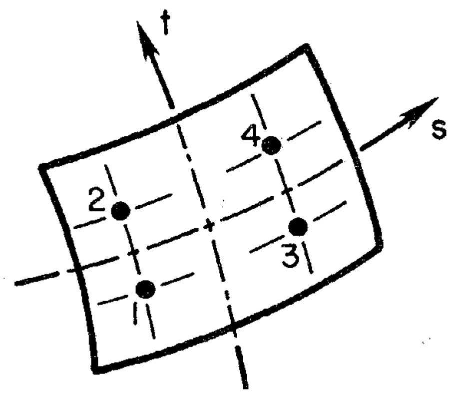

2 x 2 INTEGRATION POINTS

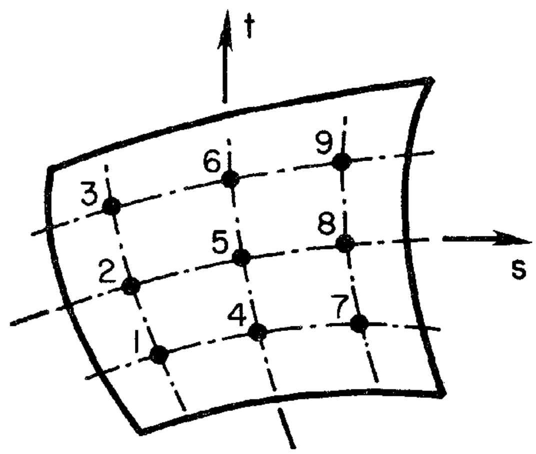

3 x 3 INTEGRATION POINTS

FIG. 5.4 INTEGRATION POINTS FOR THE QUADRILATERAL ELEMENT

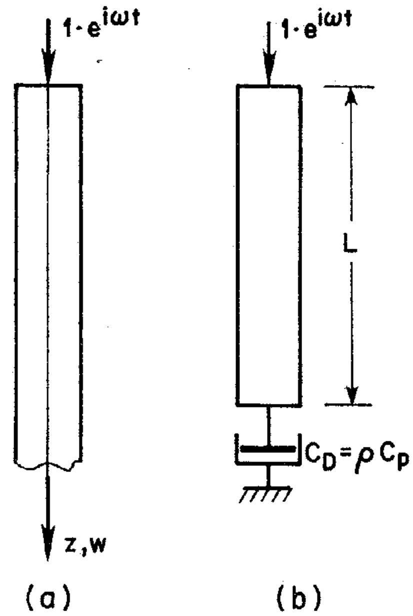

FIG. 5.5 FINITE MODEL OF SEMI-INFINITE ROD

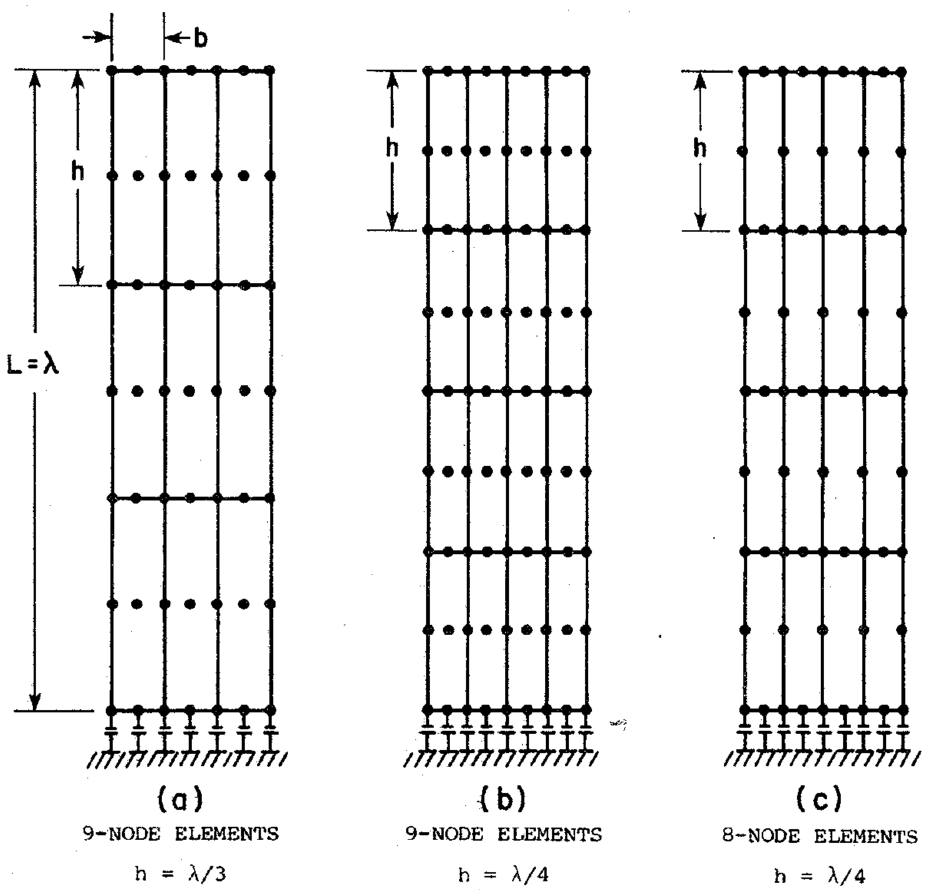

FIG. 5.6 FINITE ELEMENT MODELS

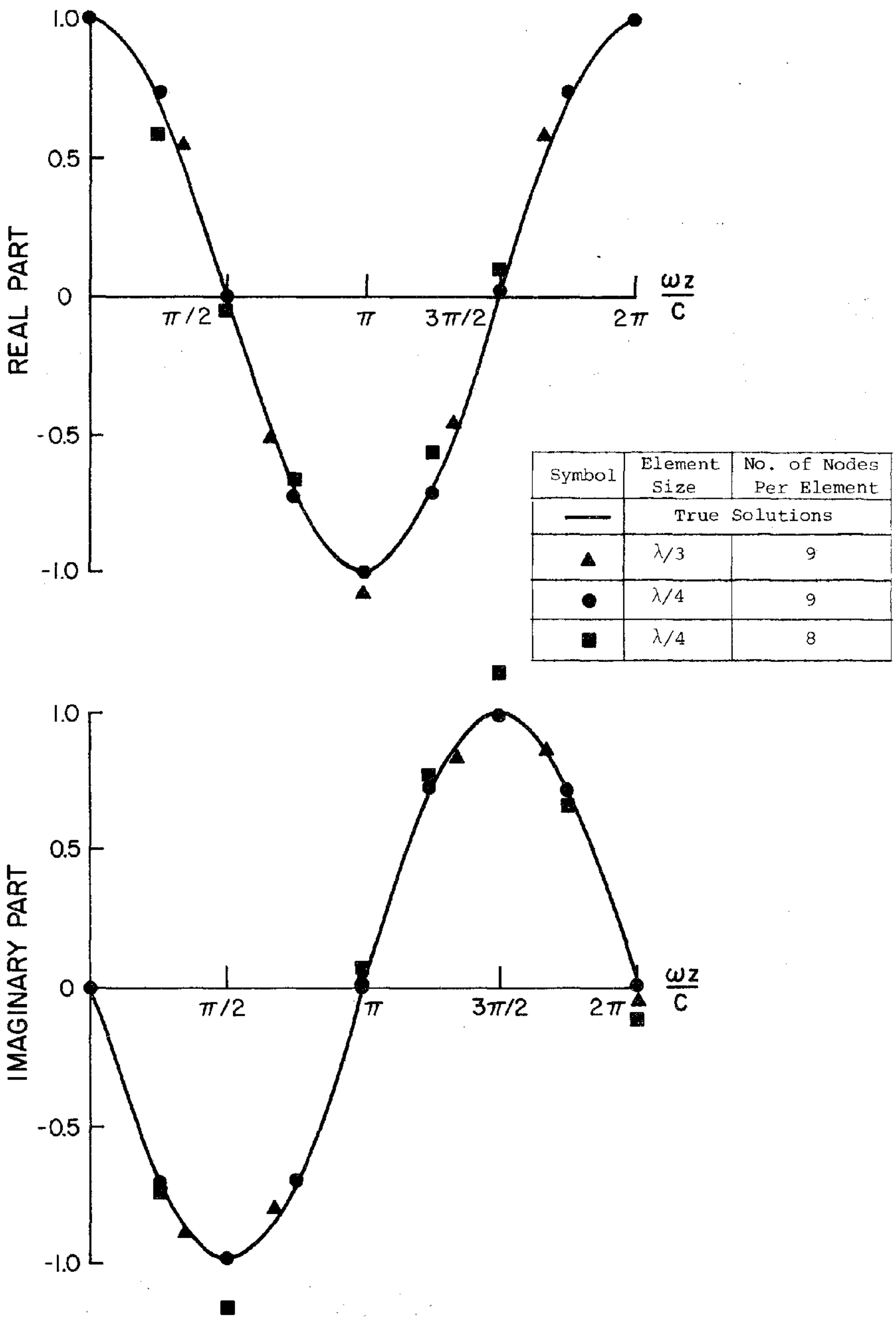

FIG. 5.7 FINITE ELEMENT ACCURACY FOR WAVE PROPAGATION

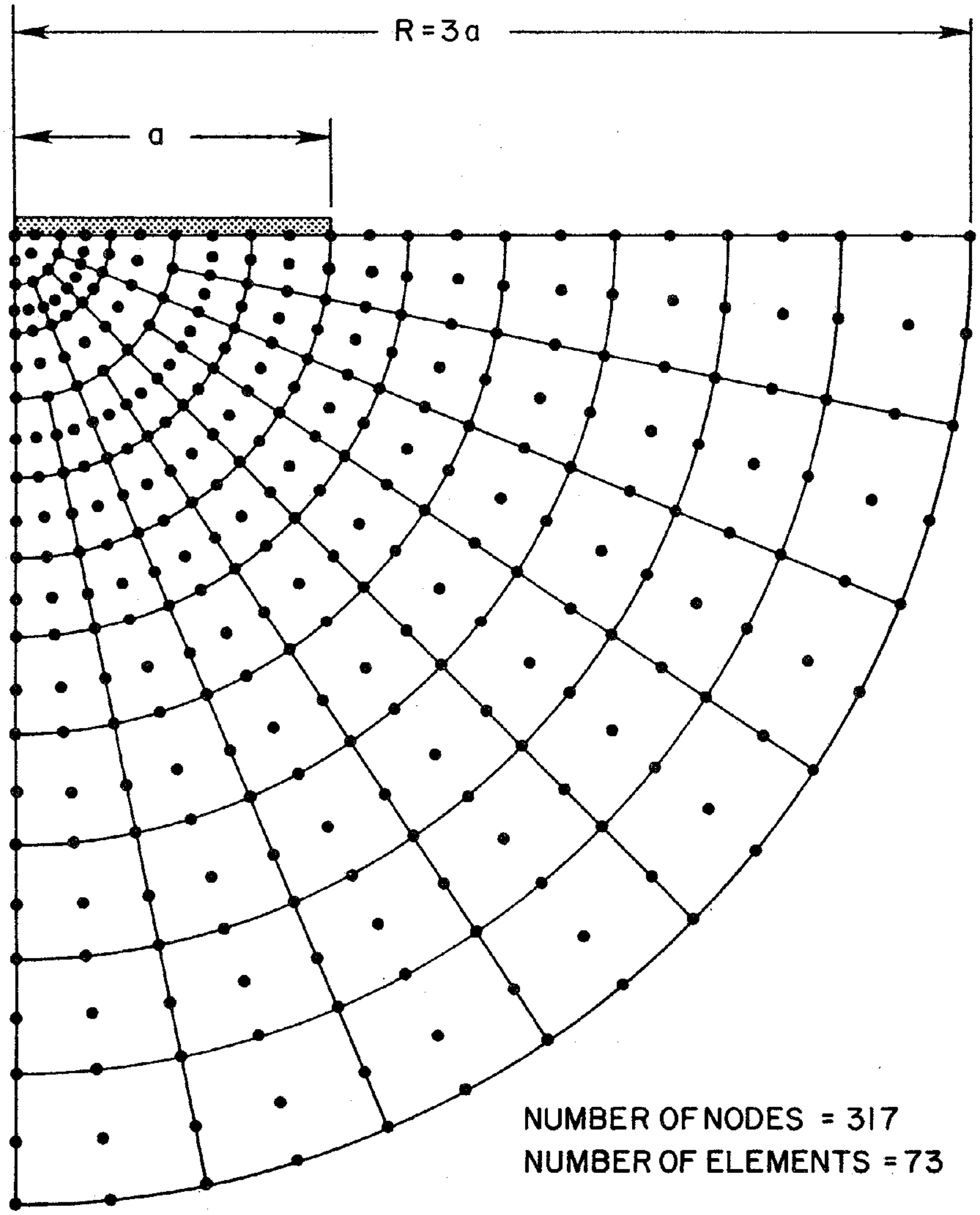

FIG. 5.8 NEAR-FIELD FINITE ELEMENT MESH FOR RIGID CIRCULAR PLATE

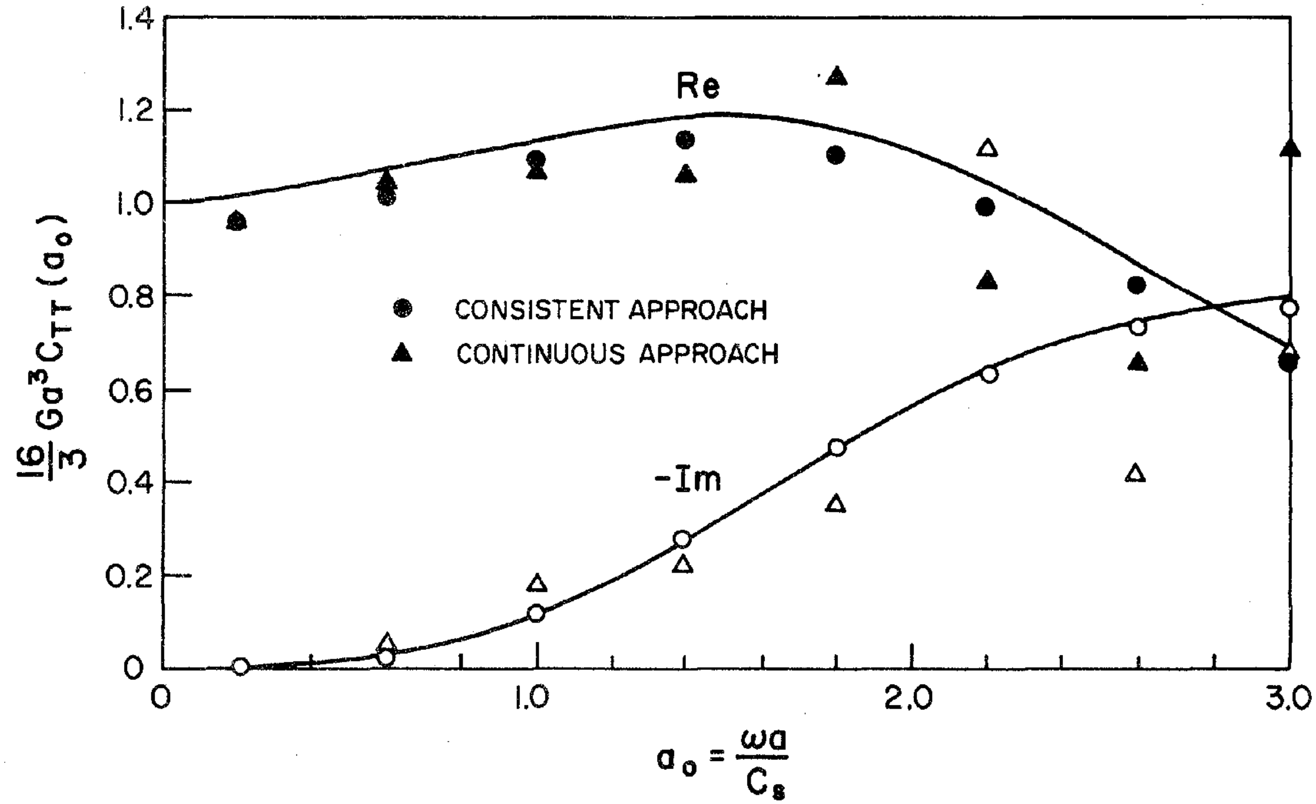

FIG. 6.1 COMPARISON OF TORSIONAL RESPONSE OF THE PLATE

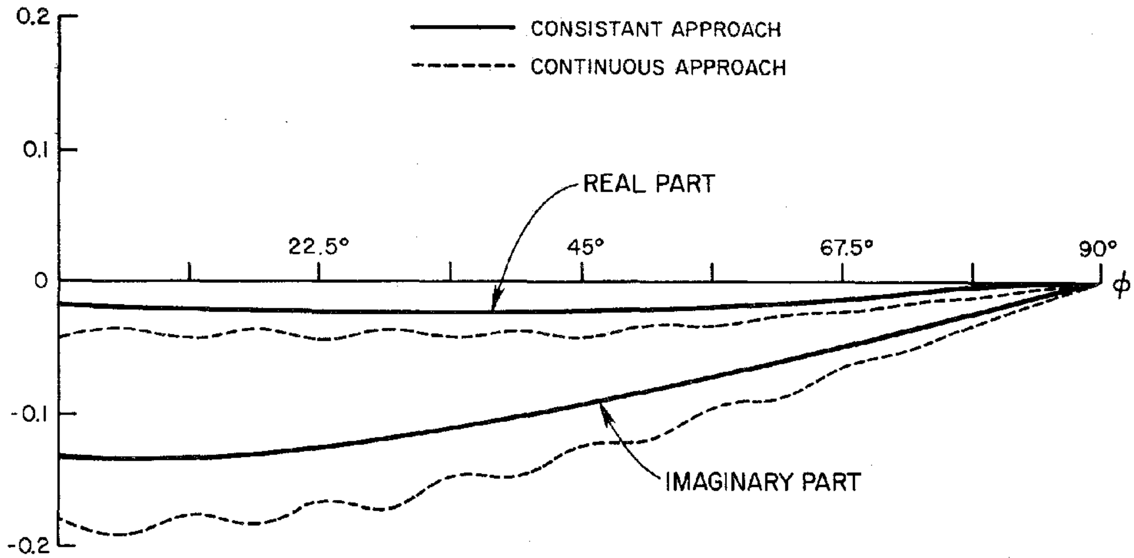

(a) $a_0 = 1.0$

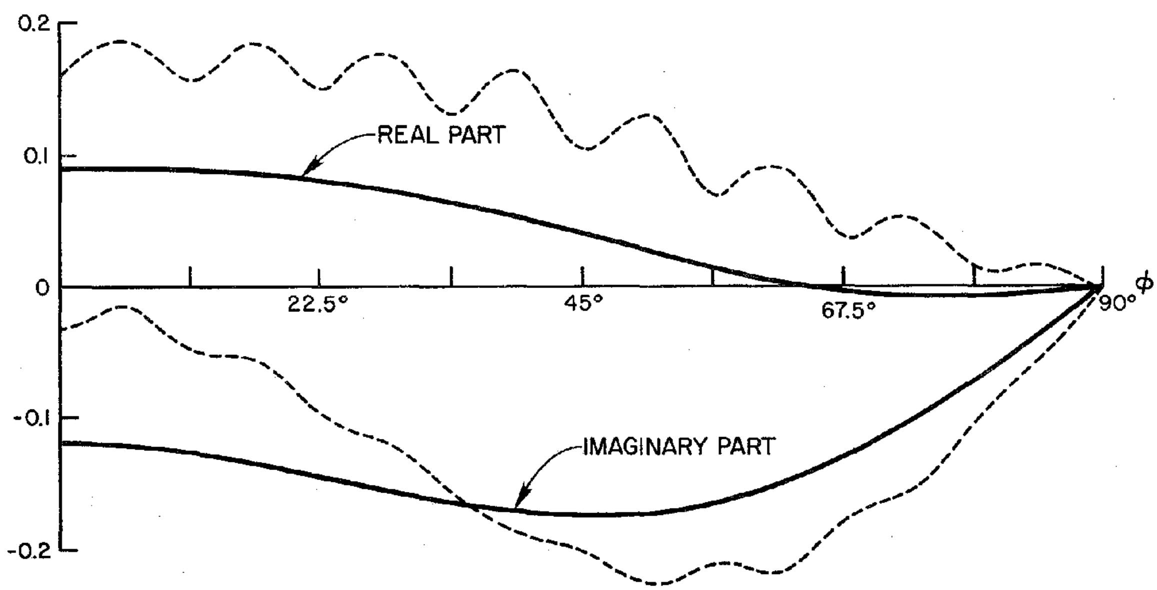

(b) $a_0 = 3.0$

FIG. 6.2 COMPARISON OF DISPLACEMENT FIELDS AT THE INTERFACE

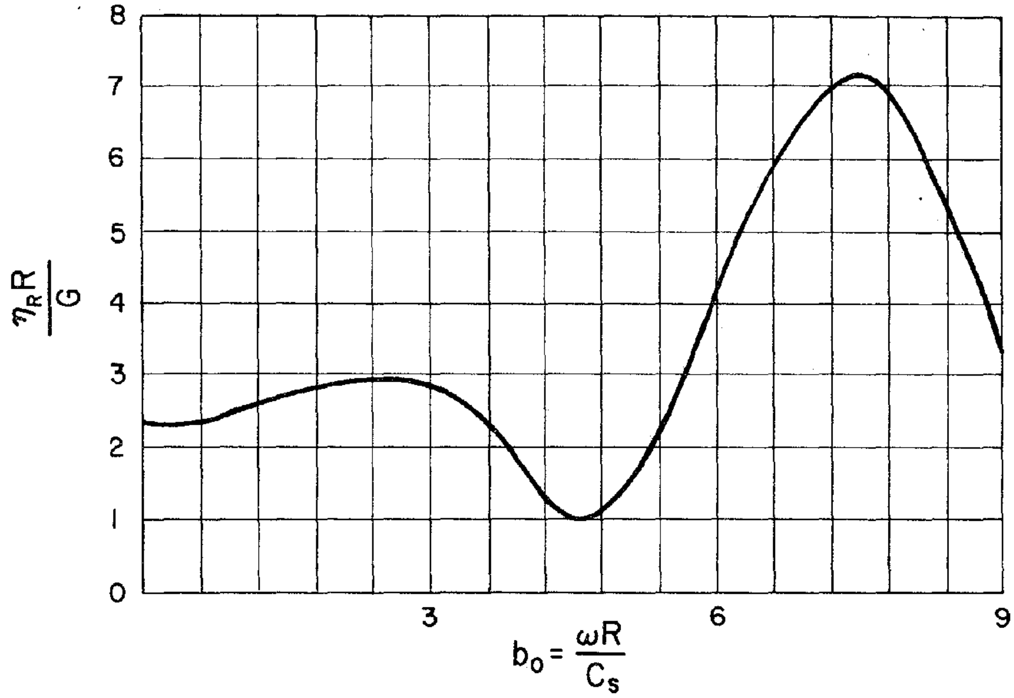

(a) REAL PART

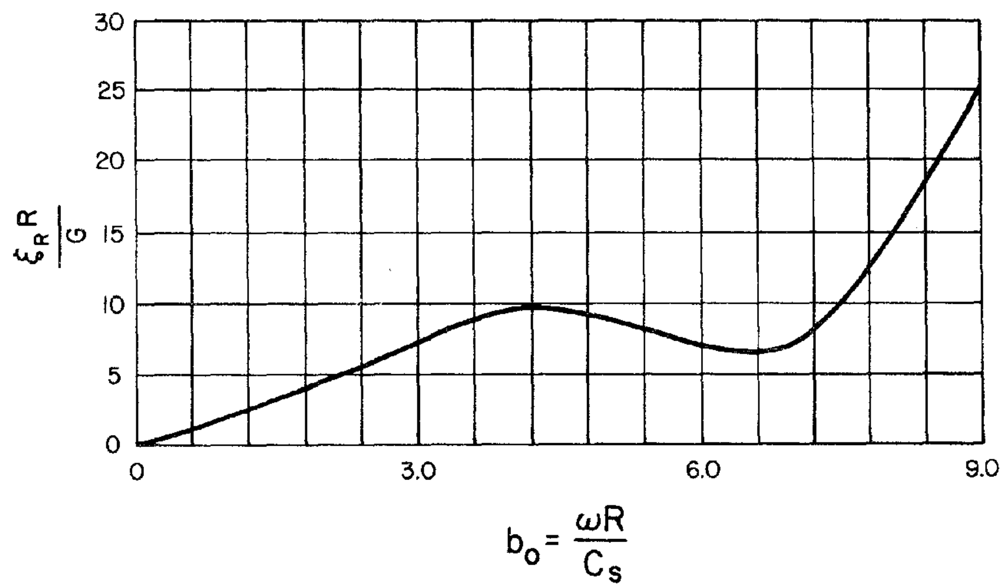

(b) IMAGINARY PART

FIG. 6.3 FAR-FIELD IMPEDANCE FUNCTIONS - NORMAL COMPONENT

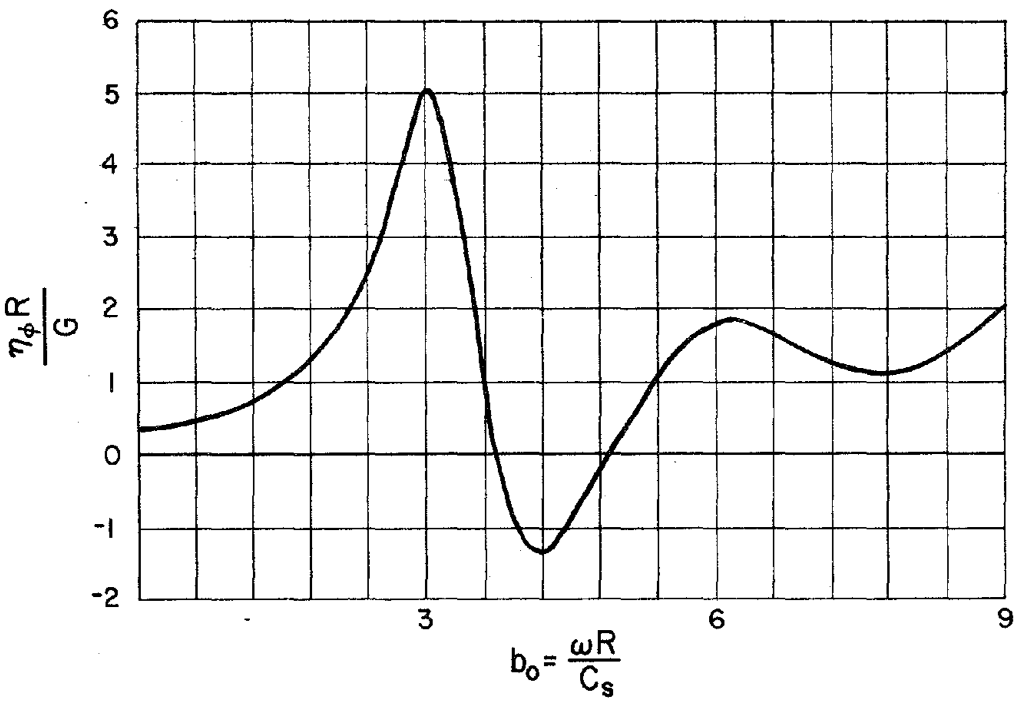

(a) REAL PART

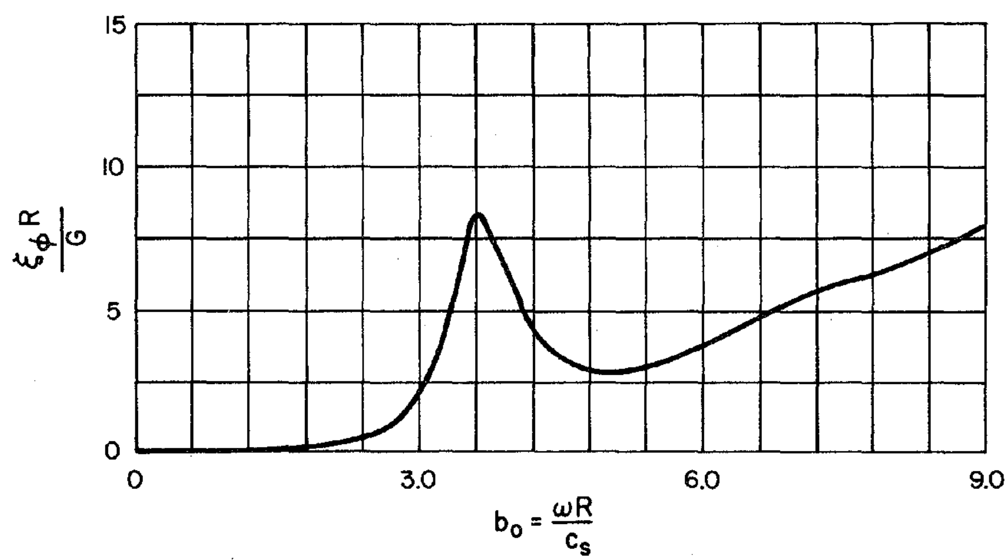

(b) IMAGINARY PART

FIG. 6.4 FAR-FIELD IMPEDANCE FUNCTIONS - TANGENTIAL COMPONENT

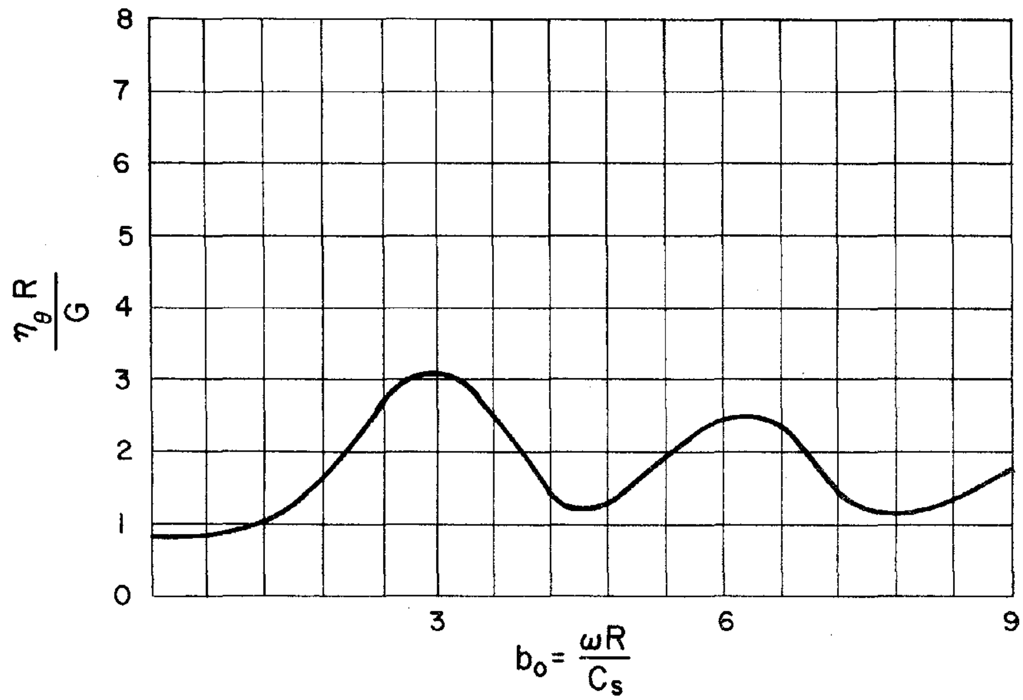

(a) REAL PART

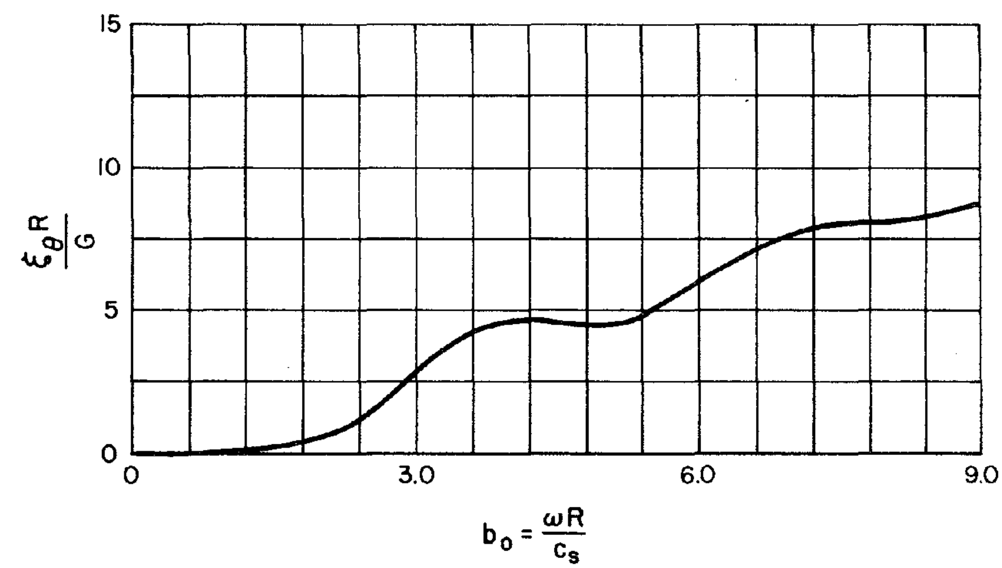

(b) IMAGINARY PART

FIG. 6.5 FAR-FIELD IMPEDANCE FUNCTIONS - CIRCUMFERENTIAL COMPONENT

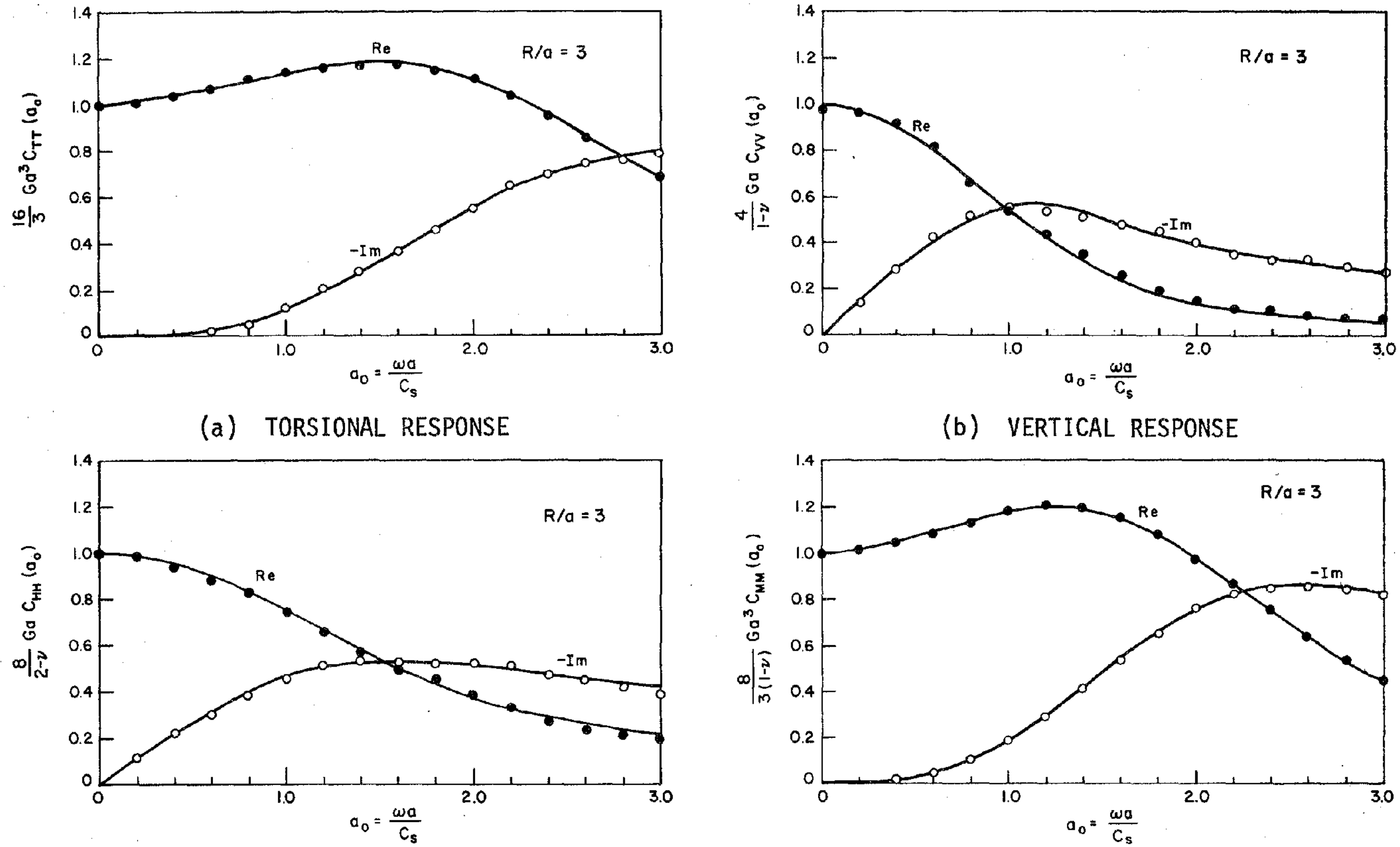

(a) TORSIONAL RESPONSE

(b) VERTICAL RESPONSE

(c) TRANSLATIONAL RESPONSE

(d) ROCKING RESPONSE

FIG. 6.6 COMPARISON OF PLATE COMPLIANCES USING IDENTIFIED IMPEDANCE FUNCTIONS

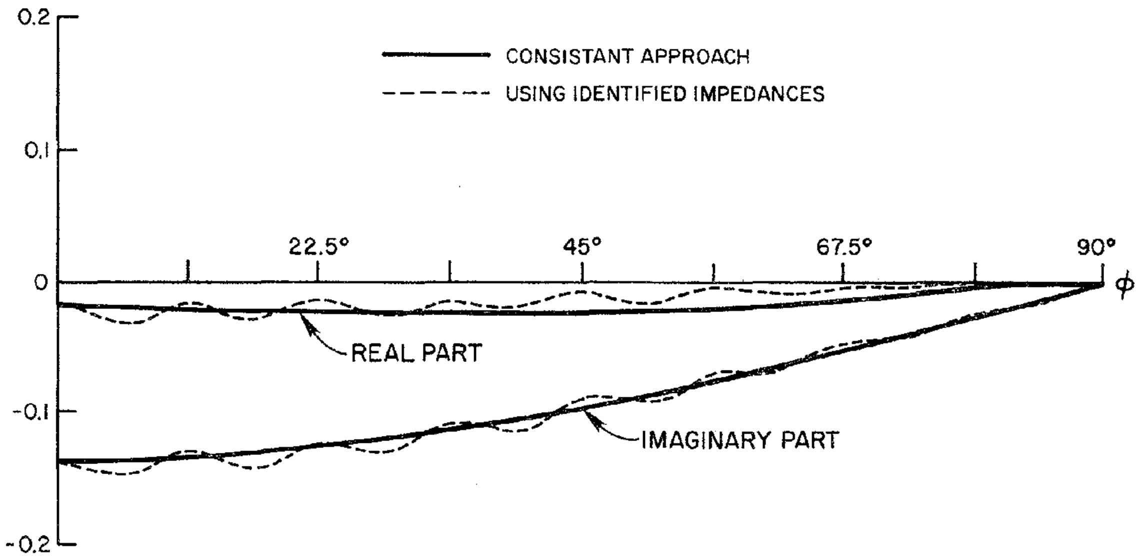

(a) a_0 = 1.0

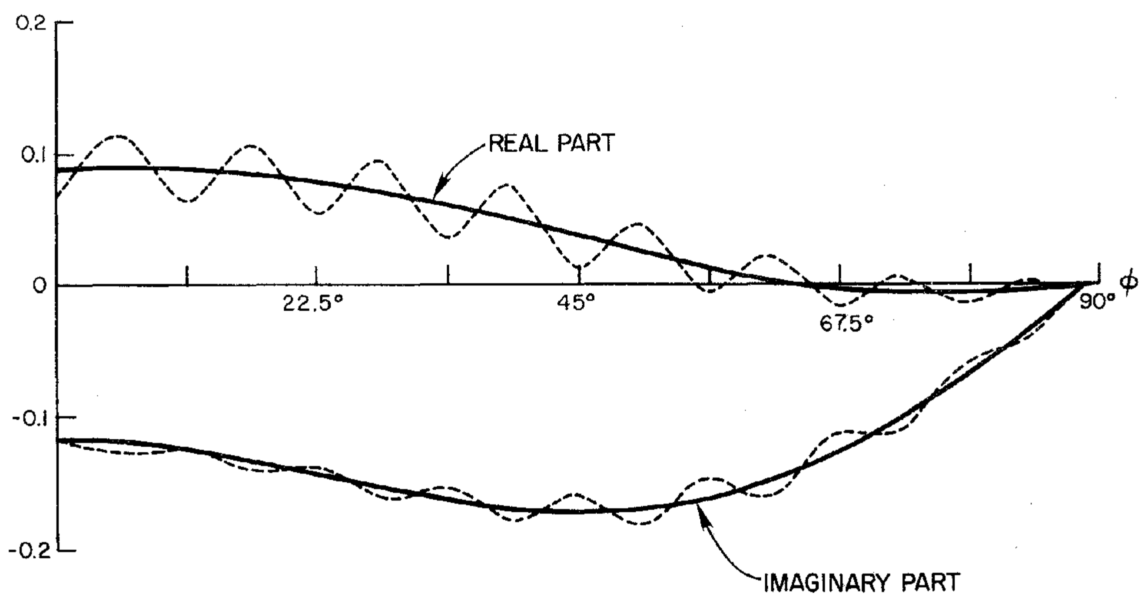

(b) a_0 = 3.0

FIG. 6.7 COMPARISON OF INTERFACE DISPLACEMENTS FOR TORSIONAL VIBRATIONS

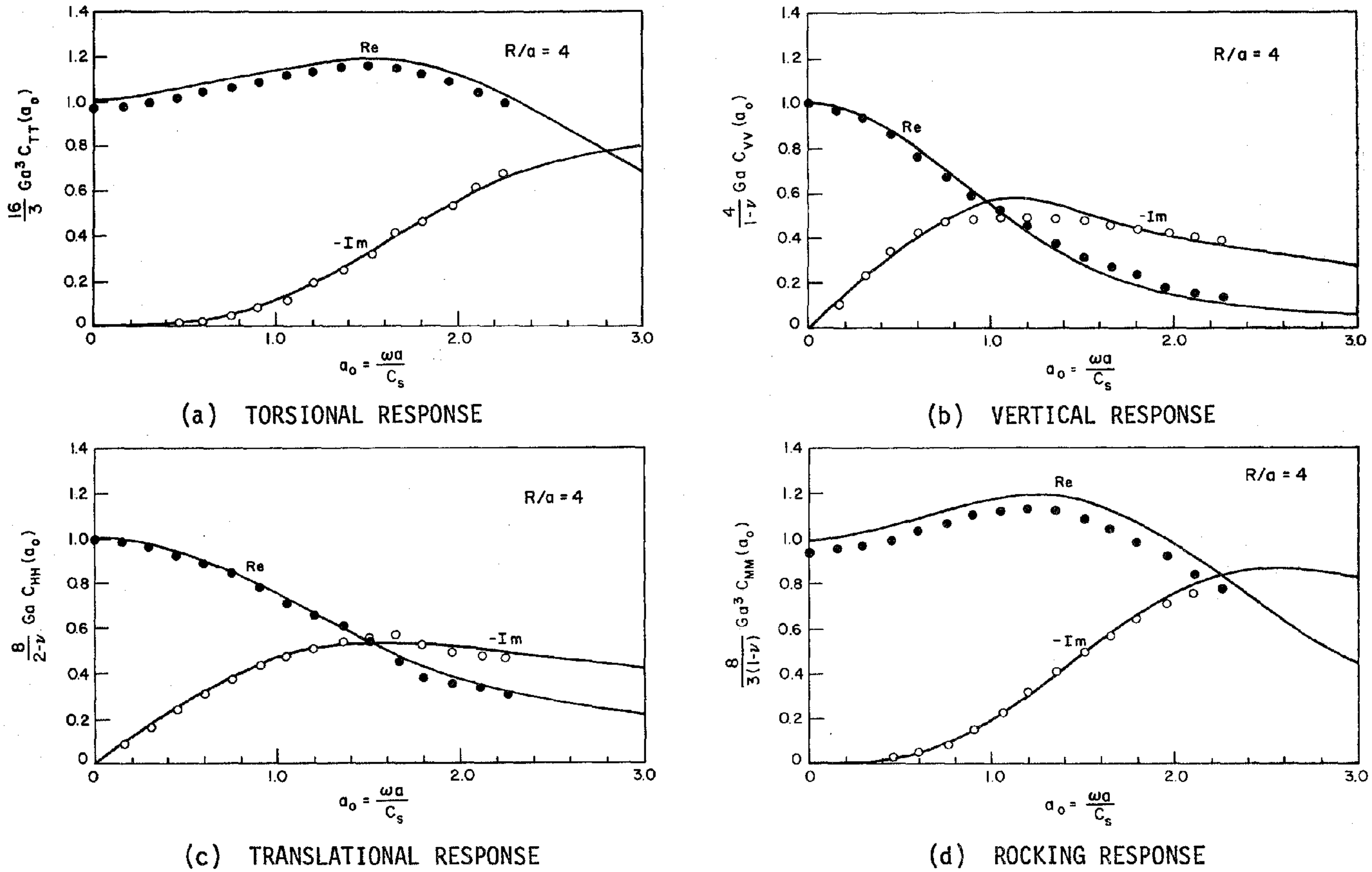

FIG. 6.8 COMPARISON OF PLATE COMPLIANCES USING IDENTIFIED IMPEDANCE FUNCTIONS

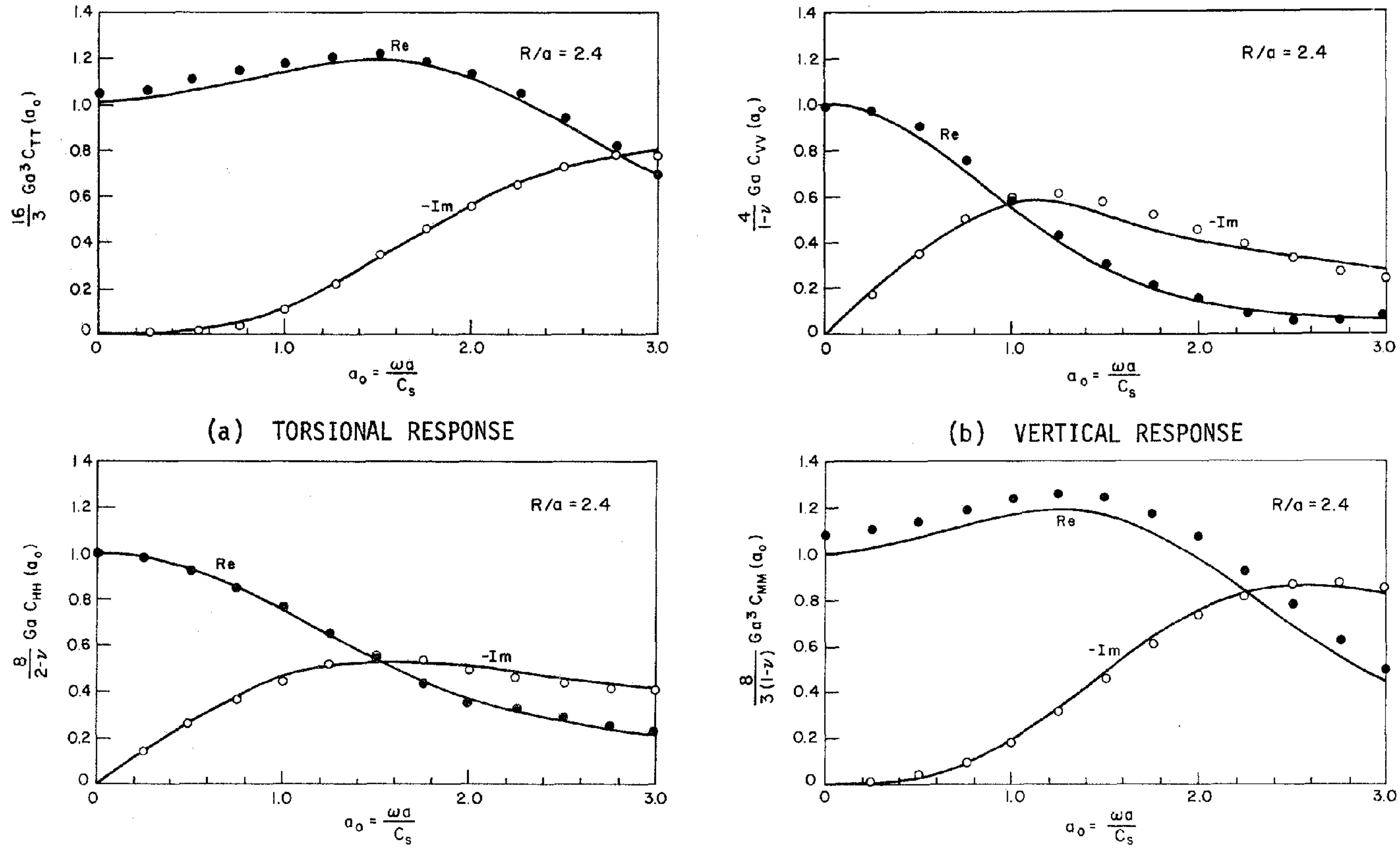

(a) TORSIONAL RESPONSE

(b) VERTICAL RESPONSE

(c) TRANSLATIONAL RESPONSE

(d) ROCKING RESPONSE

FIG. 6.9 COMPARISON OF PLATE COMPLIANCES USING IDENTIFIED IMPEDANCE FUNCTIONS

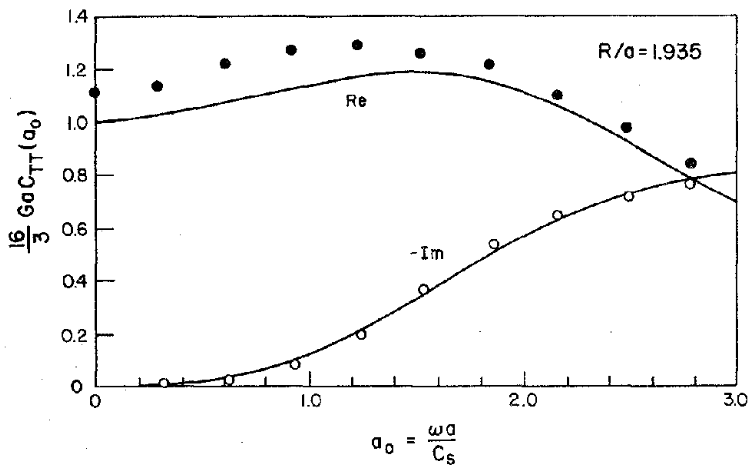

(a) TORSIONAL RESPONSE

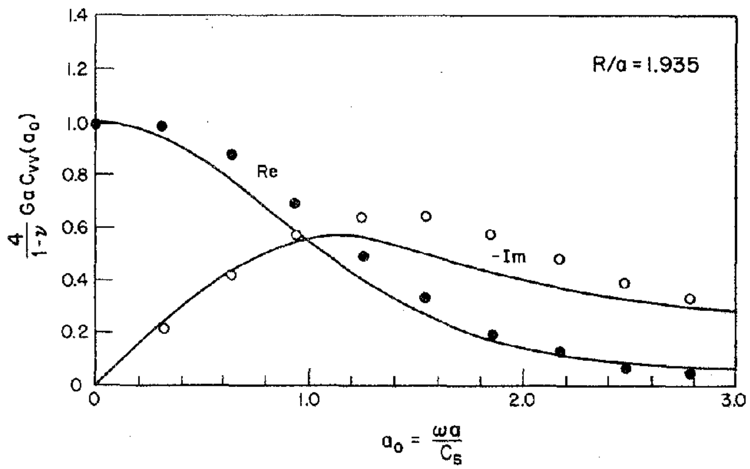

(b) VERTICAL RESPONSE

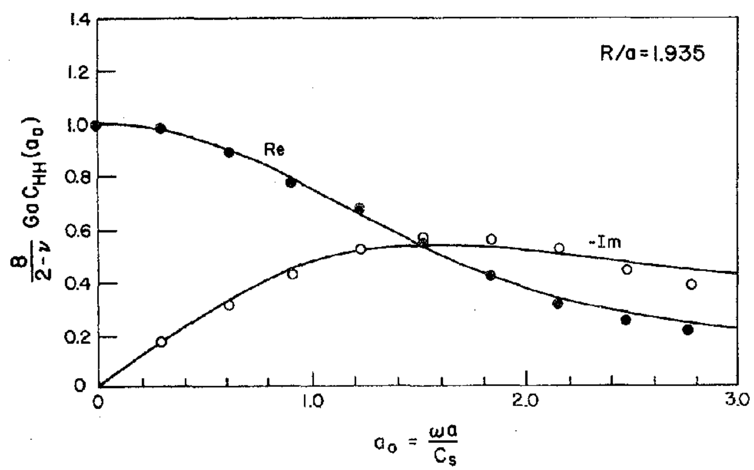

(c) TRANSALTIONAL RESPONSE

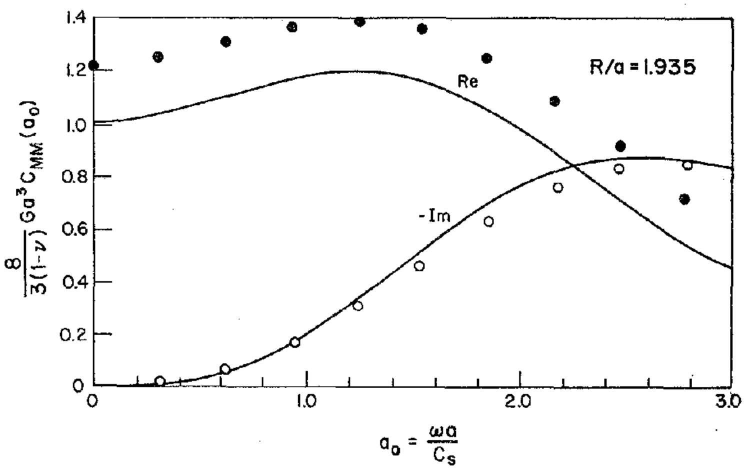

(d) ROCKING RESPONSE

FIG. 6.10 COMPARISON OF PLATE COMPLIANCES USING IDENTIFIED IMPEDANCE FUNCTIONS

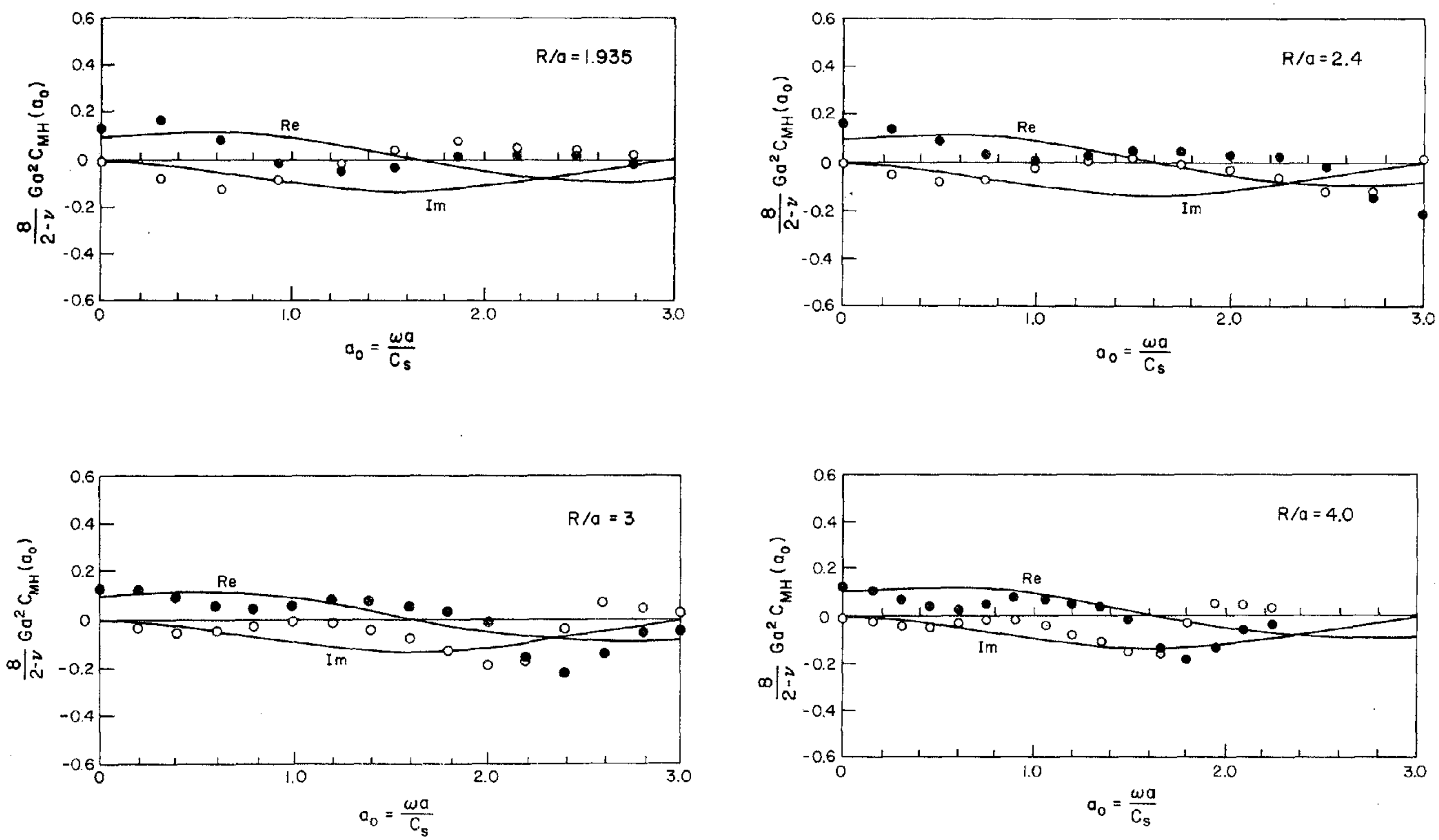

FIG. 6.11 COUPLING COMPLIANCES USING THE IDENTIFIED IMPEDANCE FUNCTIONS

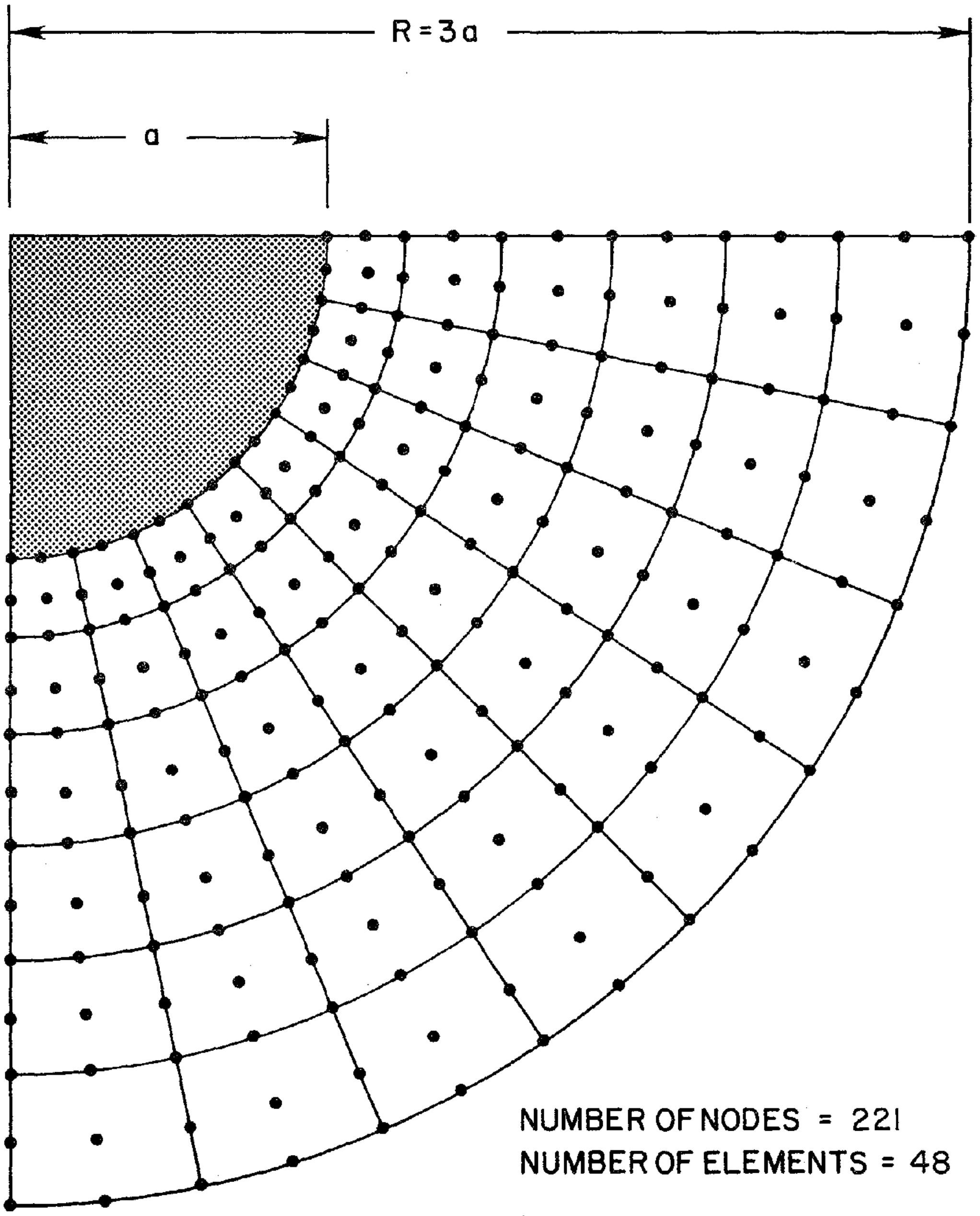

FIG. 6.12 NEAR-FIELD FINITE ELEMENT MESH FOR HEMISPHERICAL FOUNDATION

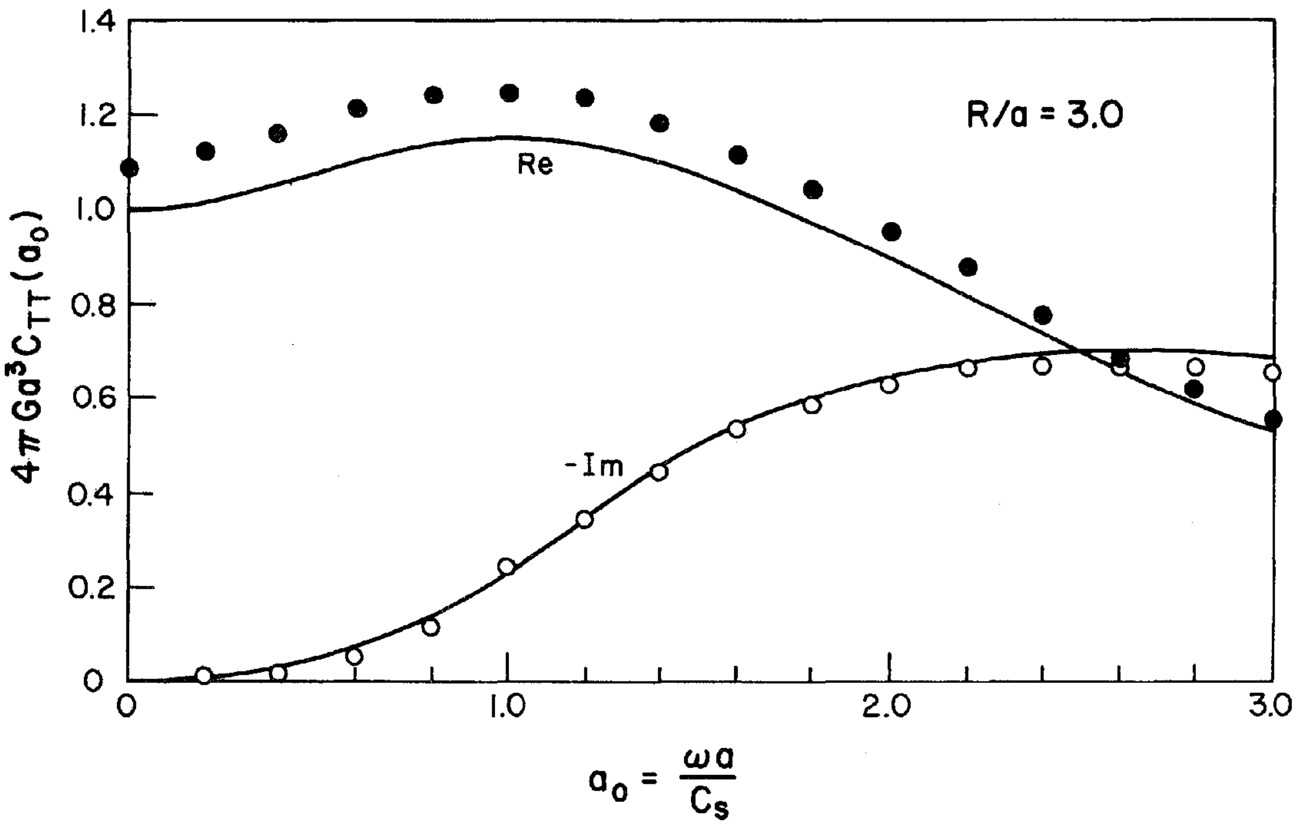

FIG. 6.13 TORSIONAL RESPONSE OF HEMISPHERICAL FOUNDATION
USING IDENTIFIED IMPEDANCE FUNCTIONS

EARTHQUAKE ENGINEERING RESEARCH CENTER REPORTS

NOTE: Numbers in parenthesis are Accession Numbers assigned by the National Technical Information Service; these are followed by a price code. Copies of the reports may be ordered from the National Technical Information Service, 5285 Port Royal Road, Springfield, Virginia, 22161. Accession Numbers should be quoted on orders for reports (PB --- ---) and remittance must accompany each order. Reports without this information were not available at time of printing. Upon request, EERC will mail inquirers this information when it becomes available.

EERC 67-1 "Feasibility Study Large-Scale Earthquake Simulator Facility," by J. Penzien, J.G. Bouwkamp, R.W. Clough and D. Rea - 1967 (PB 187 905)A07

EERC 68-1 Unassigned

EERC 68-2 "Inelastic Behavior of Beam-to-Column Subassemblages Under Repeated Loading," by V.V. Bertero - 1968 (PB 184 888)A05

EERC 68-3 "A Graphical Method for Solving the Wave Reflection-Refraction Problem," by H.D. McNiven and Y. Mengi - 1968 (PB 187 943)A03

EERC 68-4 "Dynamic Properties of McKinley School Buildings," by D. Rea, J.G. Bouwkamp and R.W. Clough - 1968 (PB 187 902)A07

EERC 68-5 "Characteristics of Rock Motions During Earthquakes," by H.B. Seed, I.M. Idriss and F.W. Kiefer - 1968 (PB 188 338)A03

EERC 69-1 "Earthquake Engineering Research at Berkeley," - 1969 (PB 187 906)A11

EERC 69-2 "Nonlinear Seismic Response of Earth Structures," by M. Dibaj and J. Penzien - 1969 (PB 187 904)A08

EERC 69-3 "Probabilistic Study of the Behavior of Structures During Earthquakes," by R. Ruiz and J. Penzien - 1969 (PB 187 886)A06

EERC 69-4 "Numerical Solution of Boundary Value Problems in Structural Mechanics by Reduction to an Initial Value Formulation," by N. Distefano and J. Schujman - 1969 (PB 187 942)A02

EERC 69-5 "Dynamic Programming and the Solution of the Biharmonic Equation," by N. Distefano - 1969 (PB 187 941)A03

EERC 69-6 "Stochastic Analysis of Offshore Tower Structures," by A.K. Malhotra and J. Penzien - 1969 (PB 187 903)A09

EERC 69-7 "Rock Motion Accelerograms for High Magnitude Earthquakes," by H.B. Seed and I.M. Idriss - 1969 (PB 187 940)A02

EERC 69-8 "Structural Dynamics Testing Facilities at the University of California, Berkeley," by R.M. Stephen, J.G. Bouwkamp, R.W. Clough and J. Penzien - 1969 (PB 189 111)A04

EERC 69-9 "Seismic Response of Soil Deposits Underlain by Sloping Rock Boundaries," by H. Dezfulian and H.B. Seed 1969 (PB 189 114)A03

EERC 69-10 "Dynamic Stress Analysis of Axisymmetric Structures Under Arbitrary Loading," by S. Ghosh and E.L. Wilson 1969 (PB 189 026)A10

EERC 69-11 "Seismic Behavior of Multistory Frames Designed by Different Philosophies," by J.C. Anderson and V. V. Bertero - 1969 (PB 190 662)A10

EERC 69-12 "Stiffness Degradation of Reinforcing Concrete Members Subjected to Cyclic Flexural Moments," by V.V. Bertero, B. Bresler and H. Ming Liao - 1969 (PB 202 942)A07

EERC 69-13 "Response of Non-Uniform Soil Deposits to Travelling Seismic Waves," by H. Dezfulian and H.B. Seed - 1969 (PB 191 023)A03

EERC 69-14 "Damping Capacity of a Model Steel Structure," by D. Rea, R.W. Clough and J.G. Bouwkamp - 1969 (PB 190 663)A06

EERC 69-15 "Influence of Local Soil Conditions on Building Damage Potential during Earthquakes," by H.B. Seed and I.M. Idriss - 1969 (PB 191 036)A03

EERC 69-16 "The Behavior of Sands Under Seismic Loading Conditions," by M.L. Silver and H.B. Seed - 1969 (AD 714 982)A07

EERC 70-1 "Earthquake Response of Gravity Dams," by A.K. Chopra - 1970 (AD 709 640)A03

EERC 70-2 "Relationships between Soil Conditions and Building Damage in the Caracas Earthquake of July 29, 1967," by H.B. Seed, I.M. Idriss and H. Dezfulian - 1970 (PB 195 762)A05

EERC 70-3 "Cyclic Loading of Full Size Steel Connections," by E.P. Popov and R.M. Stephen - 1970 (PB 213 545)A04

EERC 70-4 "Seismic Analysis of the Charaima Building, Caraballeda, Venezuela," by Subcommittee of the SEAONC Research Committee: V.V. Bertero, P.F. Fratessa, S.A. Mahin, J.H. Sexton, A.C. Scordelis, E.L. Wilson, L.A. Wyllie, H.B. Seed and J. Penzien, Chairman - 1970 (PB 201 455)A06

EERC 70-5 "A Computer Program for Earthquake Analysis of Dams," by A.K. Chopra and P. Chakrabarti - 1970 (AD 723 994)A05

EERC 70-6 "The Propagation of Love Waves Across Non-Horizontally Layered Structures," by J. Lysmer and L.A. Drake 1970 (PB 197 896)A03

EERC 70-7 "Influence of Base Rock Characteristics on Ground Response," by J. Lysmer, H.B. Seed and P.B. Schnabel 1970 (PB 197 897)A03

EERC 70-8 "Applicability of Laboratory Test Procedures for Measuring Soil Liquefaction Characteristics under Cyclic Loading," by H.B. Seed and W.H. Peacock - 1970 (PB 198 016)A03

EERC 70-9 "A Simplified Procedure for Evaluating Soil Liquefaction Potential," by H.B. Seed and I.M. Idriss - 1970 (PB 198 009)A03

EERC 70-10 "Soil Moduli and Damping Factors for Dynamic Response Analysis," by H.B. Seed and I.M. Idriss - 1970 (PB 197 869)A03

EERC 71-1 "Koyna Earthquake of December 11, 1967 and the Performance of Koyna Dam," by A.K. Chopra and P. Chakrabarti 1971 (AD 731 496)A06

EERC 71-2 "Preliminary In-Situ Measurements of Anelastic Absorption in Soils Using a Prototype Earthquake Simulator," by R.D. Borcherdt and P.W. Rodgers - 1971 (PB 201 454)A03

EERC 71-3 "Static and Dynamic Analysis of Inelastic Frame Structures," by F.L. Porter and G.H. Powell - 1971 (PB 210 135)A06

EERC 71-4 "Research Needs in Limit Design of Reinforced Concrete Structures," by V.V. Bertero - 1971 (PB 202 943)A04

EERC 71-5 "Dynamic Behavior of a High-Rise Diagonally Braced Steel Building," by D. Rea, A.A. Shah and J.G. Bouwkamp 1971 (PB 203 584)A06

EERC 71-6 "Dynamic Stress Analysis of Porous Elastic Solids Saturated with Compressible Fluids," by J. Ghaboussi and E. L. Wilson - 1971 (PB 211 396)A06

EERC 71-7 "Inelastic Behavior of Steel Beam-to-Column Subassemblages," by H. Krawinkler, V.V. Bertero and E.P. Popov 1971 (PB 211 335)A14

EERC 71-8 "Modification of Seismograph Records for Effects of Local Soil Conditions," by P. Schnabel, H.B. Seed and J. Lysmer - 1971 (PB 214 450)A03

EERC 72-1 "Static and Earthquake Analysis of Three Dimensional Frame and Shear Wall Buildings," by E.L. Wilson and H.H. Dovey - 1972 (PB 212 904)A05

EERC 72-2 "Accelerations in Rock for Earthquakes in the Western United States," by P.B. Schnabel and H.B. Seed - 1972 (PB 213 100)A03

EERC 72-3 "Elastic-Plastic Earthquake Response of Soil-Building Systems," by T. Minami - 1972 (PB 214 868)A08

EERC 72-4 "Stochastic Inelastic Response of Offshore Towers to Strong Motion Earthquakes," by M.K. Kaul - 1972 (PB 215 713)A05

EERC 72-5 "Cyclic Behavior of Three Reinforced Concrete Flexural Members with High Shear," by E.P. Popov, V.V. Bertero and H. Krawinkler - 1972 (PB 214 555)A05

EERC 72-6 "Earthquake Response of Gravity Dams Including Reservoir Interaction Effects," by P. Chakrabarti and A.K. Chopra - 1972 (AD 762 330)A08

EERC 72-7 "Dynamic Properties of Pine Flat Dam," by D. Rea, C.Y. Liaw and A.K. Chopra - 1972 (AD 763 928)A05

EERC 72-8 "Three Dimensional Analysis of Building Systems," by E.L. Wilson and H.H. Dovey - 1972 (PB 222 438)A06

EERC 72-9 "Rate of Loading Effects on Uncracked and Repaired Reinforced Concrete Members," by S. Mahin, V.V. Bertero, D. Rea and M. Atalay - 1972 (PB 224 520)A08

EERC 72-10 "Computer Program for Static and Dynamic Analysis of Linear Structural Systems," by E.L. Wilson, K.-J. Bathe, J.E. Peterson and H.H.Dovey - 1972 (PB 220 437)A04

EERC 72-11 "Literature Survey - Seismic Effects on Highway Bridges," by T. Iwasaki, J. Penzien and R.W. Clough - 1972 (PB 215 613)A19

EERC 72-12 "SHAKE-A Computer Program for Earthquake Response Analysis of Horizontally Layered Sites," by P.B. Schnabel and J. Lysmer - 1972 (PB 220 207)A06

EERC 73-1 "Optimal Seismic Design of Multistory Frames," by V.V. Bertero and H. Kamil - 1973

EERC 73-2 "Analysis of the Slides in the San Fernando Dams During the Earthquake of February 9, 1971," by H.B. Seed, K.L. Lee, I.M. Idriss and F. Makdisi - 1973 (PB 223 402)A14

EERC 73-3 "Computer Aided Ultimate Load Design of Unbraced Multistory Steel Frames," by M.B. El-Hafez and G.H. Powell 1973 (PB 248 315)A09

EERC 73-4 "Experimental Investigation into the Seismic Behavior of Critical Regions of Reinforced Concrete Components as Influenced by Moment and Shear," by M. Celebi and J. Penzien - 1973 (PB 215 884)A09

EERC 73-5 "Hysteretic Behavior of Epoxy-Repaired Reinforced Concrete Beams," by M. Celebi and J. Penzien - 1973 (PB 239 568)A03

EERC 73-6 "General Purpose Computer Program for Inelastic Dynamic Response of Plane Structures," by A. Kanaan and G.H. Powell - 1973 (PB 221 260)A08

EERC 73-7 "A Computer Program for Earthquake Analysis of Gravity Dams Including Reservoir Interaction," by P. Chakrabarti and A.K. Chopra - 1973 (AD 766 271)A04

EERC 73-8 "Behavior of Reinforced Concrete Deep Beam-Column Subassemblages Under Cyclic Loads," by O. Küstü and J.G. Bouwkamp - 1973 (PB 246 117)A12

EERC 73-9 "Earthquake Analysis of Structure-Foundation Systems," by A.K. Vaish and A.K. Chopra - 1973 (AD 766 272)A07

EERC 73-10 "Deconvolution of Seismic Response for Linear Systems," by R.B. Reimer - 1973 (PB 227 179)A08

EERC 73-11 "SAP IV: A Structural Analysis Program for Static and Dynamic Response of Linear Systems," by K.-J. Bathe, E.L. Wilson and F.E. Peterson - 1973 (PB 221 967)A09

EERC 73-12 "Analytical Investigations of the Seismic Response of Long, Multiple Span Highway Bridges," by W.S. Tseng and J. Penzien - 1973 (PB 227 816)A10

EERC 73-13 "Earthquake Analysis of Multi-Story Buildings Including Foundation Interaction," by A.K. Chopra and J.A. Gutierrez - 1973 (PB 222 970)A03

EERC 73-14 "ADAP: A Computer Program for Static and Dynamic Analysis of Arch Dams," by R.W. Clough, J.M. Raphael and S. Mojtahedi - 1973 (PB 223 763)A09

EERC 73-15 "Cyclic Plastic Analysis of Structural Steel Joints," by R.B. Pinkney and R.W. Clough - 1973 (PB 226 843)A08

EERC 73-16 "QUAD-4: A Computer Program for Evaluating the Seismic Response of Soil Structures by Variable Damping Finite Element Procedures," by I.M. Idriss, J. Lysmer, R. Hwang and H.B. Seed - 1973 (PB 229 424)A05

EERC 73-17 "Dynamic Behavior of a Multi-Story Pyramid Shaped Building," by R.M. Stephen, J.P. Hollings and J.G. Bouwkamp - 1973 (PB 240 718)A06

EERC 73-18 "Effect of Different Types of Reinforcing on Seismic Behavior of Short Concrete Columns," by V.V. Bertero, J. Hollings, O. Küstü, R.M. Stephen and J.G. Bouwkamp - 1973

EERC 73-19 "Olive View Medical Center Materials Studies, Phase I," by B. Bresler and V.V. Bertero - 1973 (PB 235 986)A06

EERC 73-20 "Linear and Nonlinear Seismic Analysis Computer Programs for Long Multiple-Span Highway Bridges," by W.S. Tseng and J. Penzien - 1973

EERC 73-21 "Constitutive Models for Cyclic Plastic Deformation of Engineering Materials," by J.M. Kelly and P.P. Gillis 1973 (PB 226 024)A03

EERC 73-22 "DRAIN - 2D User's Guide," by G.H. Powell - 1973 (PB 227 016)A05

EERC 73-23 "Earthquake Engineering at Berkeley - 1973," (PB 226 033)A11

EERC 73-24 Unassigned

EERC 73-25 "Earthquake Response of Axisymmetric Tower Structures Surrounded by Water," by C.Y. Liaw and A.K. Chopra 1973 (AD 773 052)A09

EERC 73-26 "Investigation of the Failures of the Olive View Stairtowers During the San Fernando Earthquake and Their Implications on Seismic Design," by V.V. Bertero and R.G. Collins - 1973 (PB 235 106)A13

EERC 73-27 "Further Studies on Seismic Behavior of Steel Beam-Column Subassemblages," by V.V. Bertero, H. Krawinkler and E.P. Popov - 1973 (PB 234 172)A06

EERC 74-1 "Seismic Risk Analysis," by C.S. Oliveira - 1974 (PB 235 920)A06

EERC 74-2 "Settlement and Liquefaction of Sands Under Multi-Directional Shaking," by R. Pyke, C.K. Chan and H.B. Seed 1974

EERC 74-3 "Optimum Design of Earthquake Resistant Shear Buildings," by D. Ray, K.S. Pister and A.K. Chopra - 1974 (PB 231 172)A06

EERC 74-4 "LUSH - A Computer Program for Complex Response Analysis of Soil-Structure Systems," by J. Lysmer, T. Udaka, H.B. Seed and R. Hwang - 1974 (PB 236 796)A05

EERC 74-5 "Sensitivity Analysis for Hysteretic Dynamic Systems: Applications to Earthquake Engineering," by D. Ray 1974 (PB 233 213)A06

EERC 74-6 "Soil Structure Interaction Analyses for Evaluating Seismic Response," by H.B. Seed, J. Lysmer and R. Hwang 1974 (PB 236 519)A04

EERC 74-7 Unassigned

EERC 74-8 "Shaking Table Tests of a Steel Frame - A Progress Report," by R.W. Clough and D. Tang - 1974 (PB 240 869)A03

EERC 74-9 "Hysteretic Behavior of Reinforced Concrete Flexural Members with Special Web Reinforcement," by V.V. Bertero, E.P. Popov and T.Y. Wang - 1974 (PB 236 797)A07

EERC 74-10 "Applications of Reliability-Based, Global Cost Optimization to Design of Earthquake Resistant Structures," by E. Vitiello and K.S. Pister - 1974 (PB 237 231)A06

EERC 74-11 "Liquefaction of Gravelly Soils Under Cyclic Loading Conditions," by R.T. Wong, H.B. Seed and C.K. Chan 1974 (PB 242 042)A03

EERC 74-12 "Site-Dependent Spectra for Earthquake-Resistant Design," by H.B. Seed, C. Ugas and J. Lysmer - 1974 (PB 240 953)A03

EERC 74-13 "Earthquake Simulator Study of a Reinforced Concrete Frame," by P. Hidalgo and R.W. Clough - 1974 (PB 241 944)A13

EERC 74-14 "Nonlinear Earthquake Response of Concrete Gravity Dams," by N. Pal - 1974 (AD/A 006 583)A06

EERC 74-15 "Modeling and Identification in Nonlinear Structural Dynamics - I. One Degree of Freedom Models," by N. Distefano and A. Rath - 1974 (PB 241 548)A06

EERC 75-1 "Determination of Seismic Design Criteria for the Dumbarton Bridge Replacement Structure, Vol. I: Description, Theory and Analytical Modeling of Bridge and Parameters," by F. Baron and S.-H. Pang - 1975 (PB 259 407)A15

EERC 75-2 "Determination of Seismic Design Criteria for the Dumbarton Bridge Replacement Structure, Vol. II: Numerical Studies and Establishment of Seismic Design Criteria," by F. Baron and S.-H. Pang - 1975 (PB 259 408)A11 (For set of EERC 75-1 and 75-2 (PB 259 406))

EERC 75-3 "Seismic Risk Analysis for a Site and a Metropolitan Area," by C.S. Oliveira - 1975 (PB 248 134)A09

EERC 75-4 "Analytical Investigations of Seismic Response of Short, Single or Multiple-Span Highway Bridges," by M.-C. Chen and J. Penzien - 1975 (PB 241 454)A09

EERC 75-5 "An Evaluation of Some Methods for Predicting Seismic Behavior of Reinforced Concrete Buildings," by S.A. Mahin and V.V. Bertero - 1975 (PB 246 306)A16

EERC 75-6 "Earthquake Simulator Study of a Steel Frame Structure, Vol. I: Experimental Results," by R.W. Clough and D.T. Tang - 1975 (PB 243 981)A13

EERC 75-7 "Dynamic Properties of San Bernardino Intake Tower," by D. Rea, C.-Y. Liaw and A.K. Chopra - 1975 (AD/A008 406) A05

EERC 75-8 "Seismic Studies of the Articulation for the Dumbarton Bridge Replacement Structure, Vol. I: Description, Theory and Analytical Modeling of Bridge Components," by F. Baron and R.E. Hamati - 1975 (PB 251 539)A07

EERC 75-9 "Seismic Studies of the Articulation for the Dumbarton Bridge Replacement Structure, Vol. 2: Numerical Studies of Steel and Concrete Girder Alternates," by F. Baron and R.E. Hamati - 1975 (PB 251 540)A10

EERC 75-10 "Static and Dynamic Analysis of Nonlinear Structures," by D.P. Mondkar and G.H. Powell - 1975 (PB 242 434)A08

EERC 75-11 "Hysteretic Behavior of Steel Columns," by E.P. Popov, V.V. Bertero and S. Chandramouli - 1975 (PB 252 365)A11

EERC 75-12 "Earthquake Engineering Research Center Library Printed Catalog," - 1975 (PB 243 711)A26

EERC 75-13 "Three Dimensional Analysis of Building Systems (Extended Version)," by E.L. Wilson, J.P. Hollings and H.H. Dovey - 1975 (PB 243 989)A07

EERC 75-14 "Determination of Soil Liquefaction Characteristics by Large-Scale Laboratory Tests," by P. De Alba, C.K. Chan and H.B. Seed - 1975 (NUREG 0027)A08

EERC 75-15 "A Literature Survey - Compressive, Tensile, Bond and Shear Strength of Masonry," by R.L. Mayes and R.W. Clough - 1975 (PB 246 292)A10

EERC 75-16 "Hysteretic Behavior of Ductile Moment Resisting Reinforced Concrete Frame Components," by V.V. Bertero and E.P. Popov - 1975 (PB 246 388)A05

EERC 75-17 "Relationships Between Maximum Acceleration, Maximum Velocity, Distance from Source, Local Site Conditions for Moderately Strong Earthquakes," by H.B. Seed, R. Murarka, J. Lysmer and I.M. Idriss - 1975 (PB 248 172)A03

EERC 75-18 "The Effects of Method of Sample Preparation on the Cyclic Stress-Strain Behavior of Sands," by J. Mulilis, C.K. Chan and H.B. Seed - 1975 (Summarized in EERC 75-28)

EERC 75-19 "The Seismic Behavior of Critical Regions of Reinforced Concrete Components as Influenced by Moment, Shear and Axial Force," by M.B. Atalay and J. Penzien - 1975 (PB 258 842)A11

EERC 75-20 "Dynamic Properties of an Eleven Story Masonry Building," by R.M. Stephen, J.P. Hollings, J.G. Bouwkamp and D. Jurukovski - 1975 (PB 246 945)A04

EERC 75-21 "State-of-the-Art in Seismic Strength of Masonry - An Evaluation and Review," by R.L. Mayes and R.W. Clough 1975 (PB 249 040)A07

EERC 75-22 "Frequency Dependent Stiffness Matrices for Viscoelastic Half-Plane Foundations," by A.K. Chopra, P. Chakrabarti and G. Dasgupta - 1975 (PB 248 121)A07

EERC 75-23 "Hysteretic Behavior of Reinforced Concrete Framed Walls," by T.Y. Wong, V.V. Bertero and E.P. Popov - 1975

EERC 75-24 "Testing Facility for Subassemblages of Frame-Wall Structural Systems," by V.V. Bertero, E.P. Popov and T. Endo - 1975

EERC 75-25 "Influence of Seismic History on the Liquefaction Characteristics of Sands," by H.B. Seed, K. Mori and C.K. Chan - 1975 (Summarized in EERC 75-28)

EERC 75-26 "The Generation and Dissipation of Pore Water Pressures during Soil Liquefaction," by H.B. Seed, P.P. Martin and J. Lysmer - 1975 (PB 252 648)A03

EERC 75-27 "Identification of Research Needs for Improving Aseismic Design of Building Structures," by V.V. Bertero 1975 (PB 248 136)A05

EERC 75-28 "Evaluation of Soil Liquefaction Potential during Earthquakes," by H.B. Seed, I. Arango and C.K. Chan - 1975 (NUREG 0026)A13

EERC 75-29 "Representation of Irregular Stress Time Histories by Equivalent Uniform Stress Series in Liquefaction Analyses," by H.B. Seed, I.M. Idriss, F. Makdisi and N. Banerjee - 1975 (PB 252 635)A03

EERC 75-30 "FLUSH - A Computer Program for Approximate 3-D Analysis of Soil-Structure Interaction Problems," by J. Lysmer, T. Udaka, C.-F. Tsai and H.B. Seed - 1975 (PB 259 332)A07

EERC 75-31 "ALUSH - A Computer Program for Seismic Response Analysis of Axisymmetric Soil-Structure Systems," by E. Berger, J. Lysmer and H.B. Seed - 1975

EERC 75-32 "TRIP and TRAVEL - Computer Programs for Soil-Structure Interaction Analysis with Horizontally Travelling Waves," by T. Udaka, J. Lysmer and H.B. Seed - 1975

EERC 75-33 "Predicting the Performance of Structures in Regions of High Seismicity," by J. Penzien - 1975 (PB 248 130)A03

EERC 75-34 "Efficient Finite Element Analysis of Seismic Structure - Soil - Direction," by J. Lysmer, H.B. Seed, T. Udaka, R.N. Hwang and C.-F. Tsai - 1975 (PB 253 570)A03

EERC 75-35 "The Dynamic Behavior of a First Story Girder of a Three-Story Steel Frame Subjected to Earthquake Loading," by R.W. Clough and L.-Y. Li - 1975 (PB 248 841)A05

EERC 75-36 "Earthquake Simulator Study of a Steel Frame Structure, Volume II - Analytical Results," by D.T. Tang - 1975 (PB 252 926)A10

EERC 75-37 "ANSR-I General Purpose Computer Program for Analysis of Non-Linear Structural Response," by D.P. Mondkar and G.H. Powell - 1975 (PB 252 386)A08

EERC 75-38 "Nonlinear Response Spectra for Probabilistic Seismic Design and Damage Assessment of Reinforced Concrete Structures," by M. Murakami and J. Penzien - 1975 (PB 259 530)A05

EERC 75-39 "Study of a Method of Feasible Directions for Optimal Elastic Design of Frame Structures Subjected to Earthquake Loading," by N.D. Walker and K.S. Pister - 1975 (PB 257 781)A06

EERC 75-40 "An Alternative Representation of the Elastic-Viscoelastic Analogy," by G. Dasgupta and J.L. Sackman - 1975 (PB 252 173)A03

EERC 75-41 "Effect of Multi-Directional Shaking on Liquefaction of Sands," by H.B. Seed, R. Pyke and G.R. Martin - 1975 (PB 258 781)A03

EERC 76-1 "Strength and Ductility Evaluation of Existing Low-Rise Reinforced Concrete Buildings - Screening Method," by T. Okada and B. Bresler - 1976 (PB 257 906)A11

EERC 76-2 "Experimental and Analytical Studies on the Hysteretic Behavior of Reinforced Concrete Rectangular and T-Beams," by S.-Y.M. Ma, E.P. Popov and V.V. Bertero - 1976 (PB 260 843)A12

EERC 76-3 "Dynamic Behavior of a Multistory Triangular-Shaped Building," by J. Petrovski, R.M. Stephen, E. Gartenbaum and J.G. Bouwkamp - 1976 (PB 273 279)A07

EERC 76-4 "Earthquake Induced Deformations of Earth Dams," by N. Serff, H.B. Seed, F.I. Makdisi & C.-Y. Chang - 1976 (PB 292 065)A08

EERC 76-5 "Analysis and Design of Tube-Type Tall Building Structures," by H. de Clercq and G.H. Powell - 1976 (PB 252 220) A10

EERC 76-6 "Time and Frequency Domain Analysis of Three-Dimensional Ground Motions, San Fernando Earthquake," by T. Kubo and J. Penzien (PB 260 556)A11

EERC 76-7 "Expected Performance of Uniform Building Code Design Masonry Structures," by R.L. Mayes, Y. Omote, S.W. Chen and R.W. Clough - 1976 (PB 270 098)A05

EERC 76-8 "Cyclic Shear Tests of Masonry Piers, Volume 1 - Test Results," by R.L. Mayes, Y. Omote, R.W. Clough - 1976 (PB 264 424)A06

EERC 76-9 "A Substructure Method for Earthquake Analysis of Structure - Soil Interaction," by J.A. Gutierrez and A.K. Chopra - 1976 (PB 257 783)A08

EERC 76-10 "Stabilization of Potentially Liquefiable Sand Deposits using Gravel Drain Systems," by H.B. Seed and J.R. Booker - 1976 (PB 258 820)A04

EERC 76-11 "Influence of Design and Analysis Assumptions on Computed Inelastic Response of Moderately Tall Frames," by G.H. Powell and D.G. Row - 1976 (PB 271 409)A06

EERC 76-12 "Sensitivity Analysis for Hysteretic Dynamic Systems: Theory and Applications," by D. Ray, K.S. Pister and E. Polak - 1976 (PB 262 859)A04

EERC 76-13 "Coupled Lateral Torsional Response of Buildings to Ground Shaking," by C.L. Kan and A.K. Chopra - 1976 (PB 257 907)A09

EERC 76-14 "Seismic Analyses of the Banco de America," by V.V. Bertero, S.A. Mahin and J.A. Hollings - 1976

EERC 76-15 "Reinforced Concrete Frame 2: Seismic Testing and Analytical Correlation," by R.W. Clough and J. Gidwani - 1976 (PB 261 323)A08

EERC 76-16 "Cyclic Shear Tests of Masonry Piers, Volume 2 - Analysis of Test Results," by R.L. Mayes, Y. Omote and R.W. Clough - 1976

EERC 76-17 "Structural Steel Bracing Systems: Behavior Under Cyclic Loading," by E.P. Popov, K. Takanashi and C.W. Roeder - 1976 (PB 260 715)A05

EERC 76-18 "Experimental Model Studies on Seismic Response of High Curved Overcrossings," by D. Williams and W.G. Godden - 1976 (PB 269 548)A08

EERC 76-19 "Effects of Non-Uniform Seismic Disturbances on the Dumbarton Bridge Replacement Structure," by F. Baron and R.E. Hamati - 1976 (PB 282 981)A16

EERC 76-20 "Investigation of the Inelastic Characteristics of a Single Story Steel Structure Using System Identification and Shaking Table Experiments," by V.C. Matzen and H.D. McNiven - 1976 (PB 258 453)A07

EERC 76-21 "Capacity of Columns with Splice Imperfections," by E.P. Popov, R.M. Stephen and R. Philbrick - 1976 (PB 260 378)A04

EERC 76-22 "Response of the Olive View Hospital Main Building during the San Fernando Earthquake," by S. A. Mahin, V.V. Bertero, A.K. Chopra and R. Collins - 1976 (PB 271 425)A14

EERC 76-23 "A Study on the Major Factors Influencing the Strength of Masonry Prisms," by N.M. Mostaghel, R.L. Mayes, R. W. Clough and S.W. Chen - 1976 (Not published)

EERC 76-24 "GADFLEA - A Computer Program for the Analysis of Pore Pressure Generation and Dissipation during Cyclic or Earthquake Loading," by J.R. Booker, M.S. Rahman and H.B. Seed - 1976 (PB 263 947)A04

EERC 76-25 "Seismic Safety Evaluation of a R/C School Building," by B. Bresler and J. Axley - 1976

EERC 76-26 "Correlative Investigations on Theoretical and Experimental Dynamic Behavior of a Model Bridge Structure," by K. Kawashima and J. Penzien - 1976 (PB 263 388)A11

EERC 76-27 "Earthquake Response of Coupled Shear Wall Buildings," by T. Srichatrapimuk - 1976 (PB 265 157)A07

EERC 76-28 "Tensile Capacity of Partial Penetration Welds," by E.P. Popov and R.M. Stephen - 1976 (PB 262 899)A03

EERC 76-29 "Analysis and Design of Numerical Integration Methods in Structural Dynamics," by H.M. Hilber - 1976 (PB 264 410)A06

EERC 76-30 "Contribution of a Floor System to the Dynamic Characteristics of Reinforced Concrete Buildings," by L.E. Malik and V.V. Bertero - 1976 (PB 272 247)A13

EERC 76-31 "The Effects of Seismic Disturbances on the Golden Gate Bridge," by F. Baron, M. Arikan and R.E. Hamati - 1976 (PB 272 279)A09

EERC 76-32 "Infilled Frames in Earthquake Resistant Construction," by R.E. Klingner and V.V. Bertero - 1976 (PB 265 892)A13

UCB/EERC-77/01 "PLUSH - A Computer Program for Probabilistic Finite Element Analysis of Seismic Soil-Structure Interaction," by M.P. Romo Organista, J. Lysmer and H.B. Seed - 1977

UCB/EERC-77/02 "Soil-Structure Interaction Effects at the Humboldt Bay Power Plant in the Ferndale Earthquake of June 7, 1975," by J.E. Valera, H.B. Seed, C.F. Tsai and J. Lysmer - 1977 (PB 265 795)A04

UCB/EERC-77/03 "Influence of Sample Disturbance on Sand Response to Cyclic Loading," by K. Mori, H.B. Seed and C.K. Chan - 1977 (PB 267 352)A04

UCB/EERC-77/04 "Seismological Studies of Strong Motion Records," by J. Shoja-Taheri - 1977 (PB 269 655)A10

UCB/EERC-77/05 "Testing Facility for Coupled-Shear Walls," by L. Li-Hyung, V.V. Bertero and E.P. Popov - 1977

UCB/EERC-77/06 "Developing Methodologies for Evaluating the Earthquake Safety of Existing Buildings," by No. 1 - B. Bresler; No. 2 - B. Bresler, T. Okada and D. Zisling; No. 3 - T. Okada and B. Bresler; No. 4 - V.V. Bertero and B. Bresler - 1977 (PB 267 354)A08

UCB/EERC-77/07 "A Literature Survey - Transverse Strength of Masonry Walls," by Y. Omote, R.L. Mayes, S.W. Chen and R.W. Clough - 1977 (PB 277 933)A07

UCB/EERC-77/08 "DRAIN-TABS: A Computer Program for Inelastic Earthquake Response of Three Dimensional Buildings," by R. Guendelman-Israel and G.H. Powell - 1977 (PB 270 693)A07

UCB/EERC-77/09 "SUBWALL: A Special Purpose Finite Element Computer Program for Practical Elastic Analysis and Design of Structural Walls with Substructure Option," by D.Q. Le, H. Peterson and E.P. Popov - 1977 (PB 270 567)A05

UCB/EERC-77/10 "Experimental Evaluation of Seismic Design Methods for Broad Cylindrical Tanks," by D.P. Clough (PB 272 280)A13

UCB/EERC-77/11 "Earthquake Engineering Research at Berkeley - 1976," - 1977 (PB 273 507)A09

UCB/EERC-77/12 "Automated Design of Earthquake Resistant Multistory Steel Building Frames," by N.D. Walker, Jr. - 1977 (PB 276 526)A09

UCB/EERC-77/13 "Concrete Confined by Rectangular Hoops Subjected to Axial Loads," by J. Vallenas, V.V. Bertero and E.P. Popov - 1977 (PB 275 165)A06

UCB/EERC-77/14 "Seismic Strain Induced in the Ground During Earthquakes," by Y. Sugimura - 1977 (PB 284 201)A04

UCB/EERC-77/15 "Bond Deterioration under Generalized Loading," by V.V. Bertero, E.P. Popov and S. Viwathanatepa - 1977

UCB/EERC-77/16 "Computer Aided Optimum Design of Ductile Reinforced Concrete Moment Resisting Frames," by S.W. Zagajeski and V.V. Bertero - 1977 (PB 280 137)A07

UCB/EERC-77/17 "Earthquake Simulation Testing of a Stepping Frame with Energy-Absorbing Devices," by J.M. Kelly and D.F. Tsztoo - 1977 (PB 273 506)A04

UCB/EERC-77/18 "Inelastic Behavior of Eccentrically Braced Steel Frames under Cyclic Loadings," by C.W. Roeder and E.P. Popov - 1977 (PB 275 526)A15

UCB/EERC-77/19 "A Simplified Procedure for Estimating Earthquake-Induced Deformations in Dams and Embankments," by F.I. Makdisi and H.B. Seed - 1977 (PB 276 820)A04

UCB/EERC-77/20 "The Performance of Earth Dams during Earthquakes," by H.B. Seed, F.I. Makdisi and P. de Alba - 1977 (PB 276 821)A04

UCB/EERC-77/21 "Dynamic Plastic Analysis Using Stress Resultant Finite Element Formulation," by P. Lukkunapvasit and J.M. Kelly - 1977 (PB 275 453)A04

UCB/EERC-77/22 "Preliminary Experimental Study of Seismic Uplift of a Steel Frame," by R.W. Clough and A.A. Huckelbridge 1977 (PB 278 769)A08

UCB/EERC-77/23 "Earthquake Simulator Tests of a Nine-Story Steel Frame with Columns Allowed to Uplift," by A.A. Huckelbridge - 1977 (PB 277 944)A09

UCB/EERC-77/24 "Nonlinear Soil-Structure Interaction of Skew Highway Bridges," by M.-C. Chen and J. Penzien - 1977 (PB 276 176)A07

UCB/EERC-77/25 "Seismic Analysis of an Offshore Structure Supported on Pile Foundations," by D.D.-N. Liou and J. Penzien 1977 (PB 283 180)A06

UCB/EERC-77/26 "Dynamic Stiffness Matrices for Homogeneous Viscoelastic Half-Planes," by G. Dasgupta and A.K. Chopra - 1977 (PB 279 654)A06

UCB/EERC-77/27 "A Practical Soft Story Earthquake Isolation System," by J.M. Kelly, J.M. Eidinger and C.J. Derham - 1977 (PB 276 814)A07

UCB/EERC-77/28 "Seismic Safety of Existing Buildings and Incentives for Hazard Mitigation in San Francisco: An Exploratory Study," by A.J. Meltsner - 1977 (PB 281 970)A05

UCB/EERC-77/29 "Dynamic Analysis of Electrohydraulic Shaking Tables," by D. Rea, S. Abedi-Hayati and Y. Takahashi 1977 (PB 282 569)A04

UCB/EERC-77/30 "An Approach for Improving Seismic - Resistant Behavior of Reinforced Concrete Interior Joints," by B. Galunic, V.V. Bertero and E.P. Popov - 1977 (PB 290 870)A06

UCB/EERC-78/01 "The Development of Energy-Absorbing Devices for Aseismic Base Isolation Systems," by J.M. Kelly and D.F. Tsztoo - 1978 (PB 284 978)A04

UCB/EERC-78/02 "Effect of Tensile Prestrain on the Cyclic Response of Structural Steel Connections, by J.G. Bouwkamp and A. Mukhopadhyay - 1978

UCB/EERC-78/03 "Experimental Results of an Earthquake Isolation System using Natural Rubber Bearings," by J.M. Eidinger and J.M. Kelly - 1978 (PB 281 686)A04

UCB/EERC-78/04 "Seismic Behavior of Tall Liquid Storage Tanks," by A. Niwa - 1978 (PB 284 017)A14

UCB/EERC-78/05 "Hysteretic Behavior of Reinforced Concrete Columns Subjected to High Axial and Cyclic Shear Forces," by S.W. Zagajeski, V.V. Bertero and J.G. Bouwkamp - 1978 (PB 283 858)A13

UCB/EERC-78/06 "Inelastic Beam-Column Elements for the ANSR-I Program," by A. Riahi, D.G. Row and G.H. Powell - 1978

UCB/EERC-78/07 "Studies of Structural Response to Earthquake Ground Motion," by O.A. Lopez and A.K. Chopra - 1978 (PB 282 790)A05

UCB/EERC-78/08 "A Laboratory Study of the Fluid-Structure Interaction of Submerged Tanks and Caissons in Earthquakes," by R.C. Byrd - 1978 (PB 284 957)A08

UCB/EERC-78/09 "Model for Evaluating Damageability of Structures," by I. Sakamoto and B. Bresler - 1978

UCB/EERC-78/10 "Seismic Performance of Nonstructural and Secondary Structural Elements," by I. Sakamoto - 1978

UCB/EERC-78/11 "Mathematical Modelling of Hysteresis Loops for Reinforced Concrete Columns," by S. Nakata, T. Sproul and J. Penzien - 1978

UCB/EERC-78/12 "Damageability in Existing Buildings," by T. Blejwas and B. Bresler - 1978

UCB/EERC-78/13 "Dynamic Behavior of a Pedestal Base Multistory Building," by R.M. Stephen, E.L. Wilson, J.G. Bouwkamp and M. Button - 1978 (PB 286 650)A08

UCB/EERC-78/14 "Seismic Response of Bridges - Case Studies," by R.A. Imbsen, V. Nutt and J. Penzien - 1978 (PB 286 503)A10

UCB/EERC-78/15 "A Substructure Technique for Nonlinear Static and Dynamic Analysis," by D.G. Row and G.H. Powell - 1978 (PB 288 077)A10

UCB/EERC-78/16 "Seismic Risk Studies for San Francisco and for the Greater San Francisco Bay Area," by C.S. Oliveira - 1978

UCB/EERC-78/17 "Strength of Timber Roof Connections Subjected to Cyclic Loads," by P. Gülkan, R.L. Mayes and R.W. Clough - 1978

UCB/EERC-78/18 "Response of K-Braced Steel Frame Models to Lateral Loads," by J.G. Bouwkamp, R.M. Stephen and E.P. Popov - 1978

UCB/EERC-78/19 "Rational Design Methods for Light Equipment in Structures Subjected to Ground Motion," by J.L. Sackman and J.M. Kelly - 1978 (PB 292 357)A04

UCB/EERC-78/20 "Testing of a Wind Restraint for Aseismic Base Isolation," by J.M. Kelly and D.E. Chitty - 1978 (PB 292 833)A03

UCB/EERC-78/21 "APOLLO - A Computer Program for the Analysis of Pore Pressure Generation and Dissipation in Horizontal Sand Layers During Cyclic or Earthquake Loading," by P.P. Martin and H.B. Seed - 1978 (PB 292 835)A04

UCB/EERC-78/22 "Optimal Design of an Earthquake Isolation System," by M.A. Bhatti, K.S. Pister and E. Polak - 1978 (PB 294 735)A06

UCB/EERC-78/23 "MASH - A Computer Program for the Non-Linear Analysis of Vertically Propagating Shear Waves in Horizontally Layered Deposits," by P.P. Martin and H.B. Seed - 1978 (PB 293 101)A05

UCB/EERC-78/24 "Investigation of the Elastic Characteristics of a Three Story Steel Frame Using System Identification," by I. Kaya and H.D. McNiven - 1978

UCB/EERC-78/25 "Investigation of the Nonlinear Characteristics of a Three-Story Steel Frame Using System Identification," by I. Kaya and H.D. McNiven - 1978

UCB/EERC-78/26 "Studies of Strong Ground Motion in Taiwan," by Y.M. Hsiung, B.A. Bolt and J. Penzien - 1978

UCB/EERC-78/27 "Cyclic Loading Tests of Masonry Single Piers: Volume 1 - Height to Width Ratio of 2," by P.A. Hidalgo, R.L. Mayes, H.D. McNiven and R.W. Clough - 1978

UCB/EERC-78/28 "Cyclic Loading Tests of Masonry Single Piers: Volume 2 - Height to Width Ratio of 1," by S.-W.J. Chen, P.A. Hidalgo, R.L. Mayes, R.W. Clough and H.D. McNiven - 1978

UCB/EERC-78/29 "Analytical Procedures in Soil Dynamics," by J. Lysmer - 1978

UCB/EERC-79/01 "Hysteretic Behavior of Lightweight Reinforced Concrete Beam-Column Subassemblages," by B. Forzani, E.P. Popov, and V.V. Bertero - 1979

UCB/EERC-79/02 "The Development of a Mathematical Model to Predict the Flexural Response of Reinforced Concrete Beams to Cyclic Loads, Using System Identification," by J.F. Stanton and H.D. McNiven - 1979

UCB/EERC-79/03 "Linear and Nonlinear Earthquake Response of Simple Torsionally Coupled Systems," by C.L. Kan and A.K. Chopra - 1979

UCB/EERC-79/04 "A Mathematical Model of Masonry for Predicting Its Linear Seismic Response Characteristics," by Y. Mengi and H.D. McNiven - 1979

UCB/EERC-79/05 "Mechanical Behavior of Lightweight Concrete Confined by Different Types of Lateral Reinforcement," by M.A. Manrique, V.V. Bertero and E.P. Popov - 1979

UCB/EERC-79/06 "Static Tilt Tests of a Tall Cylindrical Liquid Storage Tank," by R.W. Clough and A. Niwa - 1979

UCB/EERC-79/07 "The Design of Steel Energy Absorbing Restrainers and Their Incorporation Into Nuclear Power Plants for Enhanced Safety: Volume 1 - Summary Report," by P.N. Spencer, V.F. Zackay, and E.R. Parker - 1979

UCB/EERC-79/08 "The Design of Steel Energy Absorbing Restrainers and Their Incorporation Into Nuclear Power Plants for Enhanced Safety: Volume 2 - The Development of Analyses for Reactor System Piping," "Simple Systems" by M.C. Lee, J. Penzien, A.K. Chopra, and K. Suzuki "Complex Systems" by G.H. Powell, E.L. Wilson, R.W. Clough and D.G. Row - 1979

UCB/EERC-79/09 "The Design of Steel Energy Absorbing Restrainers and Their Incorporation Into Nuclear Power Plants for Enhanced Safety: Volume 3 - Evaluation of Commerical Steels," by W.S. Owen, R.M.N. Pelloux, R.O. Ritchie, M. Faral, T. Ohhashi, J. Toplosky, S.J. Hartman, V.F. Zackay, and E.R. Parker - 1979

UCB/EERC-79/10 "The Design of Steel Energy Absorbing Restrainers and Their Incorporation Into Nuclear Power Plants for Enhanced Safety: Volume 4 - A Review of Energy-Absorbing Devices," by J.M. Kelly and M.S. Skinner - 1979

UCB/EERC-79/11 "Conservatism In Summation Rules for Closely Spaced Modes," by J.M. Kelly and J.L. Sackman - 1979

UCB/EERC-79/12 "Cyclic Loading Tests of Masonry Single Piers Volume 3 - Height to Width Ratio of 0.5," by P.A. Hidalgo, R.L. Mayes, H.D. McNiven and R.W. Clough - 1979

UCB/EERC-79/13 "Cyclic Behavior of Dense Coarse-Grained Materials in Relation to the Seismic Stability of Dams," by N.G. Banerjee, H.B. Seed and C.K. Chan - 1979

UCB/EERC-79/14 "Seismic Behavior of Reinforced Concrete Interior Beam-Column Subassemblages," by S. Viwathanatepa, E.P. Popov and V.V. Bertero - 1979

UCB/EERC-79/15 "Optimal Design of Localized Nonlinear Systems with Dual Performance Criteria Under Earthquake Excitations," by M.A. Bhatti - 1979

UCB/EERC-79/16 "OPTDYN - A General Purpose Optimization Program for Problems with or without Dynamic Constraints," by M.A. Bhatti, E. Polak and K.S. Pister - 1979

UCB/EERC-79/17 "ANSR-II, Analysis of Nonlinear Structural Response, Users Manual," by D.P. Mondkar and G.H. Powell - 1979

UCB/EERC-79/18 "Soil Structure Interaction in Different Seismic Environments," A. Gomez-Masso, J. Lysmer, J.-C. Chen and H.B. Seed - 1979

UCB/EERC-79/19 "ARMA Models for Earthquake Ground Motions," by M.K. Chang, J.W. Kwiatkowski, R.F. Nau, R.M. Oliver and K.S. Pister - 1979

UCB/EERC-79/20 "Hysteretic Behavior of Reinforced Concrete Structural Walls," by J.M. Vallenas, V.V. Bertero and E.P. Popov - 1979

UCB/EERC-79/21 "Studies on High-Frequency Vibrations of Buildings I: The Column Effects," by J. Lubliner - 1979

UCB/EERC-79/22 "Effects of Generalized Loadings on Bond Reinforcing Bars Embedded in Confined Concrete Blocks," by S. Viwathanatepa, E.P. Popov and V.V. Bertero - 1979

UCB/EERC-79/23 "Shaking Table Study of Single-Story Masonry Houses, Volume 1: Test Structures 1 and 2," by P. Gülkan, R.L. Mayes and R.W. Clough - 1979

UCB/EERC-79/24 "Shaking Table Study of Single-Story Masonry Houses, Volume 2: Test Structures 3 and 4," by P. Gülkan, R.L. Mayes and R.W. Clough - 1979

UCB/EERC-79/25 "Shaking Table Study of Single-Story Masonry Houses, Volume 3: Summary, Conclusions and Recommendations," by R.W. Clough, R.L. Mayes and P. Gülkan - 1979

UCB/EERC-79/26 "Recommendations for a U.S.-Japan Cooperative Research Program Utilizing Large-Scale Testing Facilities," by U.S.-Japan Planning Group - 1979

UCB/EERC-79/27 "Earthquake-Induced Liquefaction Near Lake Amatitlan, Guatemala," by H.B. Seed, I. Arango, C.K. Chan, A. Gomez-Masso and R. Grant de Ascoli - 1979

UCB/EERC-79/28 "Infill Panels: Their Influence on Seismic Response of Buildings," by J.W. Axley and V.V. Bertero - 1979

UCB/EERC-79/29 "3D Truss Bar Element (Type 1) for the ANSR-II Program," by D.P. Mondkar and G.H. Powell - 1979

UCB/EERC-79/30 "2D Beam-Column Element (Type 5 - Parallel Element Theory) for the ANSR-II Program," by D.G. Row, G.H. Powell and D.P. Mondkar

UCB/EERC-79/31 "3D Beam-Column Element (Type 2 - Parallel Element Theory) for the ANSR-II Program," by A. Riahi, G.H. Powell and D.P. Mondkar - 1979

UCB/EERC-79/32 "On Response of Structures to Stationary Excitation," by A. Der Kiureghian - 1979

UCB/EERC-79/33 "Undisturbed Sampling and Cyclic Load Testing of Sands," by S. Singh, H.B. Seed and C.K. Chan - 1979

UCB/EERC-79/34 "Interaction Effects of Simultaneous Torsional and Compressional Cyclic Loading of Sand," by P.M. Griffin and W.N. Houston - 1979

UCB/EERC-80/01 "Earthquake Response of Concrete Gravity Dams Including Hydrodynamic and Foundation Interaction Effects," by A.K. Chopra, P. Chakrabarti and S. Gupta - 1980

UCB/EERC-80/02 "Rocking Response of Rigid Blocks to Earthquakes," by C.S. Yim, A.K. Chopra and J. Penzien - 1980

UCB/EERC-80/03 "Optimum Inelastic Design of Seismic-Resistant Reinforced Concrete Frame Structures," by S.W. Zagajeski and V.V. Bertero - 1980

UCB/EERC-80/04 "Effects of Amount and Arrangement of Wall-Panel Reinforcement on Hysteretic Behavior of Reinforced Concrete Walls," by R. Iliya and V.V. Bertero - 1980

UCB/EERC-80/05 "Shaking Table Research on Concrete Dam Models," by R.W. Clough and A. Niwa - 1980

UCB/EERC-80/06 "Piping With Energy Absorbing Restrainers: Parameter Study on Small Systems," by G.H. Powell, C. Oughourlian and J. Simons - 1980

UCB/EERC-80/07 "Inelastic Torsional Response of Structures Subjected to Earthquake Ground Motions," by Y. Yamazaki - 1980

UCB/EERC-80/08 "Study of X-Braced Steel Frame Structures Under Earthquake Simulation," by Y. Ghanaat - 1980

UCB/EERC-80/09 "Hybrid Modelling of Soil-Structure Interaction," by S. Gupta, T.W. Lin, J. Penzien and C.S. Yeh - 1980